UNIVERSITY OF CALIFORNIA,
IRVINE

Opsin Evolution and Sensory Physiology of the Compound Eye in *Heliconius* Butterflies

DISSERTATION

submitted in partial satisfaction of the requirements
for the degree of

DOCTOR OF PHILOSOPHY

in Ecology and Evolutionary Biology

by

Kyle Joseph McCulloch

Dissertation Committee:
Professor Adriana D. Briscoe, Chair
Professor Timothy J. Bradley
Professor Anthony D. Long

2016

DEDICATION

To

Mom and Dad, Kasey, and Bruno

TABLE OF CONTENTS

LIST OF FIGURES

CHAPTER 3

LIST OF TABLES

ACKNOWLEDGMENTS

I want to express my deep gratitude and admiration for my committee chair and adviser, Adriana D. Briscoe. Adriana, you have always had my best interests at heart, and thanks to your mentorship and example, I have learned and grown so much as a young scientist. Thank you for your investment in me, from conferences, to the course at MBL, to the *years* spent getting the ephys rig up and running. I also want to thank you for the invaluable advice outside of the lab that you have instilled in me, from politics in science to grantsmanship and speaking skills. Any future success I have I owe to you.

I would also like to thank my committee members, Professor Timothy Bradley and Professor Anthony Long. Your straight-to-the point constructive critiques are always much appreciated, and your examples of the value of good science over flashy science are something that will stick with me for the rest of my career. Thank you as well to my advancement committee members for their valuable critique and feedback, Drs. Matthew McHenry and Georg Striedter.

To Dr. Daniel Osorio, who not only came to our lab to help set up the electrophysiology rig, but whose expertise and advice made possible Chapters 1 and 2 of this dissertation, thank you. I'd also like to thank Drs. Matthew L. Aardema, Peter Andolfatto, Jorge Llorente-Bousquets, Gilbert Smith, Furong Yuan, and Ying Zhen, without whom Chapter 3 of this dissertation would not be possible.

To Aide Macias-Muñoz, who has been a truly wonderful lab-mate, scientist, salsa partner, travel buddy, and friend for most of my entire graduate career, I am forever thankful. You have made getting a Ph.D. truly fun (There's no crying in science!). Thank you also to my lab-mates past and present for your friendship and insight, Ana Catalán, Jen Briner, Susan Finkbeiner, Sebastian Höhna, Gil Smith, and Furong Yuan.

I must also thank all the other Eco Evo grad students for the friendly and social atmosphere in this department. Especially to LuAnna Dobson and Stephen Hatosy, it's been great to take this step in my life with you by my side, and I appreciate your friendship immensely. Nameer Baker, Jim Baldwin-Brown, Kate Gallagher, and Sarah Roy, you have been wonderful friends and colleagues on this journey together.

The text of Chapter 1 of this dissertation is a reprint of the material as it appears in the *Journal of Visualized Experiments* (*JoVE*) and is reproduced with permission from *JoVE*. The text of Chapter 2 is a reprint of material originally published in the *Journal of Experimental Biology* and is reproduced with permission from The Company of Biologists, Ltd. For both chapters, Dr. Adriana D. Briscoe directed, supervised, and supported this research, and co-author Dr. Daniel Osorio provided essential direction, support and feedback.
Financial support was provided by the University of California, Irvine Francisco J. Ayala School of Biological Sciences, an NSF Grant IOS-1257627 and the National Science Foundation Graduate Research Fellowship Program under Grant No. (1321846).

* * *

I am dedicating this dissertation to my family, who are the most important reasons for the success I have had so far. Your support and love have made me who I am today. Mom, Dad, you have always encouraged my scientific curiosity since as long as I can remember, from collecting starfish at the beach to salamanders in the backyard. Thank you for the crystal growing sets, seahorse kits, taking me frog and firefly catching, and for buying me hundreds of natural history books, as well as all the other things you did for me in my younger years. Also thank you so much for instilling in me the importance of and helping me with attending college, without which I could not have dreamed of graduate education. Even though the content of this dissertation might be a bit more complex than those early days, you are still the reason it exists. To Kasey, I intensely admire your fierce independence and free spirit and when you put your mind to it there's nothing you cannot do. You are an inspiration for me and I will take your example with me on the next chapter of my life. Bruno, thank you for listening to my countless practice talks, reading my drafts, and being there for me in times of stress. You are my base of support and these last few years would have been impossible without you by my side. Thank you, all.

CURRICULUM VITAE

Kyle J. McCulloch

Department of Ecology and Evolutionary Biology
University of California, Irvine
321 Steinhaus Hall
Irvine, CA 92697-2525

E-mail: mccullok@uci.edu
Phone: 774-521-8216

EDUCATION

2016 - PhD, Dept. of Ecology and Evolutionary Biology, Cumulative GPA: 4.0 University of California, Irvine, Irvine, CA. Advisor: Adriana Briscoe, PhD

2008 - B.S. Biology, with double major, Hispanic Language and Culture, Cumulative GPA: 3.5 Boston College, Chestnut Hill, MA

ADDITIONAL TRAINING

2014 - Big Data Summer School, University of Texas at Austin, Austin, TX
2012 - Sensory Ecology Course, Lund University, Lund, Sweden
2012 - Neural Systems and Behavior Course, Marine Biological Laboratories, Woods Hole, MA
2007 - Semester abroad, Universidad San Francisco de Quito, Quito, Ecuador

PROFESSIONAL EMPLOYMENT

2015-16 - Teaching Fellow, Dept. of Ecology and Evolutionary Biology, University of California Irvine: Human Physiology, Human Physiology Lab
2011-12 - Teaching Fellow, Dept. of Ecology and Evolutionary Biology, University of California Irvine: Human Physiology Lab, Color and Vision
2008-11 - Research Assistant, Harvard Medical School, Mass. Eye and Ear Infirmary, Boston, MA. Advisor: Richard Masland, PhD
2004-08 - Senior Teaching Labs Technician, Chemistry Department, Boston College, Chestnut Hill, MA

AWARDS AND FELLOWSHIPS

2016 – Grover C. Stephens Memorial Fellowship Award
2016 - Winner, Best Student Talk Competition, Society for Integrative and Comparative Biology, Division of Neurobiology
2016 - U.S. Department of Education, Graduate Assistance in Areas of National Need Fellowship
2015 - Society for the Study of Evolution Travel Award
2014 - Francisco J Ayala School of Biosciences Graduate Fellowship
2011 - National Science Foundation Graduate Research Fellowship
2011 - Francisco J. Ayala Graduate Recruitment Fellowship, School of Biological Sciences, UC Irvine

PUBLICATIONS

In Review

1. **McCulloch KJ**, Yuan F, Zhen Y, Aardema ML, Smith G, Llorente-Bousquets J, Andolfatto P, & Briscoe AD. Exceptional retinal mosaic diversity and evolution of a violet receptor in *Heliconius* butterflies. (In Review).

Published

1. *Manduca sexta* Genome Consortium*,* **McCulloch KJ** one of the authors. (**2016**) Multifaceted biological insights from a draft genome sequence of the tobacco hornworm moth, *Manduca sexta. Insect Biochemistry and Molecular Biology*. 76, 118-147.
2. **McCulloch KJ,** Osorio D, Briscoe AD. (**2016**) Sexual dimorphism in the compound eye of *Heliconius erato*: a nymphalid with at least five spectral classes of photoreceptor*. Journal of Experimental Biology.* 219, 2377-2387.
3. **McCulloch KJ,** Osorio D, Briscoe AD. (**2016**) Determination of photoreceptor cell spectral sensitivity in an insect model from *in vivo* intracellular recordings. *Journal of Visualized Experiments* 108, e53829. DOI: 10.3791/53829
4. Sümbül U, Song S, **McCulloch KJ**, Becker M, Lin B, Sanes J, Masland RH, & Seung HS. (**2014**) A genetic and computational approach to structurally classify neuronal types. *Nature Communications* 5, DOI:10.1038/ncomms4512.
5. Martin A, **McCulloch KJ,** Patel NH, Briscoe AD, Gilbert LE, & Reed RD*.* (**2014**) Multiple recent co-options of Optix associated with novel traits in adaptive butterfly wing radiations. *EvoDevo* 5, DOI: 10.1186/2041-9139-5-7.
6. Kitambi S, **McCulloch KJ**, Peterson R, & Malicki J. (**2009**) Small molecule screen for compounds that affect vascular development in the zebrafish retina. *Mechanisms of Development* 126, 464-477.
7. Zhang Y, **McCulloch KJ**, & Malicki J. (**2009**) Lens transplantation in zebrafish and its application in the analysis of eye mutants. *Journal of Visualized Experiments*, 28, DOI: 10.3791/1258.

ABSTRACT OF THE DISSERTATION

Opsin Evolution and Sensory Physiology of the Compound Eye in *Heliconius* Butterflies

By

Kyle Joseph McCulloch

Doctor of Philosophy in Ecology and Evolutionary Biology

University of California, Irvine, 2016

Professor Adriana D. Briscoe, Chair

Gene duplications sometimes result in large evolutionary shifts in adaptation, but often no phenotypic change occurs after duplication. In animals, molecular genetic changes, including duplications in opsin genes have resulted in highly diverse visual phenotypes. Unlike the diversity of vision-related phenotypes among orders and families, visual systems are mostly conserved among closely related species, and evidence is limited as to how visual traits initially diverge. The neotropical butterfly genus, *Heliconius*, is a good system for addressing these questions. *Heliconius* has duplicated UV opsin genes (*UVRh1* and *UVRh2*) coincident with a UV-yellow wing pigment, a known sexual visual cue. I hypothesized that the *Heliconius*-specific opsin duplication has led to photoreceptor neofunctionalization in the genus, which might affect visual system evolution and divergence in the genus due to the importance of UV signals in *Heliconius*.

To understand the phenotypic effects of UV gene duplication in *H. erato,* I developed an intracellular recording technique in the lab that measures photoreceptor spectral sensitivities. I also compared differences in opsin expression and retinal mosaics across 23 species in the genus, using immunohistochemistry and RNA-Sequencing. Combining this

data in a phylogenetic context, I analyzed the evolutionary history of the opsins and their expression patterns in *Heliconius.* Intracellular recordings confirm two distinct female-specific UV-sensitive cells in *H. erato* females, but males lack the UVRh1 cell. Unlike other groups with conserved eye design among closely-related species, I discovered a high diversity of both sex- and clade-specific retinal mosaics *within* the genus. I found three unique forms of sexual dimorphism, multiple independent pseudogenizations of *UVRh2*, and the independent evolution of a retinal mosaic in separate clades. The proportions of ommatidial types are tightly regulated within each species and sex. These patterns indicate that *Heliconius* species with only one UV cell subtype have higher proportions of blue cells, perhaps as a secondary method for detecting the genus-specific UV-yellow wing pigment.

The spectacular diversity in opsin expression represents the rarely-seen incipient stages of visual system divergence. Novel UV photoreceptor subtypes evolved in *Heliconius* via opsin gene duplication, and subsequent varying selection pressures have likely caused the increased diversity of retinal mosaics in *Heliconius*.

INTRODUCTION

One of the primary drivers of evolution is natural selection, which acts on the variation found in populations in nature. A major source for this variation is thought to arise when genes and genomes are duplicated, either entirely or in part. Once redundant duplicates of a particular gene exist, selection on the gene is relaxed, and mutations may accumulate in either duplicate that might otherwise be harmful to the organism, and would therefore be eliminated from the population. This process may result in subfunctionalization, or the dividing the ancestral expression pattern or phenotype between the new duplicates (Lynch & Force, 2000). If mutations in one or more duplicates result in divergent or novel phenotypes compared to the ancestor, then neofunctionalization has occurred (Lynch & Conery, 2000). Gene duplications can sometimes lead to shifts in the course of evolution, and divergence in phenotypes might quickly evolve among closely related species (Sidow, 1996; Yu et al., 2005). Even so, in most duplicated genes one of the duplicates is silenced, and traits of the descendants do not differ from the ancestral phenotype (nonfunctionalization) (Lynch & Conery, 2000). Identification of gene duplicates in a species or lineage is intriguing because of the potential for the duplication to be implicated in dramatic phenotypic evolution. However, to understand whether duplicates have indeed undergone sub- or neofunctionalization and whether or how this is adaptive, the expression patterns and phenotypes associated with the new duplicates must first be determined.

Determining changes in phenotype caused by recent gene duplicates is not always straightforward. One gene family, the opsins, is useful for this task because molecular genetic changes in opsins can lead to direct changes in phenotype (Terai et al., 2006;

Wakakuwa et al., 2010). Opsin genes encode the visual pigment proteins, part of the seven transmembrane G-protein coupled receptor superfamily (Palczewski et al., 2000). Visual opsins bind a vitamin-A derived chromophore to form the rhodopsin molecule, which is responsible for the conversion of light into a cellular signal, known as phototransduction (Shichida & Matsuyama, 2009). Phototransduction is initiated when the *cis* form of the chromophore absorbs a photon and undergoes a conformation change to all-*trans*, which then causes a conformational change in the opsin protein. This change initiates a G-protein cascade, which results in the opening of ion channels, causing a graded membrane potential change in the opsin-expressing photoreceptor cell, depending on the cell's sensitivity. Photoreceptor cell sensitivity is determined by the efficiency with which photons of a particular wavelength are absorbed by the rhodopsin expressed by that cell (Rushton, 1972). The interaction of the chromophore with particular amino acids in the opsin protein is responsible for the specific absorption spectrum of each rhodopsin molecule; thus changes to the chromophore's composition or in the amino acids that interact with it will alter the absorption spectrum (Briscoe & Chittka, 2001; Carvalho, Cowing, Wilkie, Bowmaker, & Hunt, 2007). Most animals use only one type of chromophore, so the majority of differences between photoreceptor cell sensitivities within or between individuals are caused by differences in amino acid sequence of the opsin protein (Briscoe & Chittka, 2001; Seki & Vogt, 1998).

In addition to a direct link between genotype and phenotype, opsins also serve as the molecular basis for essential visual tasks critical for survival and reproduction in many animals, from phototaxis to courtship displays (Laver & Taylor, 2011; Mazzoni, Desplan, & Blau, 2005). Furthermore, eyes and the associated neural processing necessary for vision

are metabolically costly (Niven, Anderson, & Laughlin, 2007; Niven & Laughlin, 2008). Therefore, the patterns of photoreceptors with different sensitivities that form retinal mosaics in the eye, as well as their opsin sequences and expression patterns, are generally thought to be adaptive. For highly visual animals, in particular the vertebrates and arthropods, a variety of well-developed visual systems are found, with multiple opsin genes expressed in several different subtypes of photoreceptor cells in the eye (Kelber, Vorobyev, & Osorio, 2003; Osorio & Vorobyev, 2008). Dense arrays of opsin-expressing photoreceptors (along with the associated neural processing in the brain) allow for high-resolution spatial vision. Color discrimination requires multiple opsin genes expressed in distinct subpopulations of photoreceptors. The particular opsins and set of photoreceptors in an individual are typically adapted to specific visual tasks, and are the result of ancestral opsin gene duplications (Frentiu, Bernard, Sison-Mangus, Brower, & Briscoe, 2007; Hofmann & Carleton, 2009; Spaethe & Briscoe, 2004). For instance, cichlids have multiple photoreceptor subtypes each with different sensitivities based on expression of divergent opsins. These photoreceptors are tuned to best detect intraspecific color signals under the specific light conditions of the water in which cichlids live, caused by differences in depth or turbidity, which also drives speciation (Seehausen et al., 2008). In Old-World primates, an opsin duplication is responsible for red/green discrimination, thought to benefit in detecting ripe fruit in green trees, a duplication that has been inherited in humans (Surridge, Osorio, & Mundy, 2003). Honeybees also have multiple opsins, but these are sensitive to ultraviolet (UV), blue, and green, and are adapted for foraging and navigation (Backhaus, 1993; Frisch, 1914).

Although there are many examples of opsin duplication and subsequent adaptive evolution of visual traits, not all opsin duplications result in enhanced color vision. Nor is the evolution of new important color tasks always accompanied by new opsin gene duplications or sequence evolution. For example, dragonflies have up to 30 expressed opsins (Futahashi et al., 2015), and 46 opsins are found in the genome of the water flea, *Daphnia pulex* (Colbourne et al., 2011), but these examples of hyper-duplicated opsin genes have not yet been demonstrated to have a corresponding increase in photoreceptor subtypes, suggesting considerable redundancy. In addition, several groups that live in variable light environments, with variable coloration, and variable foraging habits have minimal variation in opsin-based photoreceptor types across multiple investigated species. This is true of several comparative studies in anole lizards, birds, Old-World primates, and bees and wasps, (Hart & Hunt, 2007; Jacobs & Deegan, 1999; Loew, Fleishman, Foster, & Provencio, 2002; Peitsch et al., 1992).

A few well-studied cases exist of gene duplications that have led to a high level of diversity in opsin sequence evolution, expression patterns, photoreceptor subtypes, and retinal mosaics among related genera or families. Of these, the few comparative studies of closely related species have shown that related taxa generally display conservation of vision-related traits. Among African cichlids (family: Cichlidae), multiple opsin duplications along with rapid speciation and colonization of new habitats with different light environments have caused rapid divergence in numbers and types of photoreceptors across species (Carleton et al., 2008; Parry et al., 2005; Spady et al., 2006; Spady et al., 2005; Terai et al., 2006). However, when multiple species of the same genus (*Pundamilia*) were compared, photoreceptor subtypes and sensitivities were similar, with the greatest

difference in peak sensitivity in long wavelength receptors of about 3-4 nm (Carleton, Parry, Bowmaker, Hunt, & Seehausen, 2005). Mantis shrimps (order: Stomatopoda) are also known for their colorful displays and their extreme diversity in color receptors within individual species, with up to 16 different subtypes and sensitivities (Porter, Bok, Robinson, & Cronin, 2009). Sensitivities of some of these photoreceptors do indeed differ somewhat among species found at different depths (Cronin, Marshall, & Caldwell, 1996), and complex filtering mechanisms also tune and produce multiple short wavelength photoreceptors in the eyes of different species (Bok, Porter, & Cronin, 2015). However nearly all species investigated appear to have the same 16 photoreceptor subtypes spatially arranged in a similar way in the eye, despite some rampant opsin gene duplications whose effect on vision is not obvious (Cronin, Porter, Bok, Wolf, & Robinson, 2010; Porter et al., 2013).

In terrestrial animals too, a high level of diversity in photoreceptor subtypes can arise via opsin duplication. In the swallowtail butterflies (family: Papilionidea), six, eight, nine, and 15 photoreceptor subtypes have been described in different species, across multiple genera (Arikawa, 2003; P.-J. Chen, Awata, Matsushita, Yang, & Arikawa, 2016; P. J. Chen, Arikawa, & Yang, 2013; Matsushita, Awata, Wakakuwa, Takemura, & Arikawa, 2012). Comparative studies of visual sensitivities in butterflies within the same genus are lacking, but a single study found that at least three species of *Papilio* do not differ in the number and type of opsins expressed in the eye (P.-J. Chen et al., 2016). In some investigated lineages opsin duplications seem to be common but they do not clearly affect visual phenotypes. Those duplications that have brought about diversity in visual phenotypes is seen across larger taxonomic groups while phenotypes are conserved within single genera.

In this dissertation I aim to address the following questions: 1) Has a newly described opsin duplication resulted in sub- or neofunctionalization and does this appear to be adaptive? and 2) What are the evolutionary effects of a newly adaptive gene duplication on a group of closely related species? To determine the effects of gene duplication in the context of visual system evolution, I investigated butterflies in the genus *Heliconius.* Neotropical *Heliconius* butterflies have recently radiated into about 50 species in the past 10 to 13 million years, and the rate of speciation is still increasing (Kozak et al., 2015; Mavarez et al., 2006; Rosser, Kozak, Phillimore, & Mallet, 2015). Species in this genus are toxic and warn their visual bird predators of their unpalatability with bright aposematic coloration. *Heliconius* and other genera participate in Müllerian mimicry and have evolved similar aposematic wing signals to strengthen their collective warning signal to visual predators (Bates, 1862). Birds preferentially attack rare and novel forms, creating strong selection pressure for convergence of wing colors (Finkbeiner, Briscoe, & Reed, 2014; Langham, 2004; Pinheiro, 1996). These colorful wing patterns are also known to serve as sexual signals. *Heliconius* assortatively mate with butterflies that share their own wing color pattern over those that do not (Kronforst, Young, & Gilbert, 2007; Kronforst et al., 2006). Both predators and the butterflies themselves contribute to maintaining mimicry, but sometimes co-mimics of different species are confused for potential mates, thus there is a cost to mimicry as well (Estrada & Jiggins, 2008).

Under these conflicting selection pressures *Heliconius* have developed two genus-specific innovations that other butterfly mimics have not. In the ancestor to the genus, a duplication event occurred in the gene encoding UV opsin. At around the same time, this ancestor incorporated the compound 3-hydroxykynurenine into its yellow wing colors,

resulting in present-day *Heliconius* yellows that also reflect UV wavelengths. Both full-length UV opsins are found in several species in the genus, and one duplicate, *UVRh2*, has undergone positive selection, suggesting an adaptive function for the UV opsins (Briscoe et al., 2010). Color-space modeling suggests these two *Heliconius* synapomorphies might be related, possibly by allowing *Heliconius* to better discriminate UV wavelengths that are reflected in the wings. More than one UV photoreceptor would allow increased discrimination of different UV-yellow colors for *Heliconius* individuals, while bird visual systems are not as good at differentiating UV-yellows from non-UV-yellows (Bybee et al., 2012). If the gene duplication does improve *Heliconius* UV discrimination, then this might provide a private channel of communication where *Heliconius* can identify conspecifics while still maintaining mimicry in the eyes of their predators. Although this is an interesting hypothesis, nothing is known about the opsin protein expression patterns or functional implications for *Heliconius* photoreceptors following this UV opsin duplication.

I sought to show neofunctionalization of the UV opsin duplicates in *Heliconius*, implicating the duplicate UV genes in adaptive evolution. By characterizing spatial expression patterns of opsins and spectral sensitivities of photoreceptor cells in *Heliconius* butterflies in a comparative, phylogenetic context, I aimed to understand whether and how the duplication has contributed to compound eye evolution during 10 million years of speciation. In this dissertation I review and develop a method for recording intracellular photoreceptor responses in butterflies (Chapter 1). Next I address the question of whether the UV opsin duplicates have resulted in distinct photoreceptor subtypes with different spectral sensitivities in *Heliconius erato*, and I identify a filtering mechanism in the eye that leads to a red-sensitive cell (Chapter 2). I then comparatively survey opsin spatial

expression patterns, retinal mosaics, and evolutionary history of opsin and photoreceptor subtypes in 23 species within *Heliconius* and close outgroups (Chapter 3).

References

Arikawa, K. (2003). Spectral organization of the eye of a butterfly, *Papilio*. *J Comp Physiol A Neuroethol Sens Neural Behav Physiol, 189*(11), 791-800. doi:10.1007/s00359-003-0454-7

Backhaus. (1993). Color vision and color choice behavior of the honey bee. *Apidologie, 24*, 309-331.

Bates, H. W. (1862). Contributions to an insect fauna of the Amazon valley (Lepidoptera, Heliconidae). *Biol J Linn Soc, 16*(1), 41-54. doi:Doi 10.1111/J.1095-8312.1981.Tb01842.X

Bok, M. J., Porter, M. L., & Cronin, T. W. (2015). Ultraviolet filters in stomatopod crustaceans: diversity, ecology and evolution. *J Exp Biol, 218*(Pt 13), 2055-2066. doi:10.1242/jeb.122036

Briscoe, A. D., Bybee, S. M., Bernard, G. D., Yuan, F., Sison-Mangus, M. P., Reed, R. D., . . . Chiao, C. C. (2010). Positive selection of a duplicated UV-sensitive visual pigment coincides with wing pigment evolution in *Heliconius* butterflies. *Proc Natl Acad Sci U S A, 107*(8), 3628-3633. doi:10.1073/pnas.0910085107

Briscoe, A. D., & Chittka, L. (2001). The evolution of color vision in insects. *Annu Rev Entomol, 46*, 471-510. doi:10.1146/annurev.ento.46.1.471

Bybee, S. M., Yuan, F., Ramstetter, M. D., Llorente-Bousquets, J., Reed, R. D., Osorio, D., & Briscoe, A. D. (2012). UV photoreceptors and UV-yellow wing pigments in *Heliconius* butterflies allow a color signal to serve both mimicry and intraspecific communication. *Am Nat, 179*(1), 38-51. doi:10.1086/663192

Carleton, K. L., Parry, J. W., Bowmaker, J. K., Hunt, D. M., & Seehausen, O. (2005). Colour vision and speciation in Lake Victoria cichlids of the genus *Pundamilia*. *Mol Ecol, 14*(14), 4341-4353. doi:10.1111/j.1365-294X.2005.02735.x

Carleton, K. L., Spady, T. C., Streelman, J. T., Kidd, M. R., McFarland, W. N., & Loew, E. R. (2008). Visual sensitivities tuned by heterochronic shifts in opsin gene expression. *BMC Biol, 6*, 22. doi:10.1186/1741-7007-6-22

Carvalho, L. S., Cowing, J. A., Wilkie, S. E., Bowmaker, J. K., & Hunt, D. M. (2007). The molecular evolution of avian ultraviolet- and violet-sensitive visual pigments. *Mol Biol Evol, 24*(8), 1843-1852. doi:10.1093/molbev/msm109

Chen, P.-J., Awata, H., Matsushita, A., Yang, E.-C., & Arikawa, K. (2016). Extreme spectral richness in the eye of the common bluebottle butterfly, *Graphium sarpedon*. *Frontiers in Ecology and Evolution, 4*. doi:10.3389/fevo.2016.00018

Chen, P. J., Arikawa, K., & Yang, E. C. (2013). Diversity of the photoreceptors and spectral opponency in the compound eye of the Golden Birdwing, *Troides aeacus formosanus*. *PLoS One, 8*(4), e62240. doi:10.1371/journal.pone.0062240

Colbourne, J. K., Pfrender, M. E., Gilbert, D., Thomas, W. K., Tucker, A., Oakley, T. H., . . . Boore, J. L. (2011). The ecoresponsive genome of *Daphnia pulex*. *Science, 331*(6017), 555-561. doi:10.1126/science.1197761

Cronin, T. W., Marshall, N. J., & Caldwell, R. L. (1996). Visual pigment diversity in two genera of mantis shrimps implies rapid evolution (Crustacea; Stomatopoda). *Journal of Comparative Physiology A, 179*(3). doi:10.1007/bf00194991

Cronin, T. W., Porter, M. L., Bok, M. J., Wolf, J. B., & Robinson, P. R. (2010). The molecular genetics and evolution of colour and polarization vision in stomatopod crustaceans. *Ophthalmic Physiol Opt, 30*(5), 460-469. doi:10.1111/j.1475-1313.2010.00762.x

Estrada, C., & Jiggins, C. D. (2008). Interspecific sexual attraction because of convergence in warning colouration: is there a conflict between natural and sexual selection in mimetic species? *J Evol Biol, 21*(3), 749-760. doi:10.1111/j.1420-9101.2008.01517.x

Finkbeiner, S. D., Briscoe, A. D., & Reed, R. D. (2014). Warning signals are seductive: relative contributions of color and pattern to predator avoidance and mate attraction in *Heliconius* butterflies. *Evolution, 68*(12), 3410-3420. doi:10.1111/evo.12524

Frentiu, F. D., Bernard, G. D., Sison-Mangus, M. P., Brower, A. V., & Briscoe, A. D. (2007). Gene duplication is an

evolutionary mechanism for expanding spectral diversity in the long-wavelength photopigments of butterflies. *Mol Biol Evol, 24*(9), 2016-2028. doi:10.1093/molbev/msm132

Frisch, K. v. (1914). Der Farbensinn und Formensinn der Biene. *Jahrbucher Abteilung fuer Allgemeine Zoologie und Physiologie der Tiere, 37*, 1-238. doi:10.5962/bhl.title.11736

Futahashi, R., Kawahara-Miki, R., Kinoshita, M., Yoshitake, K., Yajima, S., Arikawa, K., & Fukatsu, T. (2015). Extraordinary diversity of visual opsin genes in dragonflies. *Proc Natl Acad Sci U S A, 112*(11), E1247-1256. doi:10.1073/pnas.1424670112

Hart, N. S., & Hunt, D. M. (2007). Avian visual pigments: characteristics, spectral tuning, and evolution. *Am Nat, 169 Suppl 1*, S7-26. doi:10.1086/510141

Hofmann, C. M., & Carleton, K. L. (2009). Gene duplication and differential gene expression play an important role in the diversification of visual pigments in fish. *Integr Comp Biol, 49*(6), 630-643. doi:10.1093/icb/icp079

Jacobs, G. H., & Deegan, J. F., 2nd. (1999). Uniformity of colour vision in Old World monkeys. *Proc Biol Sci, 266*(1432), 2023-2028. doi:10.1098/rspb.1999.0881

Kelber, A., Vorobyev, M., & Osorio, D. (2003). Animal colour vision – behavioural tests and physiological concepts. *Biological Reviews of the Cambridge Philosophical Society, 78*(1), 81-118. doi:10.1017/s1464793102005985

Kozak, K. M., Wahlberg, N., Neild, A., Dasmahapatra, K. K., Mallet, J., & Jiggins, C. D. (2015). Multilocus Species Trees Show the Recent Adaptive Radiation of the Mimetic Heliconius Butterflies. *Syst Biol*. doi:10.1093/sysbio/syv007

Kronforst, M. R., Young, L. G., & Gilbert, L. E. (2007). Reinforcement of mate preference among hybridizing *Heliconius* butterflies. *J Evol Biol, 20*(1), 278-285. doi:10.1111/j.1420-9101.2006.01198.x

Kronforst, M. R., Young, L. G., Kapan, D. D., McNeely, C., O'Neill, R. J., & Gilbert, L. E. (2006). Linkage of butterfly mate preference and wing color preference cue at the genomic location of *wingless*. *Proc Natl Acad Sci U S A, 103*(17), 6575-6580. doi:10.1073/pnas.0509685103

Langham, G. M. (2004). Specialized avian predators repeatedly attack novel color morphs of *Heliconius* butterflies. *Evolution, 58*(12), 2783-2787.

Laver, C. R., & Taylor, J. S. (2011). RT-qPCR reveals opsin gene upregulation associated with age and sex in guppies (*Poecilia reticulata*) - a species with color-based sexual selection and 11 visual-opsin genes. *BMC Evol Biol, 11*, 81. doi:10.1186/1471-2148-11-81

Loew, E. R., Fleishman, L. J., Foster, R. G., & Provencio, I. (2002). Visual pigments and oil droplets in diurnal lizards: a comparative study of Caribbean anoles. *J Exp Biol, 205*(Pt 7), 927-938.

Lynch, M., & Conery, J. S. (2000). The evolutionary fate and consequences of duplicate genes. *Science, 290*(5494), 1151-1155.

Lynch, M., & Force, A. (2000). The probability of duplicate gene preservation by subfunctionalization. *Genetics, 154*(1), 459-473.

Matsushita, A., Awata, H., Wakakuwa, M., Takemura, S. Y., & Arikawa, K. (2012). Rhabdom evolution in butterflies: insights from the uniquely tiered and heterogeneous ommatidia of the Glacial Apollo butterfly, *Parnassius glacialis*. *Proc Biol Sci, 279*(1742), 3482-3490. doi:10.1098/rspb.2012.0475

Mavarez, J., Salazar, C. A., Bermingham, E., Salcedo, C., Jiggins, C. D., & Linares, M. (2006). Speciation by hybridization in *Heliconius* butterflies. *Nature, 441*(7095), 868-871. doi:10.1038/nature04738

Mazzoni, E. O., Desplan, C., & Blau, J. (2005). Circadian pacemaker neurons transmit and modulate visual information to control a rapid behavioral response. *Neuron, 45*(2), 293-300. doi:10.1016/j.neuron.2004.12.038

Niven, J. E., Anderson, J. C., & Laughlin, S. B. (2007). Fly photoreceptors demonstrate energy-information trade-offs in neural coding. *PLoS Biol, 5*(4), e116. doi:10.1371/journal.pbio.0050116

Niven, J. E., & Laughlin, S. B. (2008). Energy limitation as a selective pressure on the evolution of sensory systems. *J Exp Biol, 211*(Pt 11), 1792-1804. doi:10.1242/jeb.017574

Osorio, D., & Vorobyev, M. (2008). A review of the evolution of animal colour vision and visual communication signals. *Vision Res, 48*(20), 2042-2051. doi:10.1016/j.visres.2008.06.018

Palczewski, K., Kumasaka, T., Hori, T., Behnke, C. A., Motoshima, H., Fox, B. A., . . . Miyano, M. (2000). Crystal structure of rhodopsin: A G protein-coupled receptor. *Science, 289*(5480), 739-745. doi:10.1126/science.289.5480.739

Parry, J. W., Carleton, K. L., Spady, T., Carboo, A., Hunt, D. M., & Bowmaker, J. K. (2005). Mix and match color vision: tuning spectral sensitivity by differential opsin gene expression in Lake Malawi cichlids. *Curr*

Biol, 15(19), 1734-1739. doi:10.1016/j.cub.2005.08.010
Peitsch, D., Fietz, A., Hertel, H., de Souza, J., Ventura, D. F., & Menzel, R. (1992). The spectral input systems of hymenopteran insects and their receptor-based colour vision. *Journal of Comparative Physiology A, 170*(1), 23-40. doi:10.1007/bf00190398
Pinheiro, C. (1996). Palatablility and escaping ability in Neotropical butterflies: tests with wild kingbirds (*Tyrannus melancholicus*, Tyrannidae). *Biological Journal of the Linnean Society, 59*(4), 351-365. doi:10.1111/j.1095-8312.1996.tb01471.x
Porter, M. L., Bok, M. J., Robinson, P. R., & Cronin, T. W. (2009). Molecular diversity of visual pigments in Stomatopoda (Crustacea). *Vis Neurosci, 26*(3), 255-265. doi:10.1017/S0952523809090129
Porter, M. L., Speiser, D. I., Zaharoff, A. K., Caldwell, R. L., Cronin, T. W., & Oakley, T. H. (2013). The evolution of complexity in the visual systems of stomatopods: insights from transcriptomics. *Integr Comp Biol, 53*(1), 39-49. doi:10.1093/icb/ict060
Rosser, N., Kozak, K. M., Phillimore, A. B., & Mallet, J. (2015). Extensive range overlap between heliconiine sister species: evidence for sympatric speciation in butterflies? *BMC Evol Biol, 15*, 125. doi:10.1186/s12862-015-0420-3
Rushton, W. (1972). Review Lecture. Pigments and signals in colour vision. *J. Physiol., 220*(3), 1-31.
Seehausen, O., Terai, Y., Magalhaes, I. S., Carleton, K. L., Mrosso, H. D., Miyagi, R., . . . Okada, N. (2008). Speciation through sensory drive in cichlid fish. *Nature, 455*(7213), 620-626. doi:10.1038/nature07285
Seki, T., & Vogt, K. (1998). Evolutionary Aspects of the Diversity of Visual Pigment Chromophores in the Class Insecta. *Comparative Biochemistry and Physiology Part B: Biochemistry and Molecular Biology, 119*(1), 53-64. doi:10.1016/s0305-0491(97)00322-2
Shichida, Y., & Matsuyama, T. (2009). Evolution of opsins and phototransduction. *Philos Trans R Soc Lond B Biol Sci, 364*(1531), 2881-2895. doi:10.1098/rstb.2009.0051
Sidow, A. (1996). Gen(om)e duplications in the evolution of early vertebrates. *Curr Opin Genet Dev, 6*(6), 715-722.
Spady, T. C., Parry, J. W., Robinson, P. R., Hunt, D. M., Bowmaker, J. K., & Carleton, K. L. (2006). Evolution of the cichlid visual palette through ontogenetic subfunctionalization of the opsin gene arrays. *Mol Biol Evol, 23*(8), 1538-1547. doi:10.1093/molbev/msl014
Spady, T. C., Seehausen, O., Loew, E. R., Jordan, R. C., Kocher, T. D., & Carleton, K. L. (2005). Adaptive molecular evolution in the opsin genes of rapidly speciating cichlid species. *Mol Biol Evol, 22*(6), 1412-1422. doi:10.1093/molbev/msi137
Spaethe, J., & Briscoe, A. D. (2004). Early duplication and functional diversification of the opsin gene family in insects. *Mol Biol Evol, 21*(8), 1583-1594. doi:10.1093/molbev/msh162
Surridge, A. K., Osorio, D., & Mundy, N. I. (2003). Evolution and selection of trichromatic vision in primates. *Trends in Ecology & Evolution, 18*(4), 198-205. doi:10.1016/s0169-5347(03)00012-0
Terai, Y., Seehausen, O., Sasaki, T., Takahashi, K., Mizoiri, S., Sugawara, T., . . . Okada, N. (2006). Divergent selection on opsins drives incipient speciation in Lake Victoria cichlids. *PLoS Biol, 4*(12), e433. doi:10.1371/journal.pbio.0040433
Wakakuwa, M., Terakita, A., Koyanagi, M., Stavenga, D. G., Shichida, Y., & Arikawa, K. (2010). Evolution and mechanism of spectral tuning of blue-absorbing visual pigments in butterflies. *PLoS One, 5*(11), e15015. doi:10.1371/journal.pone.0015015
Yu, J., Wang, J., Lin, W., Li, S., Li, H., Zhou, J., . . . Yang, H. (2005). The Genomes of *Oryza sativa*: a history of duplications. *PLoS Biol, 3*(2), e38. doi:10.1371/journal.pbio.0030038

CHAPTER 1

Determination of Photoreceptor Cell Spectral Sensitivity in an Insect Model from *In Vivo* Intracellular Recordings

Abstract

Intracellular recording is a powerful technique used to determine how a single cell may respond to a given stimulus. In vision research, intracellular recording has historically been a common technique used to study sensitivities of individual photoreceptor cells to different light stimuli that is still being used today. However, there remains a dearth of detailed methodology in the literature for researchers wishing to replicate intracellular recording experiments in the eye. Here we present the insect as a model for examining eye physiology more generally. Insect photoreceptor cells are located near the surface of the eye and therefore easy to reach, and many of the mechanisms involved in vision are conserved across animal phyla. We describe the basic procedure for *in vivo* intracellular recording of photoreceptor cells in the eye of a butterfly, with the goal of making this technique more accessible to researchers with little prior experience in electrophysiology. We introduce the basic equipment needed, how to prepare a live butterfly for recording, how to insert a glass microelectrode into a single cell, and finally the recording procedure itself. We also explain the basic analysis of raw response data for determining spectral sensitivity of individual cell types. Although our protocol focuses on determining spectral

sensitivity, other stimuli (e.g., polarized light) and variations of the method are applicable to this setup.

Introduction

The electrical properties of cells such as neurons are observed by measuring ion flow across cell membranes as a change in voltage or current. A variety of electrophysiological techniques have been developed to measure bioelectric events in cells. Neurons found in the eyes of animals are accessible and their circuitry is often less complex than in the brain, making these cells good candidates for electrophysiological study. Common applications of electrophysiology in the eye include electroretinography (ERG)(Beckmann et al., 2015; Leboulle et al., 2013) and microelectrode intracellular recording. ERG involves placing an electrode in or on the eye of an animal, applying a light stimulus, and measuring the change in voltage as a sum of the responses of all nearby cells(Knox et al., 2003; Martinez-Harms et al., 2012; Salcedo et al., 1999; Salcedo, Zheng, Phistry, Bagg, & Britt, 2003). If one is specifically interested in characterizing spectral sensitivities of individual photoreceptor cells, often multiple cell types simultaneously respond at different strengths and frequencies to a given stimulus; thus it can be difficult to determine the sensitivities of specific cell types from ERG data especially if there are several different kinds of spectrally-similar photoreceptor cells in the eye. One potential solution is to create transgenic *Drosophila* with the photoreceptor (opsin) gene of interest expressed in the majority R1-6 cells in the eye and then perform ERGs(Vilinsky & Johnson, 2012). Potential drawbacks of this method include no to low-expression of the photoreceptor protein(Hu, Leming, Whaley, & O'Tousa, 2014), and the long time frame for

the generation and screening of transgenic animals. For eyes with fewer kinds of spectrally distinct photoreceptors, adaptation of the eye with colored filters can help with lowering the contribution of some cell types to the ERG, thereby permitting estimation of spectral sensitivity maxima(Telles et al., 2014).

Intracellular recording is another technique where a fine electrode impales a cell and a stimulus is applied. The electrode records only that individual cell's response so that recording from and analyzing multiple individual cells can yield specific sensitivities of physiologically different cell types(Arikawa, Mizuno, Kinoshita, & Stavenga, 2003; Arikawa et al., 1999; Cronin, Jarvilehto, Weckstrom, & Lall, 2000; Skorupski, Doring, & Chittka, 2007; Stalleicken, Labhart, & Mouritsen, 2006). Although our protocol focuses on analysis of spectral sensitivity, the basic principles of intracellular recording with sharp electrodes are modifiable for other applications. Using a different preparation of a specimen, for instance, and using sharp quartz electrodes, one may record from deeper in the optic lobe or other regions in the brain, depending on the question being asked. For example, response times of individual photoreceptor cells(Skorupski & Chittka, 2011), cell activity in the optic lobes(E.-C. Yang & Osorio, 1991) (lamina, medulla or lobula(E. C. Yang, Lin, & Hung, 2004)), brain(Rosner & Homberg, 2013) or other ganglia(Trager & Homberg, 2011) can also be recorded with similar techniques, or color stimuli could be replaced with polarization(Greiner, Cronin, Ribi, Wcislo, & Warrant, 2007; Heinze & Reppert, 2011; Stowasser & Buschbeck, 2012) or motion stimuli(Nordstrom, Barnett, Moyer de Miguel, Brinkworth, & O'Carroll, 2008; Osorio, 1986).

Phototransduction, the process by which light energy is absorbed and converted into an electrochemical signal, is an ancient trait common to nearly all present-day animal

phyla(Plachetzki, Fong, & Oakley, 2010). The visual pigment found in photoreceptor cells and responsible for initiating visual phototransduction is rhodopsin. Rhodopsins in all animals are made up of an opsin protein, a member of the 7 transmembrane G protein-coupled receptor family, and an associated chromophore which is derived from retinal or a similar molecule(Feuda, Hamilton, McInerney, & Pisani, 2012; Palczewski et al., 2000). Opsin amino acid sequence and chromophore structure affect the absorbance of rhodopsin to different wavelengths of light. When a photon is absorbed by the chromophore the rhodopsin becomes activated, initiating a G-protein cascade in the cell that ultimately leads to the opening of membrane-bound ion channels(Hardie & Raghu, 2001). Unlike most neurons, photoreceptor cells undergo graded potential changes that can be measured as a relative change in response amplitude with changing light stimulus. Typically a given photoreceptor type expresses only one opsin gene (though exceptions exist(Arikawa et al., 2003; Hu et al., 2014; Katti et al., 2010; Sison-Mangus, Bernard, Lampel, & Briscoe, 2006; Smith, Price, Greenberg, & Battelle, 1993)). Sophisticated color vision, of the kind found in many vertebrates and arthropods, is achieved with a complex eye of hundreds or thousands of photoreceptor cells each expressing one or occasionally more rhodopsin types. Visual information is captured by comparing responses over the photoreceptor mosaic via complex downstream neural signaling in the eye and brain, resulting in the perception of an image complete with color and motion.

After measuring the raw responses of a photoreceptor cell to different wavelengths of light via intracellular recording, it is possible to calculate its spectral sensitivity. This calculation is based on the Principle of Univariance, which states that a photoreceptor cell's response is dependent on the number of photons it absorbs, but not on the particular

properties of the photons it absorbs(Rushton, 1972). Any photon that is absorbed by rhodopsin will induce the same kind of response. In practice, this means that a cell's raw response amplitude will increase due to either an increase in light intensity (more photons to absorb), *or* to a shift in wavelength toward its peak sensitivity (higher probability of rhodopsin absorbing that wavelength). We make use of this principle in relating cellular responses at known intensity and the same wavelength to responses at different wavelengths and the same intensity but unknown relative sensitivity. Cell types are often identified by the wavelength at which their sensitivity peaks.

Here we show one method for intracellular recording and analysis of spectral sensitivity of photoreceptors in the eye of a butterfly, with a focus on making this method more accessible to the wider research community. Although intracellular recording remains common in the literature, particularly with respect to color vision in insects, we have found that descriptions of materials and methods are usually too brief to allow for reproduction of the technique. We present this method in video format with the aim of permitting its easier replication. We also describe the technique using easily obtainable and affordable equipment. We address common caveats that often are not reported, which slow down research when optimizing a new and complex technique.

Protocol

All animals were treated as humanely as possible in accordance with University of California ethics guidelines for insects. Insects were shipped as pupae from Costa Rica Entomological Supply, Costa Rica.

1. *Heliconius* Pupae Care

1. Hang all pupae spaced 2-3 cm apart in a humidified chamber using insect pins.
2. After eclosion, allow wings to dry then keep butterflies alive for at least 1 day in a humidified chamber and feed a dilute honey solution daily before recording.
    1. Dilute honey with water to about a 20% honey solution by volume, and pour into a shallow Petri dish.
    2. Bring individual butterflies to the Petri dish, one by one. Upon touching the solution with their front tarsi, the butterflies will automatically extend their proboscides and drink from the Petri dish. If their proboscis does not automatically extend, use forceps to pull the proboscis out and introduce it to the honey solution.

2. Optical Track, Calibration, and Measurement of Experimental Light Conditions.

1. Place a Xenon arc lamp with housing and universal power supply and an attached condenser lens assembly on one end of a table at least one meter long to deliver bright white light. CAUTION: Xenon arc lamps produce extremely bright light with strong UV intensities. Protective eyewear should be worn at all times and the lamp should be used as directed by the manufacturer to prevent accumulation of ozone caused by interaction of UV light with atmospheric oxygen.
2. Set up an optical track one meter in length for the light exiting the housing assembly to pass through.
    1. Place in the following order on the optical track with approximate distances apart: 1) a convex silica or quartz lens 40 cm from the condenser assembly, 2) a neutral density filter wheel (with no filters currently in the light path) 22 cm further along the track, 3) a shutter with drive unit 14 cm from the ND

filters, 4) a concave silica or quartz lens immediately adjacent following the shutter, and 5) a collimating beam probe 6 cm further along the far end of the track.

2. Affix a 600 µm diameter fiber optic cable to the collimating beam probe.

   Note: Depending on light intensity, a 5-10 mm diameter fiber optic cable may be required to deliver enough light to other preps and may be substituted for this.

3. Adjust the distance, height and angle of each optical element so that the light beam exiting the assembly is at the highest intensity possible.
4. As optical track elements may differ slightly with different applications, ensure that all elements transmit light in the UVA and visible range (315 – 700 nm).

3. Once the optical track is assembled, measure the light that passes through the setup using a spectrometer. It is necessary to calibrate the spectrometer first using a calibration lamp with a known spectrum and Spectra Suite software. Note: We describe the following set up using Ocean Optics products for clarity but other manufacturers (e.g. Ayantes) sell comparable products.
   1. Turn on the LS-1-Cal calibration lamp at least 45 minutes before taking measurements.
   2. To calibrate, attach the spectrometer via USB to a computer with the Spectra Suite software installed. Then connect the spectrometer to the LS-1-Cal lamp via a UV-visible transmitting cosine corrector.

3. In Spectra Suite, select “New Absolute Irradiance Measurement” from the “File” tab, and select the spectrometer as the “Source.”
4. Follow the prompts to create a new calibration “cal” file. When prompted, load the provided data file for the known spectrum of the LS-1-Cal lamp in the visible light range (300-800 nm) into the software, which automatically calculates the corrected spectrum from the spectrometer output.
5. Save the calibration file. This file should be loaded when initializing the software for all future measurements of light spectra using the spectrometer.

4. Once the spectrometer is calibrated, it may be used to record the light spectra from the experimental setup. Hereafter when Spectra Suite is opened, select “New Absolute Irradiance Measurement” and load the previously saved calibration file. Next take a dark spectrum by blocking all light to the spectrometer.
    1. With the spectrometer currently measuring the desired experimental light conditions, adjust the integration time (4 ms), scans to average (5), and boxcar width (5), so the spectrum is properly scaled and smoothed. These settings should remain the same for all spectral measurements, so that light intensities from different measurements can be compared.
5. Measure spectra for unattenuated white light, for all neutral density filters to be used during experiments, and for each bandpass interference filter (Figure 5).
    1. Measure the white light spectrum without any filters in the light path by affixing the free end of the fiber optic cable from step 2.2.2 to the spectrometer. With the calibration file loaded from step 2.3, save the white light spectrum using the spectrometer’s software as a text file. Note: Spectra

saved as text files list the wavelength (x coordinates) in one column and the intensity of light (y coordinates) in the second column, so that the data may be loaded into a spreadsheet for step 2.6.

2. Using the same setup as step 2.5.1, record the spectrum from each optical density (OD) (0-3.5 OD) used during experiments by rotating the neutral density (ND) filter wheel in the optical track, and save the text file for each OD.
3. Using the same setup as step 2.5.1, place the 10 nm half bandwidth interference filters one by one into the light path and record the spectrum observed for each filter. Repeat this procedure for each of 41 different interference filters with peak transmittances spaced every 10 nm from 300 to 700 nm. Filters spaced further apart (20 nm) are acceptable for most applications (for spectra, see Figure 5).

6. Correct for differences in intensity of light when interference filters are placed in the light path. Each interference filter allows a different total number of photons to pass, and the low transmission of some filters makes it difficult to further attenuate intensity so that all filters allow equal numbers of photons.
    1. To calculate the relative intensity (I) for each 10 nm bandwidth interference filter, solve for I in the expression, I = T/sec, where T is the area under the spectral curve of each 10 nm interference filter (from 2.5.3), and s is the maximum absolute irradiance (y value of saved text file from 2.5.1) of white light at the peak wavelength of each filter (See Figure 2 for an example at 520 nm).

2. Divide all calculated intensities by the max intensity value calculated in 2.6.1 to normalize to one, and take the reciprocal of the relative normalized values for use as a correction factor applied to the raw sensitivity at each wavelength (see Step 6.4).

7. Perform steps 2.1 through 2.6 only once before a set of experiments. Over the course of an experiment periodically record the absolute irradiance of the Xenon arc lamp under bright light and neutral density filters, to make sure the intensity of the light stimulus does not change.
8. During the course of an experiment, if any cellular response to light transmitted through the interference filters approaches the maximum response amplitude, use the ND filters to attenuate the signal. If ND filters are used during an experiment, account for the corresponding decrease in intensity during the calculation of spectral sensitivity.
9. Set up optical track, calibration, and filters days or weeks before experiments begin. Keep filters covered to prevent dust accumulation.

3. Recording Equipment Setup

1. Feed the same fiber optic cable used for calibration through a Faraday cage and mount on a goniometric device such as a Cardan arm perimeter (see Figure 4 for diagram). The cable will be about 10 cm away from the eye of the specimen.
2. Place a metal stage on a vibrationally isolated table with an electrode holder mounted directly above the stage under control of a micromanipulator. Place the Cardan arm so that the specimen's head is at the center of the sphere created by the arm's rotational movement.

3. Using an intracellular preamplifier system, which includes an amplifier (outside the Faraday cage) and preamplifier (headstage, near the prep inside the Faraday cage) mount the headstage above the metal stage where the specimen will be placed.
    1. Connect a coaxial cable to the headstage via a BNC connection. Split open only the tip on the other end of the coaxial cable, and separate the outer metal sheath of the cable from the inner wire.
    2. Solder the outer sheath (kept at ground potential) to one end of an insulated copper wire with an alligator clip on the other end. This alligator clip will attach to the metal reference electrode on the specimen platform (Step 5.1.4).
    3. Solder the inner wire of the coaxial cable to a thin silver wire, to serve as the recording electrode. This wire should be thin enough to be fed into the solution-filled glass electrode in Step 5.2.3.
4. Place a stereomicroscope attached to a swinging arm and base on the wooden bench outside the Faraday cage, so that it may be swung in to lower the electrode into the eye, and swung back out again once the electrode is in the eye.
5. Make sure everything metal inside the Faraday cage is properly grounded.
6. Outside the Faraday cage, attach the preamplifer to the input of a 50-60 Hz noise reducer (optional), and connect the output to one channel of an oscilloscope using a BNC T-adapter.
7. Using the other end of the T-adapter, connect the signal passing through the oscilloscope to one channel of the Powerlab hardware. Attach this hardware to a

computer by a USB cable, which will allow responses recorded with the preamplifier to be read by software on the computer.

8. Attach the shutter driver from the optical track to the second channel of the oscilloscope using another T-adapter and connect this to a pulse generator that will control the frequency and duration of light flashes delivered to the eye (Step 5.5). Note: Set up of the rig itself should only need to be done once. Break here until ready to begin recordings.

4. Prep on the Day of Recording

1. Turn on the Xenon lamp at least 45 minutes before the experiment and turn on the glass microelectrode puller at least 30 minutes before pulling glass electrodes.
2. Turn on all recording equipment (shutter, amplifier, Humbug, pulse generator, oscilloscope, and Powerlab hardware) and make sure the shutter is closed by default so no light passes through the fiber optic cable.
3. Pull fine borosilicate (or aluminosilicate) glass microelectrodes (100-250 MΩ resistance is ideal) using a glass microelectrode puller. Use glass electrodes within only a few hours of being pulled.
4. Backfill the electrodes with 3 M Potassium chloride (KCl). Note that this solution may be modified according to the researcher's needs, e.g. dye injection.

5. Specimen Prep and Recording Procedure

1. Prepare the specimen.
    1. Affix an individual butterfly inside a small plastic tube with hot wax so the head is immobile and protruding from one end of the tube. Wax down proboscis, antennae, and wings.

2. Hold down the abdomen with a dry piece of wax and keep the tube humidified by placing a wet tissue inside the tube behind the abdomen. Make sure the specimen is completely immobile.
3. Mount the tube using a small piece of wax onto a small platform with a ball-and-socket joint that is attached to a magnetic base.
4. Under a dissecting microscope, insert a silver wire of 0.125 mm diameter into the head via the mouthparts to be used as the reference electrode. Before the experiment, permanently fix the wire to the platform in such a way that the copper wire in Step 3.3.2 may clip on to it once the platform is placed on the stage for recording.
5. Once the reference electrode is in a suitable position it may be kept in place by quickly melting and then cooling wax around the wire.
6. Using a breakable carbon steel razor blade, grip part of the blade with a blade holder and break off a small piece to use for cutting the cornea.
7. Cut a small hole (~10 ommatidia in diameter) in the left cornea using the razorblade and seal the hole with Vaseline to prevent desiccation.

2. Once the cornea is cut, insert the recording electrode into the eye as quickly as possible because hemolymph in the eye will quickly harden and make it impossible to insert an electrode. If possible perform the dissection in the rig where the recording will take place.
    1. If not already on the stage, place the mounted specimen and platform onto the stage in the recording rig. Connect the headstage ground wire from step

3.3.2 to the reference electrode on the specimen platform using alligator clips.

2. Use a light source with gooseneck attachments to briefly light the specimen under a stereoscope while lowering the recording electrode into the eye.
3. Insert the silver wire connected to the headstage from step 3.3.3 into the KCl solution in the back of a glass microelectrode. Mount the glass electrode on the electrode holder.
4. Adjust the electrode holder so the microelectrode is directly over the hole previously cut in the cornea, about a millimeter above the cornea. Lower the microelectrode into the eye using the micromanipulator until a circuit is completed, as shown by a large change in potential (mV) on the oscilloscope.

3. Once in the eye, swing the stereoscope outside the Faraday cage, and turn off the light source illuminating the specimen. The room should be kept dark so the eye becomes dark adapted.
4. Check the resistance of the electrode by applying a 1 nA current from the amplifier and noting the change in voltage. Resistance should typically be in the range between 100 – 250 MΩ. (Higher resistances are indicative of blockage or bending of the electrode, and low resistances of electrode breakage.)
5. Activate the pulse generator so the shutter opens allowing a flash of light with a 50 msec duration every 0.5 sec, and allow it to continue flashing for the duration of the experiment.
    1. Adjust the pulse generator so it allows flashes of up to 50 msec duration. This duration and 0.5 sec pause between flashes keeps the specimen as near to

dark adapted as possible during the experiment. Fifty msec is close to the shortest flash duration that will elicit the same amplitude in response as longer flash durations.

2. Re-measure responses at both the beginning and end of the experiment (Step 5.16). Over the course of about a twenty minute experiment, these flash settings do not degrade the response over time. Different preps may require adjustments to these flash settings.

6. Position the Cardan arm so that the fiber optic cable is directed toward the eye.
7. Check the oscilloscope for voltage change with each light flash. A negative change in voltage signifies that the electrode has not yet entered a cell.
8. Move the Cardan arm around the specimen until it is positioned at an angle to the eye at which there is a maximum voltage response.
9. Rotate the micromanipulator back and forth, causing very small vertical movements of the electrode in both directions while lightly tapping the base of the electrode holder or using the Buzz function on the preamplifier. Continue making small adjustments until a depolarizing light response appears on the oscilloscope (Figure 6).
10. Adjust the Cardan arm again to find the angle of incidence where a flash of light produces the largest depolarizing signal. Make small adjustments with the micromanipulator and use the Buzz function on the amplifier as needed to make sure the electrode is stably recording the cell and that it will stay in the cell for the whole experiment (See Step 5.11).

11. Once the setup is stable, begin recording. A stable recording should have little to no change in resting potential, low background noise, and a consistently large depolarizing response (at least a 10:1 signal to noise ratio).
    1. Run the LabChart software on the computer, and begin a "new experiment," which will open a pop up window with four channels.
    2. Adjust the voltage scale at the top right corner of the software window to 500 mV. The first channel will display the responses recorded from the electrode in real time, while the second channel will record the square wave produced by the function generator, if the signal is fed to the data aquisition hardware via the oscilloscope, showing when the shutter is open. The other two channels are unneeded.
    3. Click "Start" at the bottom right hand corner to begin recording, and allow the software to run for the duration of the experiment. Adjust the zoom of the x (time) and y (voltage) axes so that the responses are clear.
12. First, with white light, record up to 10 individual responses with the ND filter wheel at 3.5 OD (about 5-10 s).
13. Next record the same number of responses at 3.3 OD, then 3.1, 3.0, 2.5, 2.3, 2.1, etc. in every combination until 0.0 OD. These response amplitudes to the ND filter series will provide the response-log intensity curve in Section 6. If bleaching occurs, use fewer flashes of bright stimuli during the course of the experiment.
14. Record the response of the cell to all wavelengths, using the interference filters.
    1. First find the peak wavelength. Without ND filters in the light path (0.0 OD), place a UV transmitting filter in the light path and briefly observe the

response amplitude. Repeat with a blue transmitting filter, a green transmitting filter, and a red transmitting filter, which should give some idea of where the peak response will be.

2. Use filters at about 350, 450, 550, 650 nm to find the general region of peak sensitivity in step 5.14.1. The exact wavelength does not matter in this initial search phase because all wavelengths will be recorded in the next step. If estimates exist of peak sensitivities, or they have been previously recorded, use known wavelengths to quickly identify the peak response.
3. Once the peak response or close to it is identified, record at this wavelength for 10 responses (about 5 s).
4. After recording at the wavelength of peak response, record with the other interference filters, from 300-700 nm at 10 nm steps. Start from the peak and step out toward both shorter and longer wavelengths by swapping the filters out from the light path one by one (*e.g.* if the peak response is at 520 nm, record responses at this wavelength first, then 510 nm, followed by 530 nm, 500 nm, 540 nm, 490 nm, 550 nm, and so on until no there is no response).
5. Allow for up to 10 responses per filter (5 s each). When swapping interference filters, allow the cell to respond to 1-2 flashes of white light without any filter in the light path, which is helpful to monitor whether the peak response is degrading over time. Reduce number of responses or increase the OD if bleaching occurs.

15. If the response under any interference filter is too close to the maximum response under white light at 0 OD, then attenuate with ND filters. The interference filters and

size of the fiber optic cable used in this experiment greatly attenuate the intensity of light and so ND filters are typically not needed.

16. If the recording remains stable, re-record wavelengths around the peak response, which serves as a pseudoreplicate for confirming previous response amplitudes and helps to ensure response has not degraded over time. Once all wavelengths are recorded, re-record the responses under the ND series, as in step 5.12.
17. Once recording is complete click “Stop” on the LabChart software, and save the recording for analysis.
18. After an experiment, sacrifice the individual by freezing, or cooling for several minutes followed by swiftly severing the head and crushing the thorax.
19. Shut down all equipment. Break here if needed before doing the analysis.

6. Spectral Sensitivity Analysis

1. With the software used to record raw responses, calculate the mean response amplitude of 10 individual responses for each filter in the ND series and for each interference filter.
2. Create a response-log intensity (VlogI) function from the ND filter series recorded in Steps 5.12-5.13 (Figure 7). Do this by plotting log units of intensity (OD) on the X axis, and response to each intensity on the y axis.
    1. To derive spectral sensitivity of the cell at different wavelengths, typically fit the Naka-Rushton equation to the data from step 6.2, and use this equation to relate experimentally obtained spectral responses of different wavelengths to relative photons required to elicit that response under a constant wavelength (in this case white light).

Note: The Naka-Rushton equation is: $V/V_{max} = I^n/(I^n + K^n)$, where I is the stimulus intensity, V is the response amplitude, V_{max} is the maximum response amplitude, K is the stimulus intensity giving ½ V_{max}, and n is the exponential slope. Various methods can be used to fit this equation to the VlogI data, including curve fitting software, or code-based statistical packages.

2. To fit the Naka-Rushton equation using simple calculations and a spreadsheet program, transform the VlogI response data for each stimulus intensity: $\log[(V_{max}/V) - 1]$. Then perform linear regression on the transformed data to get the equation of the line of best fit.

   Note: V_{max} must be greater than any measured responses; to keep this consistent, this method estimates V_{max} as 1% greater than the highest measured response.

3. From the equation of the regression line, estimate the exponent (n) by taking the negative slope, and log(K) = y-intercept/n.

3. Once the parameters for V_{max}, n, and K have been estimated, one can determine the relative number of photons required to elicit the spectral response of the cell at each wavelength by plugging in the measured spectral response at a given wavelength as (V) and solving for I.
4. Multiply the calculated stimulus intensity (I) from step 6.3 by the correction factor for each interference filter (from step 2.4.3) at each wavelength.

5. To get sensitivity, all intensities must be related to the V log-I curve so they can be compared. Do this by relating each wavelength intensity to ½ V_{max} or K, calculated in Step 6.2.3.
    1. Subtract each corrected wavelength intensity (Step 6.4) from K.
    2. Then for each wavelength intensity, add this "distance from K" value to K, and multiply by (-1).
    3. Next bring all data points positive by adding the absolute value of the lowest data point in the series to each wavelength.
6. Find sensitivity at each wavelength by taking the reciprocal of all newly calculated intensities from Step 6.5.1. Transform the data so that the sensitivity spectrum falls between 0 and 1.
7. After recording from more than one cell of the same type average the final responses and plot with standard error bars or 95% confidence intervals (Figure 8).

Representative Results

For many elements of the recording setup, a written description does not provide enough detail. Figure 1 is a composite image showing several setup and equipment features. Figure 2 shows several steps in the preparation of a butterfly for the experiment. Figure 3 is a schematic of the elements involved in the complete recording setup. Figure 4 shows photos and a diagram of the Cardan arm that was used for these experiments. In Figure 5, spectra are plotted for white light and each interference filter to give a sense of why a correction factor is needed and what is needed for to calculate this correction.

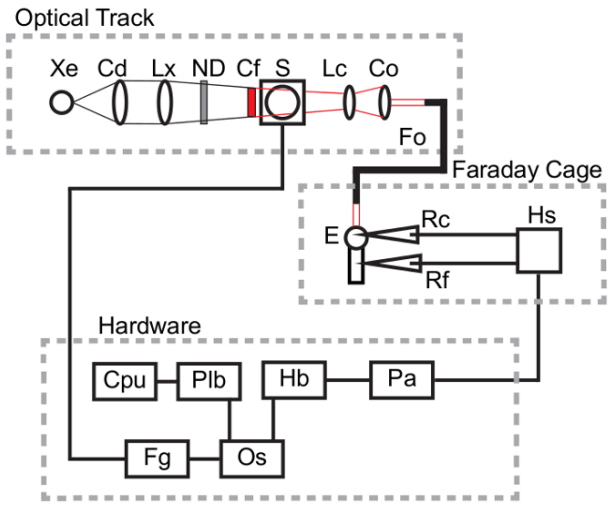

Figure 1: Schematic of Recording Components. Components of the light path, specimen setup, and recording hardware are indicated. Optical track sits on the wooden bench outside the Faraday cage. *Xe*, xenon arc lamp, *Cd*, condenser assembly, *Lx*, convex lens, *ND*, neutral density filter wheel, *Cf*, interference filter, *S*, shutter, *Lc*, concave lens, *Co*, collimating beam probe, *Fo,* fiber optic cable. The Faraday cage sits on the wooden bench around the specimen. The wooden bench sits above but does not touch the vibrationally isolated marble table underneath. Recording (*Rc*) and reference (*Rf*) electrodes are attached to the headstage (*Hs*). *Rc* is introduced into the eye (*E*) and *Rf* is introduced into another part of the body. The headstage is part of the preamplifier (*Pa*) setup outside the Faraday cage. The signal is passed from the preamplifier through the Humbug noise reducer (*Hb*), and into the oscilloscope (*Os*). From the oscilloscope the signal is passed through the Powerlab hardware (*Plb*) and into the laptop computer (*Cpu*) where it is read by the Labchart software. The shutter is controlled by a function generator (*Fg*) which is passed through a second channel on the oscilloscope, and may also be passed through a second channel on the Powerlab hardware if this signal is going to be recorded as well.

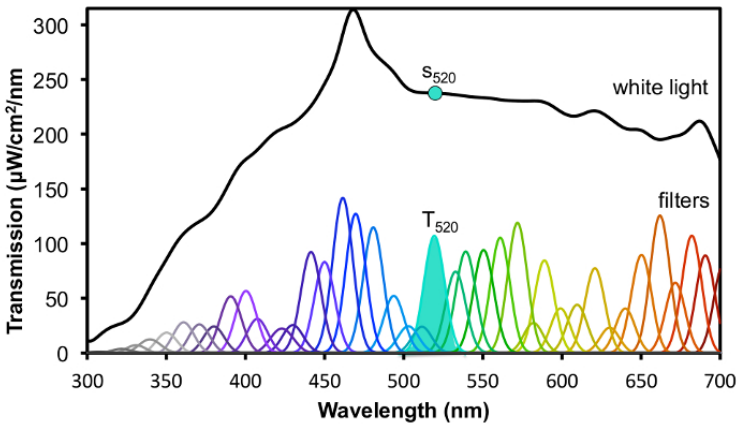

Figure 2: White Light and Interference Filter Spectra Used to Calculate Correction Factors. The spectra measured in step 2.5 of the protocol are shown from 300 to 700 nm, for white light as well as each of the 41 interference filters. Each interference filter spectrum is measured with only that filter in the light path. T_{520} corresponds to the area under the spectrum for the filter with peak 520 nm, and s_{520} corresponds to the intensity of white light at peak wavelength of the filter, 520 nm. These values are used in calculating the correction factors for each filter (in this case 520 nm) as described in step 2.6 in the protocol.

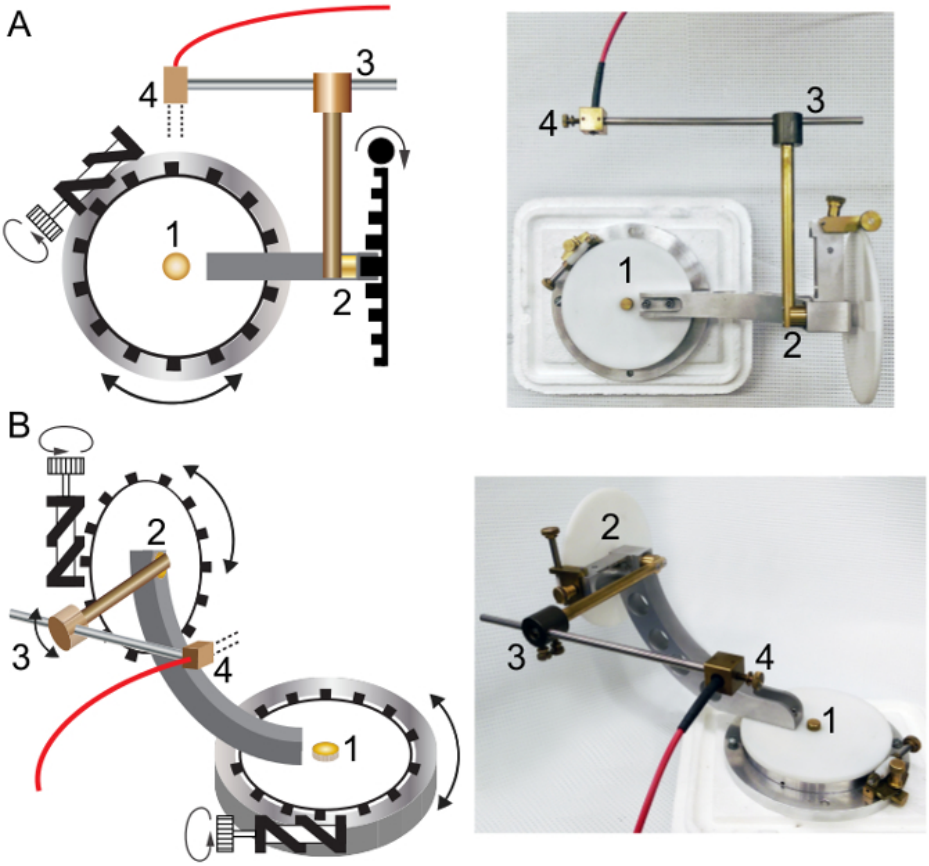

Figure 3: Description of the Cardan Arm Perimeter Used in the Experiments. The Cardan arm holds the fiber optic cable and allows full spherical rotation and angular adjustment so that light may be delivered at the proper angle of incidence to the cell being recorded. (**A**) Top down view. (**B**) View from the side at an angle. Numbers correspond to the same part in all panels. (1) The bottom plate allows full circular rotation in the horizontal plane. (2) The vertical plate allows full circular rotation of the arm in a vertical plane. (3) This cylinder holds the metal arm with the fiber optic cable on the end, and it allows a second vertical plane of circular rotation perpendicular to (2). (4) The fiber optic cable is held in place at the end of the arm, and light is directed toward the location of the specimen in the experimental setup.

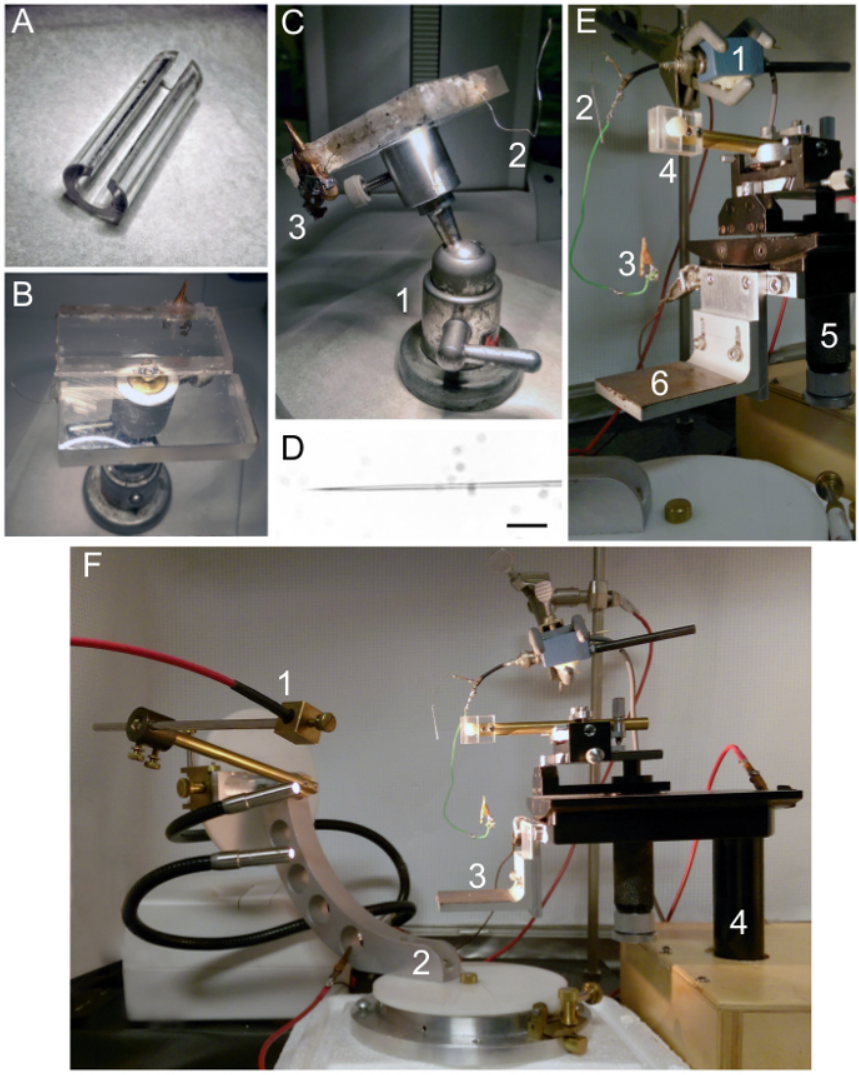

Figure 4: Components of the Recording Setup. (**A**) Plastic tube used to hold the specimen. (**B**) Overhead view of the platform on which the specimen and tube are mounted. (**C**) Side view of ball-and-joint platform with magnetic base (1). Reference electrode kept immobile with glue and wax on side of platform (2). Reference electrode wrapped around alligator clip and soldered in place, providing an attachment area where the headstage reference electrode can clip (3). (**D**) Electrode tip under 20X magnification. Scale bar, 25 µm. (**E**) Stage, electrode holder, and micromanipulator setup. The headstage (1) is fixed above the apparatus with the silver recording wire (2), and the reference electrode with alligator clip (3) attached. The electrode holder (4) is fixed to a manual micromanipulator (5) with a post below that may be adjusted with a knob for vertical movement or may be pushed or pulled for horizontal movement of the electrode holder. The magnetic platform with specimen sits on the stage (6) just below the electrode holder. (**F**) The Faraday cage surrounds the recording setup with a screen that can be pulled up or down in the front. Aluminum foil is placed underneath all equipment with rubber pads on top. The fiber optic cable (1) leads into the cage from the optical track outside, and is directed by the Cardan arm (2) toward the stage (3). The recording stage and manipulator apparatus is placed in a sand box (4) resting on a marble table underneath the setup. All other equipment rests on the wooden bench top that does not touch the marble table. The sand box sits on top of the marble table in a hole cut out of the wooden table, so that the specimen is completely vibrationally isolated from the equipment on the wooden tabletop.

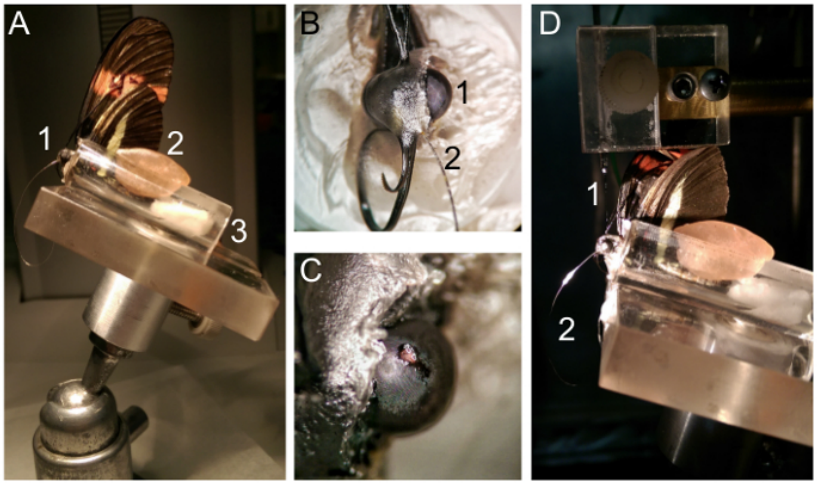

Figure 5: Butterfly Prep. (**A**) The butterfly is inserted into the tube and the head, wings, and antennae are immobilized with hot wax. The indifferent electrode is inserted into the mouthparts (1), a piece of dry wax is used to hold down the abdomen (2), and a wet tissue is placed behind the specimen. (**B**) Close-up of the head waxed down. The eye to be recorded from (1) is kept clear from wax or debris, and the reference electrode (2) is inserted into the mouthparts and hot wax is quickly melted over it to keep it in place. (**C**) A hole cut into the eye where the pink-white photoreceptor cell layer can be seen. Black pigment and yellow hemolymph are absent. (**D**) Lateral view of the specimen with a glass recording electrode (1) placed in the eye, and the indifferent electrode (2) attached to the head stage, which should complete a circuit as seen on the oscilloscope.

Once a recording begins, a *negative* change in voltage in response to a light flash means that the electrode is outside of a cell, as in Figure 6a. The strength of the response depends on the proximity of the electrode tip to a photoreceptor cell, and the angle of incidence of the light flash. The response should be large (> 30 mV) before the tip is near enough to a cell to impale. Figure 6b shows a clear *depolarizing* response to a light stimulus, signifying entry into a photoreceptor cell. The resting potential should be stable and the response amplitude should be large (at least 40 mV), although the absolute amplitude may vary considerably. We measure *relative* response, so it is more important that the signal to noise ratio is high. If the resting potential changes greatly, the response waveform looks unusual, or the maximum response is too low, then comparing relative responses across all interference filters becomes impossible. Examples of unusable recordings are shown in Figure 6c, d.

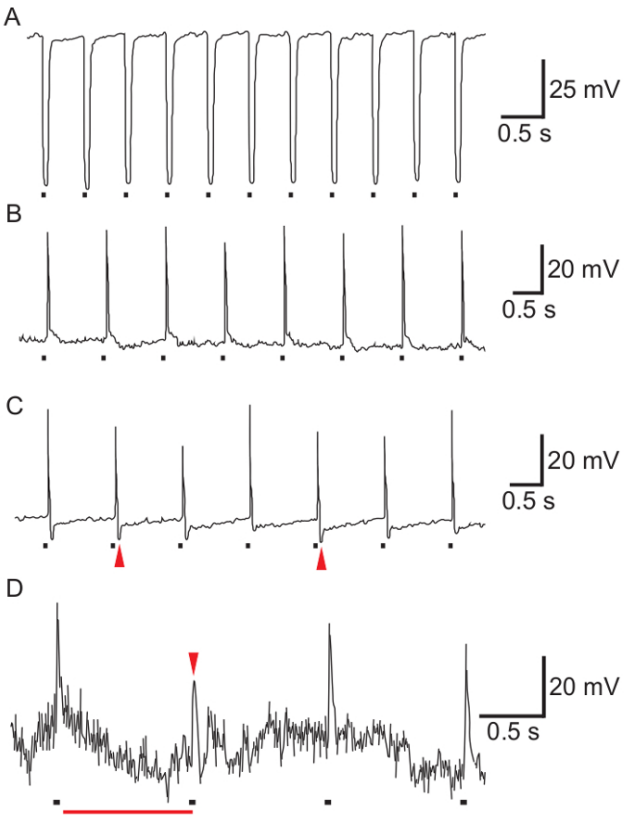

Figure 6: Raw Responses from Sample Recordings. Each response corresponds to a single light flash of 50 msec duration (black bars). (**A**) An example of the large negative voltage change that should be seen just before entering a cell. (**B**) A clean recording should have little background noise and a large depolarizing response, typically of at least 40 mV. (**C**) An example of a poor recording due to the negative potential change after the main peak (arrowheads). (**D**) Another example of a bad recording. The resting potential is undergoing large fluctuations (red bar) and the large amount of background noise can obscure the amplitude of response (arrowhead).

After completing a successful recording, the ND responses must be plotted and the Naka-Rushton equation should be fitted to the data(Naka & Rushton, 1966), shown in Figure 7. This figure is plotted using the ND filter series without any interference filters. If the recording is stable, the data from the ND filter series should be similar before and after the experiment. Spectral sensitivity is determined by fitting the Naka-Rushton equation to the VlogI plot in Figure 7, then solving for (I) for each response (V) at a given wavelength, as explained in the calculations of Section 6 of the protocol.

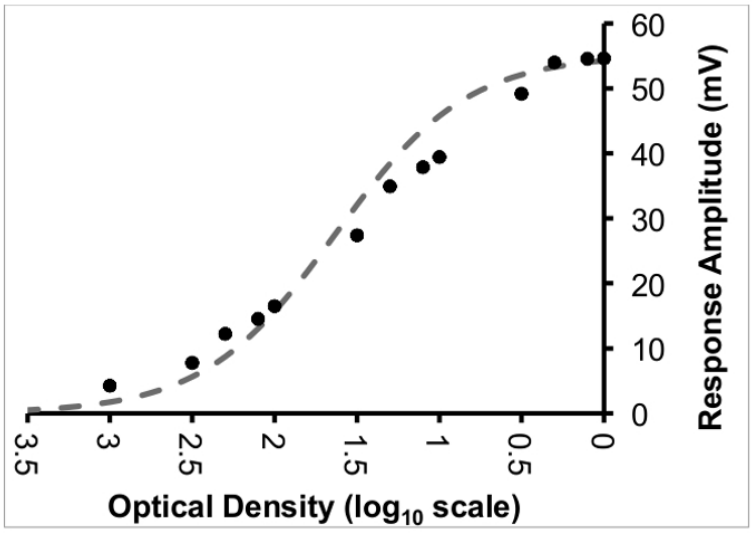

Figure 7: Response-Intensity Log-Linear Function. Solid circles show the measured responses of a cell from 3.5 to 0 OD, for this experimental setup. Light intensity is on a logarithmic scale. At very high intensities the response is saturated, and at very low intensities a small response persists instead of dropping to zero along the line. The Naka-Rushton equation[33] is fitted to this non-linear shape (dotted line).

A representative example of spectral sensitivity derived from a single recording is plotted in Figure 8a (please note this example shows real calculated data, but the peak has been shifted as this result is unpublished). Cell types may be classified by peak sensitivity at a similar wavelength and overall shape of the sensitivity spectrum. Similar cell types are then averaged and the mean sensitivity is plotted with standard error bars at each wavelength in Figure 8b. Spectral sensitivities of three typical cell types found in an insect are shown in Figure 8c (magnitude and error bars are calculated from real data, but the peaks are shifted).

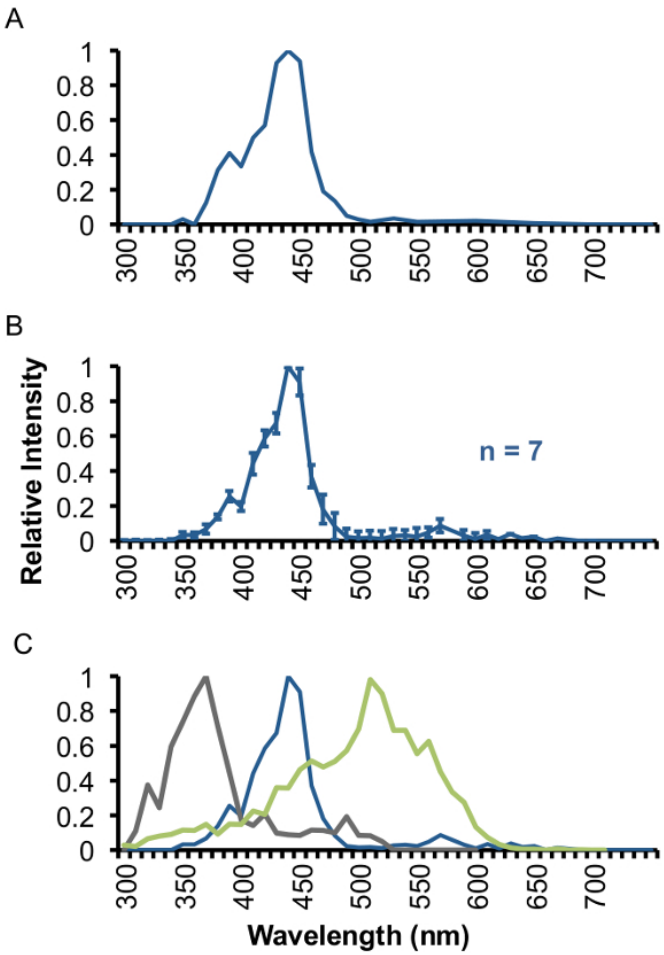

Figure 8: Spectral Sensitivity Examples. (**A**) A single representative cell's responses were recorded and relative spectral sensitivity was calculated. The peak of this cell is at 440 nm, meaning it responds best to blue light. Single cell data may look noisy (peak at 380 nm). (**B**) Cells with the same relative peak and shape are averaged together and standard error bars are added. Here, seven blue cells from seven individuals were averaged providing strong evidence that a cell type exists in this species maximally sensitive to light at 440 nm. (**C**) This process can be repeated for all cell types found, and plotted together. Insect eyes vary widely in their spectral sensitivities but a typical insect may have peaks shown here, at 370 nm, 440 nm, and 510 nm. Note, these spectral sensitivities are all calculated using real data, but the peaks have been shifted because the data is not yet published for this species.

Discussion

Intracellular recording can be a difficult technique to master due to the many technical steps involved. For successful experiments several important points must be considered. First, it is important to have a properly vibrationally-isolated table on which the experiment is performed. Many researchers use air tables, which completely separate

the tabletop from the base, giving superior vibration isolation. Our setup involves a thick marble table with a sandbox on top, into which is placed the micromanipulator/electrode holder/specimen stage apparatus. This is an effective and more affordable alternative to an air table, especially if access to in-house gas or compressed air is a limitation. Additional vibration-absorbing measures may be taken such as passive air suspension, or the addition of cushioning elements to the table legs (e.g., opened tennis balls, bike tubes, thick gel pads). Furthermore, it is essential that the experimental setup be inside a Faraday cage with everything properly grounded. The Faraday cage should have a metal screen in the front that can be removed when working inside the cage and replaced easily when recording. Even a small amount of ambient electrical noise (especially 50 Hz noise from the main AC power supply) can make an otherwise good recording unusable.

When preparing the specimen, hemolymph and pigment layers surrounding the ommatidia may prevent successful recordings. If the hole in the cornea is cut too large, normal pumping of hemolymph in the body causes the liquid surface to move up and down at the cut site, resulting in an unstable recording. Once the hole is cut, hemolymph and surface pigment layers will clot rapidly into an impenetrable scab even when sealed with Vaseline, so it is important to get the electrode into the eye as soon as possible. Ringer's solution may also be used instead of Vaseline. The ground electrode may be introduced into the mouthparts or into the stump of a cut antenna.

Additionally, it is important to keep the animal as dark-adapted as possible. For this method, steps include keeping the recording room very dark, blocking stray light from the Xenon lamp from entering the Faraday cage, short duration stimulus flashes (30-50 ms), and a low enough frequency between flashes (0.5 or greater). When a visual pigment

absorbs a photon, the chromophore in rhodopsin switches from 11-*cis*-retinal to all-*trans*-retinal, inducing the conformational change of the opsin protein, and activating the entire complex as metarhodopsin, which initiates the G protein cascade. Photo-bleaching occurs when high intensity light causes the chromophore to physically separate from the opsin protein before photoisomerization back to 11-*cis*-retinal can occur. Time is a limiting factor in this experiment because the electrode will only stably record responses from within the cell for a certain period of time before it falls out or the membrane is damaged. For this reason we do not break to allow the cell to recover, but we do use a flash duration and frequency that we have found does not degrade the cell's response over time. It is important to decrease both frequency and intensity of light if photo-bleaching occurs.

During recording, a large electrode tip or large movement by the electrode may damage the cell when penetrating the membrane. Only fine tips (at least ~100 MΩ) and small movements should be used when approaching a cell for recording. If intracellular recording is applied to other applications, such as brain recordings, extremely fine, sturdy electrodes may be pulled using quartz glass, but a specialized puller must be used for these electrodes. When first making an electrode pulling program, we checked tip resistance by backfilling the electrode, securing it to the electrode holder in a mock setup, and placing the tip and ground electrode in saline solution. Next we applied a current to measure change in voltage on the oscilloscope. To move the electrode tip we use a manual micromanipulator that moves along two axes. Other manipulators exist including digital ones that allow movement along all three axes and these may be used for this or more complex applications. There are many ways to build a stage for recording, and there are many

different types of hardware and software used in recording and analyzing the observed data. Our setup represents one simple, easy, and affordable setup of the recording rig.

In constructing the VlogI curve, functions developed by Naka and Rushton(Naka & Rushton, 1966) and others(Lipetz, 1971; Matić & Laughlin, 1981) account for the non-linear portions of the plotted responses. Various methods are used to fit this curve to the data, and we plotted the results of one such method that does not require curve-fitting software, though other methods are also suitable(Aylward, 1989; Evans, Peachey, & Marchese, 1993) (Figure 7). It may also be useful to compare spectral sensitivities to models of rhodopsin absorbance at a given peak wavelength. Several published models aim to reproduce rhodopsin absorbance spectra(Bernard, 1979; Stavenga, Smits, & Hoenders, 1993). A more precise idea of the absorbance spectrum of the visual pigment expressed in an insect photoreceptor cell may be modeled by taking into account ommatidial properties such as filtering pigments, but this requires measurement of additional physiological and anatomical parameters(Arikawa et al., 1999; Ogawa et al., 2012).

One limitation of the method is that if the study organism expresses more than one genetically similar opsin in the eye, it can be difficult to identify which opsin mRNA likely corresponds to which spectral class of photoreceptor cell. To overcome this problem, this method has been combined with dye-injections and *in situ* hybridization or immunohistochemistry to successfully identify the opsins expressed in recorded cells(Arikawa et al., 2003).

Our method is simple and accessible for researchers unfamiliar with visual electrophysiology. This technique is common in neuroscience, but specific and clear methods are absent in the literature, making this method difficult to reproduce. Although

many variations of this technique exist, we offer a straightforward way to measure spectral sensitivity in the compound eye. The physiological data is an important piece of evidence in stories of visual ecology and evolution(Briscoe & Chittka, 2001). Opsin sequence variation is linked closely with the sensitivity of a photoreceptor cell, making this method ideal for studies examining the genetic basis for phenotypic change. Measurement of photoreceptor cell sensitivities may also be paired with behavioral color discrimination assays, showing the physiological basis for important discrimination thresholds in color vision(Blackiston, Briscoe, & Weiss, 2011; Kelber, Balkenius, & Warrant, 2002; Kelber, Thunell, & Arikawa, 2001; Koshitaka, Kinoshita, Vorobyev, & Arikawa, 2008; Sison-Mangus, Briscoe, Zaccardi, Knuttel, & Kelber, 2008). In genetic or therapeutic manipulations in *Drosophila* for example, this technique can be a good way to measure proper physiological function of the eye or brain as well(Luan, Reddig, & Li, 2014; Schneuwly et al., 1989). Although ours is not the first or the most complex method of intracellular recording in the eye, our hope is that we can make this method more easily available for reproduction and integration in research programs outside of formal neuroscience.

References

Arikawa, K., Mizuno, S., Kinoshita, M., & Stavenga, D. G. (2003). Coexpression of two visual pigments in a photoreceptor causes an abnormally broad spectral sensitivity in the eye of the butterfly *Papilio xuthus*. *J Neurosci, 23*(11), 4527-4532.

Arikawa, K., Mizuno, S., Scholten, D. G., Kinoshita, M., Seki, T., Kitamoto, J., & Stavenga, D. G. (1999). An ultraviolet absorbing pigment causes a narrow-band violet receptor and a single-peaked green receptor in the eye of the butterfly *Papilio*. *Vision Res, 39*(1), 1-8.

Aylward, G. W. (1989). A simple method of fitting the Naka-Rushton equation. *Clinical Vision Sciences, 4*(3), 275-277.

Beckmann, H., Hering, L., Henze, M. J., Kelber, A., Stevenson, P. A., & Mayer, G. (2015). Spectral sensitivity in Onychophora (velvet worms) revealed by electroretinograms, phototactic behaviour and opsin gene expression. *J Exp Biol, 218*(Pt 6), 915-922. doi:10.1242/jeb.116780

Bernard, G. D. (1979). Red-absorbing visual pigment of butterflies. *Science, 203*(4385), 1125-1127. doi:10.1126/science.203.4385.1125

Blackiston, D., Briscoe, A. D., & Weiss, M. R. (2011). Color vision and learning in the monarch butterfly, *Danaus*

plexippus (Nymphalidae). *J Exp Biol, 214*(Pt 3), 509-520. doi:10.1242/jeb.048728
Briscoe, A. D., & Chittka, L. (2001). The evolution of color vision in insects. *Annu Rev Entomol, 46*, 471-510. doi:10.1146/annurev.ento.46.1.471
Cronin, T. W., Jarvilehto, M., Weckstrom, M., & Lall, A. B. (2000). Tuning of photoreceptor spectral sensitivity in fireflies (Coleoptera: Lampyridae). *J. Comp. Physiol. A, 186*(1), 1-12. doi:10.1007/s003590050001
Evans, L. S., Peachey, N. S., & Marchese, A. L. (1993). Comparison of three methods of estimating the parameters of the Naka-Rushton equation. *Documenta Ophthalmologica, 84*(1), 19-30. doi:10.1007/bf01203279
Feuda, R., Hamilton, S. C., McInerney, J. O., & Pisani, D. (2012). Metazoan opsin evolution reveals a simple route to animal vision. *Proc. Natl. Acad. Sci. U.S.A., 109*(46), 18868-18872. doi:10.1073/pnas.1304582110
Greiner, B., Cronin, T. W., Ribi, W. A., Wcislo, W. T., & Warrant, E. J. (2007). Anatomical and physiological evidence for polarisation vision in the nocturnal bee *Megalopta genalis*. *J. Comp. Physiol. A, 193*(6), 591-600. doi:10.1007/s00359-007-0214-1
Hardie, R. C., & Raghu, P. (2001). Visual transduction in *Drosophila*. *Nature, 413*(6852), 186-193. doi:10.1038/35093002
Heinze, S., & Reppert, S. M. (2011). Sun compass integration of skylight cues in migratory monarch butterflies. *Neuron, 69*(2), 345-358. doi:10.1016/j.neuron.2010.12.025
Hu, X., Leming, M. T., Whaley, M. A., & O'Tousa, J. E. (2014). Rhodopsin coexpression in UV photoreceptors of *Aedes aegypti* and *Anopheles gambiae* mosquitoes. *J Exp Biol, 217*(Pt 6), 1003-1008. doi:10.1242/jeb.096347
Katti, C., Kempler, K., Porter, M. L., Legg, A., Gonzalez, R., Garcia-Rivera, E., . . . Battelle, B. A. (2010). Opsin co-expression in *Limulus* photoreceptors: differential regulation by light and a circadian clock. *J Exp Biol, 213*(Pt 15), 2589-2601. doi:10.1242/jeb.043869
Kelber, A., Balkenius, A., & Warrant, E. J. (2002). Scotopic colour vision in nocturnal hawkmoths. *Nature, 419*(6910), 922-925. doi:10.1038/nature01065
Kelber, A., Thunell, C., & Arikawa, K. (2001). Polarisation-dependent colour vision in *Papilio* butterflies. *J Exp Biol, 204*(Pt 14), 2469-2480.
Knox, B. E., Salcedo, E., Mathiesz, K., Schaefer, J., Chou, W. H., Chadwell, L. V., . . . Barlow, R. B. (2003). Heterologous expression of *Limulus* rhodopsin. *J Biol Chem, 278*(42), 40493-40502. doi:10.1074/jbc.M304567200
Koshitaka, H., Kinoshita, M., Vorobyev, M., & Arikawa, K. (2008). Tetrachromacy in a butterfly that has eight varieties of spectral receptors. *Proc. Biol. Sci., 275*(1637), 947-954. doi:10.1098/rspb.2007.1614
Leboulle, G., Niggebrugge, C., Roessler, R., Briscoe, A. D., Menzel, R., & Hempel de Ibarra, N. (2013). Characterisation of the RNA interference response against the long-wavelength receptor of the honeybee. *Insect Biochem Mol Biol, 43*(10), 959-969. doi:10.1016/j.ibmb.2013.07.006
Lipetz, L. E. (1971). The Relation of Physiological and Psychological Aspects of Sensory Intensity. In W. R. Loewenstein (Ed.), *Principles of Receptor Physiology* (Vol. 1, pp. 191-225): Springer Berlin Heidelberg.
Luan, Z., Reddig, K., & Li, H. S. (2014). Loss of Na(+)/K(+)-ATPase in *Drosophila* photoreceptors leads to blindness and age-dependent neurodegeneration. *Exp Neurol, 261*, 791-801. doi:10.1016/j.expneurol.2014.08.025
Martinez-Harms, J., Vorobyev, M., Schorn, J., Shmida, A., Keasar, T., Homberg, U., . . . Menzel, R. (2012). Evidence of red sensitive photoreceptors in *Pygopleurus israelitus* (Glaphyridae: Coleoptera) and its implications for beetle pollination in the southeast Mediterranean. *J. Comp. Physiol. A, 198*(6), 451-463. doi:10.1007/s00359-012-0722-5
Matić, T., & Laughlin, S. B. (1981). Changes in the intensity-response function of an insect's photoreceptors due to light adaptation. *J. Comp. Physiol. A, 145*(2), 169-177. doi:10.1007/bf00605031
Naka, K. I., & Rushton, W. A. (1966). S-potentials from luminosity units in the retina of fish (Cyprinidae). *J. Physiol., 185*(3), 587-599.
Nordstrom, K., Barnett, P. D., Moyer de Miguel, I. M., Brinkworth, R. S., & O'Carroll, D. C. (2008). Sexual dimorphism in the hoverfly motion vision pathway. *Curr Biol, 18*(9), 661-667. doi:10.1016/j.cub.2008.03.061
Ogawa, Y., Awata, H., Wakakuwa, M., Kinoshita, M., Stavenga, D. G., & Arikawa, K. (2012). Coexpression of three middle wavelength-absorbing visual pigments in sexually dimorphic photoreceptors of the butterfly *Colias erate*. *J Comp Physiol A Neuroethol Sens Neural Behav Physiol, 198*(12), 857-867.

doi:10.1007/s00359-012-0756-8
Osorio, D. (1986). Directionally selective cells in the locust medulla. *J. Comp. Physiol. A, 159*(6), 841-847. doi:10.1007/bf00603737
Palczewski, K., Kumasaka, T., Hori, T., Behnke, C. A., Motoshima, H., Fox, B. A., . . . Miyano, M. (2000). Crystal structure of rhodopsin: A G protein-coupled receptor. *Science, 289*(5480), 739-745. doi:10.1126/science.289.5480.739
Plachetzki, D. C., Fong, C. R., & Oakley, T. H. (2010). The evolution of phototransduction from an ancestral cyclic nucleotide gated pathway. *Proc. Biol. Sci., 277*(1690), 1963-1969. doi:10.1098/rspb.2009.1797
Rosner, R., & Homberg, U. (2013). Widespread sensitivity to looming stimuli and small moving objects in the central complex of an insect brain. *J Neurosci, 33*(19), 8122-8133. doi:10.1523/JNEUROSCI.5390-12.2013
Rushton, W. (1972). Review Lecture. Pigments and signals in colour vision. *J. Physiol., 220*(3), 1-31.
Salcedo, E., Huber, A., Henrich, S., Chadwell, L. V., Chou, W. H., Paulsen, R., & Britt, S. G. (1999). Blue- and green-absorbing visual pigments of *Drosophila*: ectopic expression and physiological characterization of the R8 photoreceptor cell-specific Rh5 and Rh6 rhodopsins. *Journal of Neuroscience, 19*(24), 10716-10726.
Salcedo, E., Zheng, L., Phistry, M., Bagg, E. E., & Britt, S. G. (2003). Molecular basis for ultraviolet vision in invertebrates. *J Neurosci, 23*(34), 10873-10878.
Schneuwly, S., Shortridge, R. D., Larrivee, D. C., Ono, T., Ozaki, M., & Pak, W. L. (1989). *Drosophila ninaA* gene encodes an eye-specific cyclophilin (cyclosporine A binding protein). *Proc. Natl. Acad. Sci. U.S.A.*
Sison-Mangus, M. P., Bernard, G. D., Lampel, J., & Briscoe, A. D. (2006). Beauty in the eye of the beholder: the two blue opsins of lycaenid butterflies and the opsin gene-driven evolution of sexually dimorphic eyes. *J Exp Biol, 209*(Pt 16), 3079-3090. doi:10.1242/jeb.02360
Sison-Mangus, M. P., Briscoe, A. D., Zaccardi, G., Knuttel, H., & Kelber, A. (2008). The lycaenid butterfly *Polyommatus icarus* uses a duplicated blue opsin to see green. *J Exp Biol, 211*(Pt 3), 361-369. doi:10.1242/jeb.012617
Skorupski, P., & Chittka, L. (2011). Photoreceptor processing speed and input resistance changes during light adaptation correlate with spectral class in the bumblebee, *Bombus impatiens*. *PLoS One, 6*(10), e25989. doi:10.1371/journal.pone.0025989
Skorupski, P., Doring, T. F., & Chittka, L. (2007). Photoreceptor spectral sensitivity in island and mainland populations of the bumblebee, *Bombus terrestris*. *J. Comp. Physiol. A, 193*(5), 485-494. doi:10.1007/s00359-006-0206-6
Smith, W. C., Price, D. A., Greenberg, R. M., & Battelle, B. A. (1993). Opsins from the lateral eyes and ocelli of the horseshoe crab, *Limulus polyphemus*. *Proc. Natl. Acad. Sci. U.S.A., 90*(13), 6150-6154.
Stalleicken, J., Labhart, T., & Mouritsen, H. (2006). Physiological characterization of the compound eye in monarch butterflies with focus on the dorsal rim area. *J. Comp. Physiol. A, 192*(3), 321-331. doi:10.1007/s00359-005-0073-6
Stavenga, D. G., Smits, R. P., & Hoenders, B. J. (1993). Simple exponential functions describing the absorbance bands of visual pigment spectra. *Vision Res, 33*(8), 1011-1017.
Stowasser, A., & Buschbeck, E. K. (2012). Electrophysiological evidence for polarization sensitivity in the camera-type eyes of the aquatic predacious insect larva *Thermonectus marmoratus*. *J Exp Biol, 215*(Pt 20), 3577-3586. doi:10.1242/jeb.075028
Telles, F. J., Lind, O., Henze, M. J., Rodriguez-Girones, M. A., Goyret, J., & Kelber, A. (2014). Out of the blue: the spectral sensitivity of hummingbird hawkmoths. *J. Comp. Physiol. A, 200*(6), 537-546. doi:10.1007/s00359-014-0888-0
Trager, U., & Homberg, U. (2011). Polarization-sensitive descending neurons in the locust: connecting the brain to thoracic ganglia. *J Neurosci, 31*(6), 2238-2247. doi:10.1523/JNEUROSCI.3624-10.2011
Vilinsky, I., & Johnson, K. G. (2012). Electroretinograms in *Drosophila*: a robust and genetically accessible electrophysiological system for the undergraduate laboratory. *J. Undergrad. Neurosci. Educ., 11*(1), A149-157.
Yang, E.-C., & Osorio, D. (1991). Spectral sensitivities of photoreceptors and lamina monopolar cells in the dragonfly, *Hemicordulia tau*. *J. Comp. Physiol. A, 169*(6). doi:10.1007/bf00194895
Yang, E. C., Lin, H. C., & Hung, Y. S. (2004). Patterns of chromatic information processing in the lobula of the honeybee, *Apis mellifera* L. *J Insect Physiol, 50*(10), 913-925. doi:10.1016/j.jinsphys.2004.06.010

CHAPTER 2

Sexual Dimorphism in the Compound Eye of *Heliconius erato*: a Nymphalid Butterfly with at Least Five Spectral Classes of Photoreceptor

Abstract

Most butterfly families expand the number of spectrally-distinct photoreceptors in their compound eye by opsin gene duplications together with lateral filter pigments, however most nymphalid genera have limited diversity, with only three or four spectral types of photoreceptor. Here we examine the spatial pattern of opsin expression and photoreceptor spectral sensitivities in *Heliconius erato,* a nymphalid with duplicate ultraviolet opsin genes, *UVRh1* and *UVRh2*. We find that the *H. erato* compound eye is sexually dimorphic. Females express the two UV opsin proteins in separate photoreceptors, but males do not express UVRh1. Intracellular recordings confirmed that females have three short wavelength-sensitive photoreceptors (λ_{max} = 356 nm, ~390 nm and 470 nm), while males have two (λ_{max} = 390 nm and ~470 nm). We also found two long wavelength-sensitive photoreceptors (green, λ_{max} ~555 nm, and red, λ_{max} ~600 nm), which express the same LW opsin. The red cell's shifted sensitivity is probably due to perirhabdomal filtering pigments. Sexual dimorphism of the UV-absorbing rhodopsins may reflect the females' need to discriminate conspecifics from co-mimics. Red-green color vision may be used to detect differences in red coloration on *Heliconius* wings, or for host-plant identification. Among nymphalids so far investigated, only *H. erato* is known to possess five spectral

classes of photoreceptor; sexual dimorphism of the eye via suppression of one class of opsin (here UVRh1 in males) has not--to our knowledge--been reported in any animal.

Introduction

As vision incurs energetic costs (Moran, Softley, & Warrant, 2015; Niven, Anderson, & Laughlin, 2007; Niven & Laughlin, 2008), selective pressure for efficiency leads us to expect that the number of spectral receptor types, their tuning, and the way in which they are distributed across the retinal mosaic will reflect the evolutionary significance of color to an animal. Accordingly, sex differences in color vision might be expected where the sexes forage differently for food, and especially where one sex (normally females) chooses mates by their coloration. It is therefore surprising that within some taxonomic groups for which color is ecologically important, such as old-world primates, birds, and bees, there is little variation in photoreceptor spectral sensitivities between species within a given clade (Bloch, 2015; Osorio & Vorobyev, 2005), or between sexes. Aquatic taxa including teleost fish (Bowmaker & Hunt, 2006; Carleton & Kocher, 2001) and stomatopods (Cronin & Marshall, 1989; Porter, Bok, Robinson, & Cronin, 2009) do have substantial spectral diversity of photoreceptors between related species, which can often be related to the spectral variation in ambient illumination in water. Among terrestrial animals dragonflies (Futahashi et al., 2015) and butterflies (Briscoe, 2008) are known for the diversity of their photoreceptor spectral sensitivities, but the evolutionary causes and physiological significance of these differences remain unclear, and there is limited evidence for sexual dimorphism in photoreceptor spectral sensitivities (but see below).

Ancestral holometabolous insects probably had compound eyes with three spectral types of photoreceptor, each containing a unique type of opsin (Briscoe & Chittka, 2001; Henze & Oakley, 2015). The butterfly eye ground plan seems to have retained the ancestral form with three opsins, UV, B, and LW, having sensitivity maxima (λ_{max}) at about 360 nm, 470 nm, and 560 nm respectively (Briscoe, 2008; Briscoe & Chittka, 2001). Butterfly ommatidia contain nine photoreceptor cells R1-R9, whose photosensitive membranes form a fused rhabdom (Figure 1A-C); (Wernet, Perry, & Desplan, 2015). In the nomenclature used for butterflies, R1 and R2 cells are long visual fiber (LVF) photoreceptors, which lie on opposite sides of the rhabdom, and typically express either *UVRh* or *BRh* mRNAs (encoding SW opsins) (Figure 1C). R3-R8 cells are short visual fiber (SVF) photoreceptors, which express *LWRh* mRNAs (Figure 1C), and the R9 cell is a tiny LVF, which contributes a few microvilli to the proximal tip of the rhabdom (Briscoe, 2008).

Butterflies are known for the diversity in their photoreceptor spectral sensitivities (Arikawa, Inokuma, & Eguchi, 1987; Arikawa, Wakakuwa, Qiu, Kurasawa, & Stavenga, 2005; Briscoe, 2008; Ogawa et al., 2012; Sison-Mangus, Bernard, Lampel, & Briscoe, 2006). In several butterfly families, this diversity has been achieved by independent increases in the number of spectrally distinct photoreceptors in the adult compound eye, via three mechanisms. First, opsin gene duplication followed by subfunctionalization and spectral tuning produces divergent sensitivities of the resulting photoreceptor cells. Second, photostable lateral filtering pigments typically absorb short wavelengths, narrowing the shape and shifting the peak of a cell's spectral sensitivity toward longer wavelengths without any change in the endogenous opsin sequence or expression level. Finally, two opsins may be expressed together in the same cell to broaden spectral sensitivity.

The swallowtails (Papilionidae) have the greatest known number of photoreceptor spectral sensitivities among butterflies. *Papilio xuthus* uses the three processes above to produce at least eight spectrally-distinct types of photoreceptors (Arikawa, Mizuno, Kinoshita, & Stavenga, 2003; Arikawa, Mizuno, et al., 1999; Arikawa, Scholten, Kinoshita, & Stavenga, 1999; Kitamoto, Ozaki, & Arikawa, 2000; Kitamoto, Sakamoto, Ozaki, Mishina, & Arikawa, 1998; Stavenga & Arikawa, 2006). *Papilio glaucus* has eight visual opsins, six of which result from LW opsin duplications (Briscoe, 2000; Cong, Borek, Otwinowski, & Grishin, 2015), while another papilionid, the birdwing *Troides aeaca* has nine spectral classes of photoreceptor (Chen, Arikawa, & Yang, 2013). Duplicated LW opsin genes are found in several species including a representative from the basal lineage of the family, *Parnassius glacialis*, suggesting the LW opsin duplication may have been present in the ancestral papilionid (Matsushita, Awata, Wakakuwa, Takemura, & Arikawa, 2012).

In other butterfly families, similar mechanisms have resulted in expansions of photoreceptor classes. At least one species in the Riodinidae has duplicated a LW opsin (Frentiu, Bernard, Sison-Mangus, Brower, & Briscoe, 2007). B opsin gene duplications have resulted in spectrally distinct receptors in the range 435 nm – 500 nm in the family Lycaenidae (Sison-Mangus et al., 2006; Sison-Mangus, Briscoe, Zaccardi, Knuttel, & Kelber, 2008) and independently in Pieridae. In addition, both *Pieris* and *Colias* (Pieridae) have complex patterns of lateral filtering pigments, which in *Colias erate*, results in nine spectral classes of photoreceptor, including multiple red-sensitive cells (Arikawa et al., 2005; Awata, Wakakuwa, & Arikawa, 2009; Ogawa et al., 2012; Ogawa, Kinoshita, Stavenga, & Arikawa, 2013; Qiu & Arikawa, 2003; Qiu, Vanhoutte, Stavenga, & Arikawa, 2002).

In contrast to other investigated butterfly families, the photoreceptor spectral sensitivities in the largest butterfly family, Nymphalidae, have not diverged from the ancestral holometablous insect form (Briscoe, Bernard, Szeto, Nagy, & White, 2003; Sauman et al., 2005; Stalleicken, Labhart, & Mouritsen, 2006). Nymphalids with three known spectral types of photoreceptor include iconic and cosmopolitan species such as the monarch, *Danaus plexippus,* and the painted lady, *Vanessa cardui*. The satyrine butterfly *Hermeuptychia hermes,* is an exception with a single *LWRh* duplication (Frentiu et al., 2007). Although perirhabdomal filtering pigments are common to many insects, including butterflies (Stavenga, 2002a, 2002b), they seem to be absent from some nymphalid eyes, thus eliminating one way to generate additional photoreceptor spectral sensitivities (Briscoe & Bernard, 2005; Frentiu et al., 2007). The narrower spectral variability in this speciose and colorful group of butterflies highlights the general problem of relating color vision to visual ecology (Osorio & Vorobyev, 2008), where the underlying ecological and evolutionary processes responsible for the observed patterns of visual traits are difficult to identify.

In this context the genus *Heliconius* is of particular interest owing to the presence of two evolutionary innovations (synapomorphies), namely a duplicated UV opsin gene that evolved under positive selection (Briscoe et al. 2010), and the use of the UV-yellow-reflecting molecule, 3-hydroxykynurenine (3-OHK), for wing pigmentation (Briscoe et al., 2010; Keith S. Brown, 1967; Bybee et al., 2012). Color space modeling predicts that the presence of two UV receptors would be beneficial for discriminating *Heliconius* 3-OHK wing pigmentation from co-mimics belonging to other genera that use a different non-UV reflecting wing pigment (Bybee et al., 2012). Thus, the novel wing pigment and enhanced

UV color vision may be important in the success of *Heliconius*, allowing the genus to benefit from defensive mimicry without losing the ability to recognize conspecifics and select mates by their color (Bates, 1862; K. S. Brown, Sheppard, & Turner, 1974; *Heliconius* Genome Consortium, 2012; Hines et al., 2011; Merrill et al., 2015)

If *Heliconius* use 3-OHK UV-yellows as a private channel of communication to identify conspecifics while maintaining mimicry in the eyes of predators (Bybee et al., 2012), we would expect that *Heliconius* do indeed have two types of UV receptors with different spectral sensitivities. In attempt to answer this question using *in situ* hybridization, a previous experiment found that *H. erato UVRh1* and *UVRh2* transcripts co-localized to the same R1 and R2 photoreceptor cells (Zaccardi, Kelber, Sison-Mangus, & Briscoe, 2006b). We could not, however, rule out the possibility of cross-hybridization of the riboprobes due to the high nucleotide sequence similarity between the duplicated genes. We next attempted to estimate UVRh1 and UVRh2 visual pigment (opsin + chromophore) absorbance by epi-microspectrophotometric densitometry on *H. erato in vivo*, which yields peak absorbances through reflectance measurements of a group of (~20) ommatidia (Briscoe et al., 2010). This method identified separate peak absorbances at 355 nm and 398 nm, as expected for an eye with two functional UV opsins, but strong evidence linking specific UV opsins to specific photoreceptors with divergent sensitivities was still missing.

Due to their significance for understanding the co-evolution of color vision and communication signals, we aimed to characterize the photoreceptor subtypes and ommatidial classes in *H. erato* compound eyes. We predicted that the duplicate UV opsins are expressed in distinct R1 and R2 photoreceptor subtypes with different spectral

sensitivities, consistent with sub- and neo-functionalization after gene duplication. Among nymphalids, *H. erato* is notable for the ability to discriminate color in the red range (Zaccardi et al. 2006b), and as only one LW opsin gene is found in gDNA (Hsu, 2001) or cDNA synthesized from head tissue (Zaccardi, Kelber, Sison-Mangus, & Briscoe, 2006a), we predicted a red-sensitive photoreceptor cell is present in the eye of *H. erato,* probably due to filter pigments.

This study uses immunohistochemistry to determine the pattern of opsin expression in photoreceptor cells and intracellular recordings to measure photoreceptor spectral sensitivities. We confirm that the UV opsins are expressed in separate R1 and R2 photoreceptor subtypes, and we provide evidence for the presence of a red-sensitive photoreceptor. Unexpectedly, *H. erato's* compound eye is sexually dimorphic, with the male lacking UVRh1 expression. This is the first instance, to our knowledge, of a nymphalid using both an opsin duplication and filtering pigments to increase the number of spectral receptor types, and the first case of a sexually-dimorphic eye in the family Nymphalidae.

Materials and Methods

Animals

We obtained *H. erato petiverana* pupae from The Butterfly Farm - Costa Rica Entomological Supply. After eclosion, butterflies were housed for at least a day in a humidified chamber, and were fed a diluted honey solution daily before recording. Animals were sacrificed by rapidly severing the head and crushing the thorax.

Cryosectioning and Immunohistochemistry

Freshly severed butterfly heads were cut in two to separate the eyes, and immediately fixed in 4% paraformaldehyde (Electron Microscopy Sciences, Hatfield, PA, USA) in 0.1 M phosphate buffered saline (PBS) for 30 minutes at room temperature. Eyes were then sucrose-protected in successive concentrations of 10%, 20%, and 30% sucrose in PBS, either for one hour at room temperature or overnight at 4°C. Excess cuticle around each eye was cut away before it was placed on a bed of Tissue Tek O.C.T. compound (VWR, Radnor, PA, USA) and frozen at -20°C. Frozen eyes were sectioned at 14 μm thickness on a Microm HM 500 OM microtome cryostat (Fisher Scientific, Pittsburgh, PA, USA), and placed on slides to dry overnight at room temperature.

An antibody against the peptide DGLDSVDLAVIPEH in the N-terminal domain of *Heliconius erato* UVRh1 was generated in guinea pigs and immunoaffinity purified (Open Biosystems, Inc., Huntsville, AL, USA). An anti-blue opsin antibody was generated in rats against the *H. erato* peptide RYRAELQKRLPWMGVREAD, and also immunoaffinity purified (Life Technologies, Grand Island, NY, USA). The rabbit anti-pan-UV antibody was generated against a *Papilio glaucus* peptide CISHPKYRQELQKRMP (Lampel, Briscoe, & Wasserthal, 2005), which has a sequence similar to *H. erato* UVRh1 and UVRh2. In *H. erato*, this antibody strongly labels R1 and R2 cells that do not stain for anti-UVRh1 or anti-blue antibodies. The long-wavelength opsin antibody was generated in rabbits against the *Limenitis astyanax* sequence KYRAALYARFPALACAPEPQD (Quality Controlled Biochemicals, Hopkinton, MA, USA). After labeling, dry slides were placed in 100% ice-cold acetone for 5 minutes, then washed 3 x 10 minutes in 0.1 M PBS. Slides were then placed in 0.5% sodium dodecyl sulfate in 0.1 M PBS for 5 minutes. Each slide was blocked for one hour at room temperature using 8% (v/v) normal donkey serum and normal goat serum,

and 0.3% Triton X-100 in 0.1 M PBS. Slides were incubated with 2:75 rabbit anti-pan-UV, 1:15 rat anti-blue antibody (pooled from two animals), and 1:15 guinea pig anti-UVRh1 antibody or 1:15 rabbit anti-LWRh antibody in blocking solution overnight at 4°C. Slides were washed 3 x 10 minutes in 0.1 M PBS and then incubated with 1:1000 goat anti-rat Alexafluor 488 and 1:500 donkey anti-rabbit Cy3 or Alexafluor 555, and 1:250 goat-anti-guinea pig Alexafluor 633 (Life Technologies, Grand Island, NY, USA) in blocking solution for two hours at room temperature. Slides were washed again 3 x 10 minutes in 0.1 M PBS. Slides were stored for imaging by coverslipping with Aqua Poly/Mount (Polysciences, Inc. Warrington, PA, USA). Slides were viewed using a Zeiss Axioskop 2 under a 20x lens. Images were taken using a Zeiss Axiocam HRc and associated Axiovision software. For some images, a Leica confocal SP700 microscope was used in the UC Irvine Optical Core Facility. Stains were pseudocolored, and contrast and brightness were adjusted for clarity using Adobe Photoshop CS4 and Fiji (Schindelin et al., 2012).

Cell and Ommatidial Counts

Ommatidia were counted when images contained more than 100 ommatidia, the tissue was not sheared or folded, and cell bodies were clearly labeled without a high level of background. Images were viewed at full resolution in Adobe Illustrator and whenever possible, ommatidia were individually marked according to their R1/R2 cell staining. Background autofluorescence was retained, to reveal any unstained ommatidia. Ommatidia were not counted if the staining was unclear or the sectioned tissue was of poor quality (e.g. folded). Total ommatidia were counted over as much area as possible for a single high quality section per individual and the percentages of each class of ommatidia were

calculated due to differences in the area of different sections or partial sections. From these ommatidial classes we derived the total number of individual R1 and R2 photoreceptor subtypes in each section. The numbers of photoreceptors in each subtype were also converted to percentages. Ommatidial and photoreceptor counts of all animals were pooled by class and sex, converted to proportions, and each proportion was compared between the sexes using a two tailed Z-test. The data were tested for normality using a Shapiro-Wilk test, and a nonparametric Mann-Whitney-Wilcoxon test was performed to test for sex differences when the null hypothesis of normality was rejected.

Intracellular Recording

Before beginning an experiment the sex was determined. For *in vivo* recordings, an individual was affixed inside a small plastic tube using hot wax. The abdomen was held down with a dry piece of wax and the tube was humidified by placing a wet tissue inside. The entire tube was mounted on a stage and an indifferent silver electrode of 0.125 mm diameter inserted into the head via the mouthparts. A small hole (~10-20 ommatidia in diameter) was cut in the left cornea using a thin razorblade chip and sealed with Vaseline to prevent desiccation.

The recording setup and procedure are described in detail elsewhere (McCulloch, Osorio, & Briscoe, 2016). Briefly, we used an Oriel Xenon Arc lamp (Irvine, CA, USA) as a light source, aiming the light through a condenser lens assembly (Newport, Irvine, CA, USA, Model 60006), a convex silica lens (Newport, SPX055), a neutral density (ND) filter wheel (from 0 to 3.5 optical density), 10 nm bandwith spectral interference filters (Edmund Optics, Barrington, NJ, USA) a concave silica lens (Newport SPC034), a shutter with drive

unit (Uniblitz, Rochester NY, USA, 100-2B), a collimating beam probe (Newport 77644), and finally into an attached UV transmitting 600 μm diameter fiber optic cable (Oriel 78367), all held by an optical rail. Photoreceptors were recorded intracellularly with borosilicate capillary electrodes filled with 3M KCL (~100 MΩ resistance).

Once the recording was stable, i.e. little to no change in resting potential, low background noise, and consistently large depolarizing responses (at least 10:1 signal to noise ratio, at least ~50 mV response amplitude), recording began. Responses were recorded to narrow-band spectral flashes of 50 ms, presented at 0.5 s time-intervals and covering the spectrum from 300 nm to 700 nm in steps of 10 nm. Intensity response curves were recorded from 3.5 to 0 optical density before and after an experiment when possible. During an experiment, the ND filter wheel was left in place at an optical density that elicited a strong response from the peak interference filter wavelength but one that did not approach the maximum response with white light. intensities adjusted as appropriate using quartz neutral density filters (McCulloch et al., 2016). When possible, wavelengths near the peak spectral response were recorded more than once.

After a recording, the spectral sensitivity of each cell was derived from the recorded spectral responses. The amplitudes of responses to white light at each ND filter step were used to create a response-log Intensity (VlogI) curve. The VlogI data was used to estimate parameters for the Naka-Rushton equation: $V/V_{max} = I^n / (I^n + K^n)$, where V is the amplitude of a given response; V_{max} is the maximum response amplitude; I is the intensity of the stimulus for the given response, V; K is the intensity of the stimulus that elicits ½ of V_{max}; n is the exponential slope of the function (Figure 7) (Aylward, 1989; Naka & Rushton, 1966). Due to differences in total photon flux for each interference filter, correction factors were

calculated to approximate constant photon flux over all filters from 300 to 700 nm, and multiplied by raw intensities. Corrected intensities were divided by the maximum for each cell to calculate relative spectral sensitivity. Photoreceptors were classified by peak sensitivity and shape of the spectral sensitivity curve. Averages were taken of the same spectral class of photoreceptor for each sex, and standard error (SE) bars were applied. Each cell recording came from a different individual. To estimate peak sensitivities, we used least-squares regression to fit rhodopsin templates to our data (Stavenga, 2010).

Eyeshine and Tapetal Reflectances

Eyeshine images were taken with a 4x objective on a Zeiss Axioskop2 plus microscope using white light epi-illumination. Live butterflies were affixed to a glass slide on their side using wax, and positioned so that the ommatidia directly faced the objective, and then were allowed to dark adapt for a few minutes. To rule out the possibility of heterogeneous tapetal reflectances, we removed the photoreceptor layer from 4% paraformaldehyde-fixed eyes and visualized the tapeta under 10x magnification on a Zeiss Axioskop2.

Results

We labeled UVRh1, UVRh2, BRh, and LWRh by immunohistochemistry, and observed the distribution of labeling across the main retina (excluding the dorsal rim area) of *H. erato* (Figure 1). All R3-R8 cells express LWRh (Figure 1D,E). Each R1 and R2 photoreceptor expresses only one opsin: either UVRh1, UVRh2, or BRh, confirming and extending previous *in situ* hybridizations that could not distinguish between the two *UVRh*

opsin mRNAs (Zaccardi et al., 2006a). We identified ommatidial classes by their staining for UVRh1, UVRh2, and BRh (Figure 1F,G), and examined the sexes separately (see below). Additionally, because previous experiments and our own data show that BRh is expressed in the R1 and R2 cells that do not express UV opsin, we included double UV stains in our dataset, treating an unstained cell in either the R1 or R2 position as a blue cell. We pooled data from ommatidial classes if the same opsins were expressed in either the R1 or the R2 cells. Thus an ommatidium with BRh in R1 and UVRh in R2 would be the same as one with UVRh in R1 and BRh in R2.

Comparing sexes we found that females (n=6) express both UVRh1 and UVRh2, while males (n=8) express only UVRh2 (Figure 1F,G) in the main retina. Male ommatidia have all three possible combinations of R1-R2 cells given the loss of UVRh1 (B-UV2, UV2-UV2, and B-B), while females have three of their six possible combinations (B-UV1, UV2-UV2, or B-B). Females lack the male B-UV2 ommatidial class. There were no exceptions to these expression patterns in 24 individuals visualized under the microscope, and from 4784 ommatidia counted in high quality sections from 14 individuals. Differences in eye morphology and function along the dorso-ventral axis of the eye are common in insects (e.g., the ventral stripe in the cricket retina; (Henze, Dannenhauer, Kohler, Labhart, & Gesemann, 2012)) so we also stained longitudinal sections of the eye (n=6), but did not find any signs of regionalization (Figure 2).

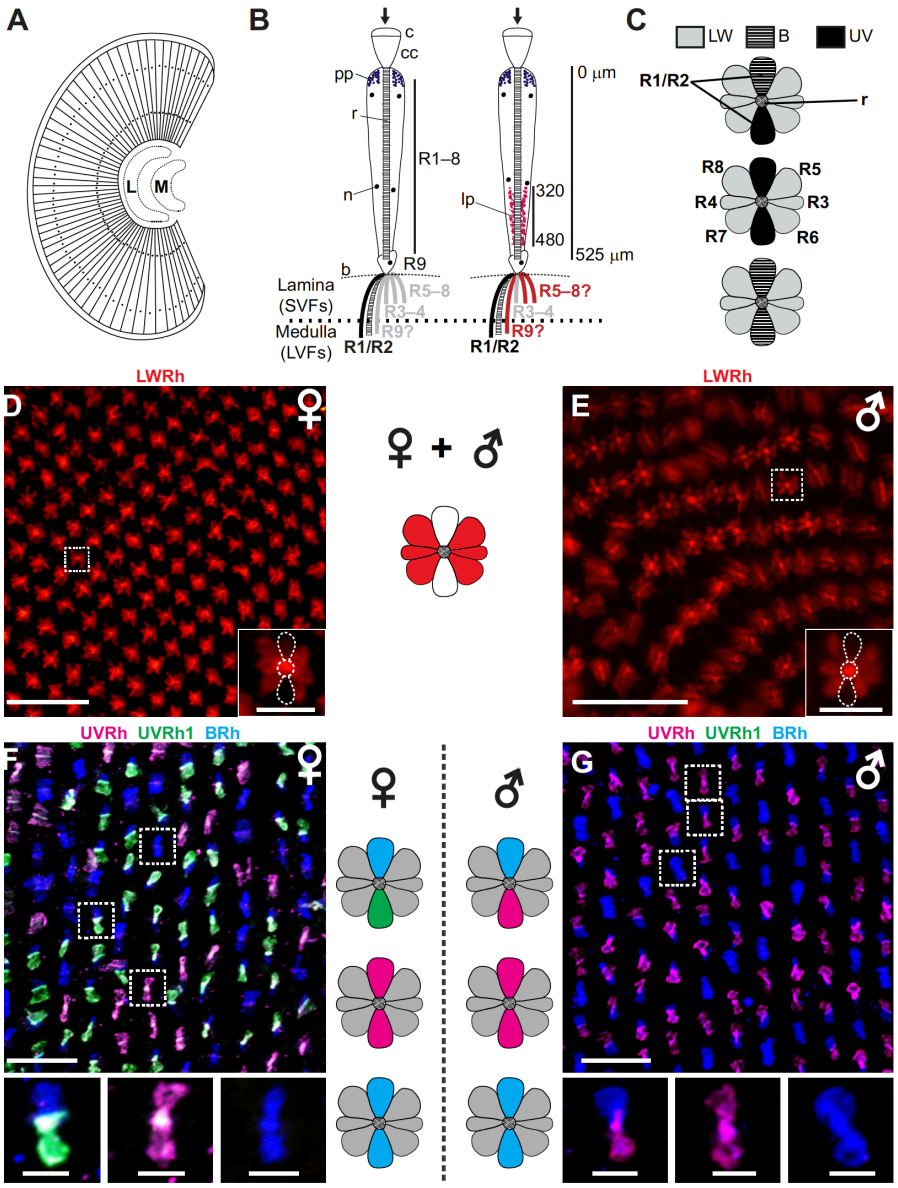

Figure 1. Butterfly compound eye anatomy and *Heliconius erato* eye sections stained for opsins (N=24). (A) Schematic diagram of a longitudinal section of ommatidia and optic lobe immediately proximal to the retina. L, lamina; M, medulla. (B) Longitudinal view of two H. erato ommatidia. The arrow indicates the direction of light entering the eye. Numbers indicate the length of the rhabdom from the most distal (0 µm)tothe most proximal point (525 µm). Perirhabdomal filtering pigment extends from about 320 to 480 µm. c, cornea; cc, crystalline cone; pp, pupillary pigment; r, rhabdom; n, cell nucleus; R1–9, photoreceptor cells; b, basement membrane through which axons from cells R1–R9 pass to reach the lamina and medulla; SVFs, short visual fibers; LVFs, long visual fibers; lp, lateral filtering pigment. (C) Transverse sections of individual ommatidia, showing R1–R8 cells. In butterflies, R1/R2 cells express SW opsins, either BRh or UVRh.R3–R8 cells (and possibly R9 cells) express LWRh. (D,E) Ommatidia stained with anti-LW opsin are shown in red. Scale bar: 50 µm. Inset shows a single ommatidium at higher magnification, where six cells, R3–R8, are immunolabeled. Dotted lines indicate R1 and R2 cells, which are not labeled. Scale bar: 10 µm. (F,G) Triple stains of pan-UVRh (magenta), UVRh1 (green) and BRh (blue) opsins. Males (N=8) and females (N=6) are sexually dimorphic, with males lacking UVRh1 expression. Cartoon ommatidia show differences in classes of ommatidia found in males and females. Scale bar: 50 µm. The boxed areas correspond to individual classes of ommatidia found in males and females, shown under higher magnification below. Scale bar: 10 µm.

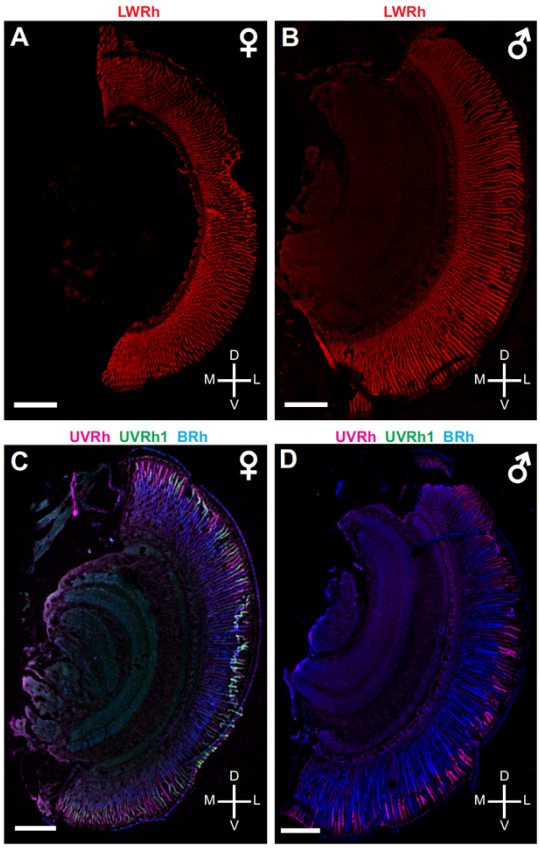

Figure 2. Longitudinal sections of the adult compound eye stained for opsins in both males (N=3) and females (N=3). (A,B) LW opsin (red) is present throughout the dorso-ventral axis of the eye in both males and females.(C,D) Triple stains show no obvious regionalization with respect to SW opsins, with UVRh1 (green), UVRh2 (magenta) and BRh (blue) cells found across the dorsal and ventral compound eye. Sexual dimorphism is evident, with the male eye lacking UVRh1 expression. Crosses show orientation along the dorsal (D)–ventral (V) axis and the lateral (L)–medial (M) axis. Scale bars: 250 μm.

To further characterize photoreceptor cell and ommatidial classes, we counted 299-730 ommatidia in the six females and 181-428 ommatidia in the eight males for which we had high quality tissue. Within the same sex, variation in the percentages of both cell and ommatidial classes is low (see boxplots in Figure 3, Table 1). Approximately half the ommatidia (46.9-55.2 %) in females are UV1-B ommatidia, and the other half are split into similar proportions of UV2-UV2 (20.3-27.5 %) and B-B ommatidia (20.7-27.5 %). Based on ommatidial counts, female R1 and R2 cells express roughly half blue cells (48.3-53.6 %) and half UV cells (46.3-51.7 %), split between either UV1 (23.5-27.6 %) or UV2 (20.4-27.5 %) opsin. Males, rather than mirroring female expression, have a much higher proportion

Table 1. Ommatidial counts in adult compound eyes of male and female *Heliconius erato*.

		Total ommatidial counts (N)							Percentage					
Specimen	Sex	UV2/UV2	UV2/B	B/B	UV1/UV1	UV1/UV2	UV1/B	Total	UV2/UV2	UV2/B	B/B	UV1/UV1	UV1/UV2	UV1/B
1	F	175	0	185	0	0	370	730	23.97	0	25.34	0	0	50.68
2	F	98	0	124	0	0	258	480	20.41	0	25.83	0	0	53.75
3	F	72	0	62	0	0	165	299	24.08	0	20.73	0	0	55.18
4	F	83	0	75	0	0	179	337	24.62	0	22.25	0	0	53.11
5	F	42	0	57	0	0	108	207	20.28	0	27.53	0	0	52.17
6	F	103	0	96	0	0	176	375	27.46	0	25.6	0	0	46.93
7	M	77	136	142	0	0	0	355	21.69	38.3	40	0	0	0
8	M	25	71	94	0	0	0	190	13.15	37.36	49.47	0	0	0
9	M	82	158	188	0	0	0	428	19.15	36.91	43.92	0	0	0
10	M	33	68	80	0	0	0	181	18.23	37.56	44.19	0	0	0
11	M	59	104	122	0	0	0	285	20.7	36.49	42.8	0	0	0
12	M	19	91	85	0	0	0	195	9.74	46.66	43.58	0	0	0
13	M	67	145	90	0	0	0	302	22.18	48.01	29.8	0	0	0
14	M	71	184	165	0	0	0	420	16.9	43.8	39.28	0	0	0

Total numbers of ommatidia were counted for each sample, excluding unclear staining or poor tissue quality. Mean percentages for each sex were calculated and used in Fig. 3. Total cell counts used in Fig. 3 were derived from ommatidial counts. F, female; M, male.

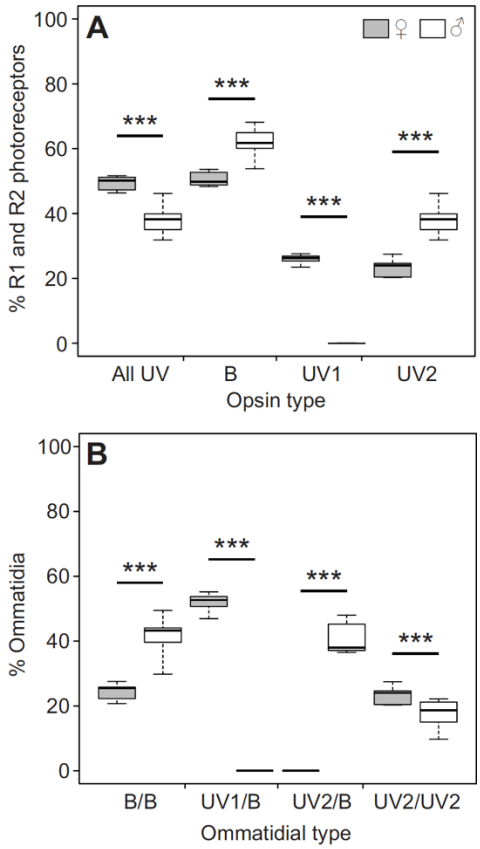

Figure 3. Boxplots of female and male photoreceptor and ommatidial classes. (A) Percentage of R1 and R2 photoreceptors in the compound eye of males (N=8) and females (N=6) expressing a particular opsin. Males lack any UVRh1 expression. 'All UV' indicates the sum of the percentage of UV1 and UV2 cells. (B) Percentage of each ommatidial class in the compound eye based on specific R1 and R2 opsin expression. Female eyes do not have UV2/B ommatidia, while male eyes do not have UV1/B ommatidia. A Z-test was performed to compare pooled male and female proportions for each photoreceptor and ommatidial class. For the Z-test, the number of photoreceptors sampled was 4712 for males and 4856 for females, and the number of ommatidia sampled was 2356 for males and 2428 for females. ***P<0.001 between the two groups.

of B-B ommatidia than UV2-UV2 ommatidia. Male R1 and R2 cells comprise between 53.8 66.9 % blue photoreceptors and 33.1-46.2 % UV2 photoreceptors. In males 29.8-49.5 % of ommatidia are B-B, 13.2-22.2 % are UV2-UV2, and 36.5-48.0 % are UV2-B ommatidia. The proportions for the same ommatidial type differ significantly between males and females (Z-test, $p < 0.001$ for all cases), as do the relative abundances for the different cell types (Z-test, $p < 0.01$ for all cases). Using a Shapiro-Wilk test, the null hypothesis of normality could not be rejected for all cell and ommatidial counts ($p > 0.05$) except for the male UV2/B ommatidial type ($p = 0.029$). Females do not express this ommatidial subtype, so we were still confident that the difference in expression was real. A nonparametric

Mann-Whitney-Wilcoxon test was performed, which showed that the sex difference in the number of the UV2/B ommatidial type was significant ($p = 0.00159$). Ommatidia are expressed spatially in a stochastic manner, but the proportion of each type of ommatidium is consistent within each sex, as in other insects (Wernet et al., 2015).

Intracellular recordings of *H. erato* photoreceptor cells between 300 and 700 nm are reported from 42 cells. As expected from opsin expression, we found that females have two UV and one blue spectral receptor type, with λ_{max} at 356 ± 1.5 nm (n = 3) (SE after fitting a rhodopsin template to our data, see Methods), 389 ± 1.6 nm (n = 3), and 470 ± 2.0 nm (n = 7), respectively (Figure 4A). Males have one UV and one blue receptor type with λ_{max} at 390 ± 1.2 nm (n = 4) and 469 ± 1.8 nm (n = 4) (Figure 4B). Based on sexually dimorphic opsin labeling together with sexually dimorphic intracellular recordings, we infer that the UVRh1 is present in the female-specific 356 nm-sensitive photoreceptors, while the UVRh2 is found in the ~390 nm-sensitive photoreceptors found in both sexes. Both sexes have

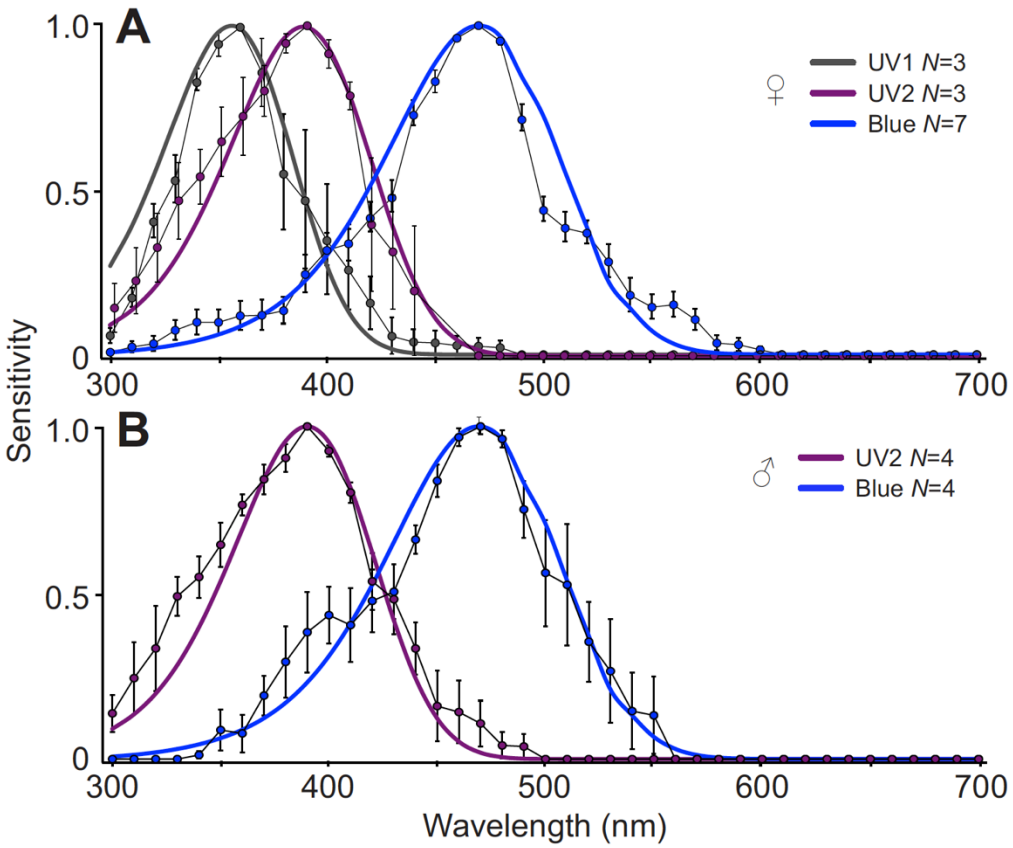

Figure 4. Short-wavelength (SW) photoreceptor cell spectral sensitivities in *H. erato*. Data are means±s.e.m. for (A) females and (B) males. Sensitivity was normalized to 1. Females have a UVRh1 photoreceptor cell with λmax=356± 1.5 nm, which males do not possess. UVRh2 cells in females have λmax=389± 1.6 nm and in males λmax=390±1.2 nm, while BRh cells in females have λmax=470±2.0 nm and in males λmax=469±1.8 nm.

typical butterfly LW receptors with λ_{max} = 555 ± 1.0 nm for females (n = 12) and λ_{max} = 556 ± 2.2 nm for males (n = 7). We also found single examples of red sensitive cells in each sex, with λ_{max} ~ 600 nm (Figure 5). The spectral sensitivity of the red receptor is narrowed in a manner that is consistent with tuning by a red filter pigment associated with LW opsin expression. Qualitatively, the spectral curve dips at the peak wavelengths of the green-sensitive photoreceptor, from ~540 nm to 570 nm, and then rises to a sharp, narrow-band peak sensitivity at ~600 nm (Figure 5). Red pigment that may be responsible for heterogeneous eyeshine reflectance *in vivo* (Figure 6), and that could produce such an effect on sensitivity, is visible in plastic sectioned eyes of *H. erato* (Zaccardi et al., 2006a).

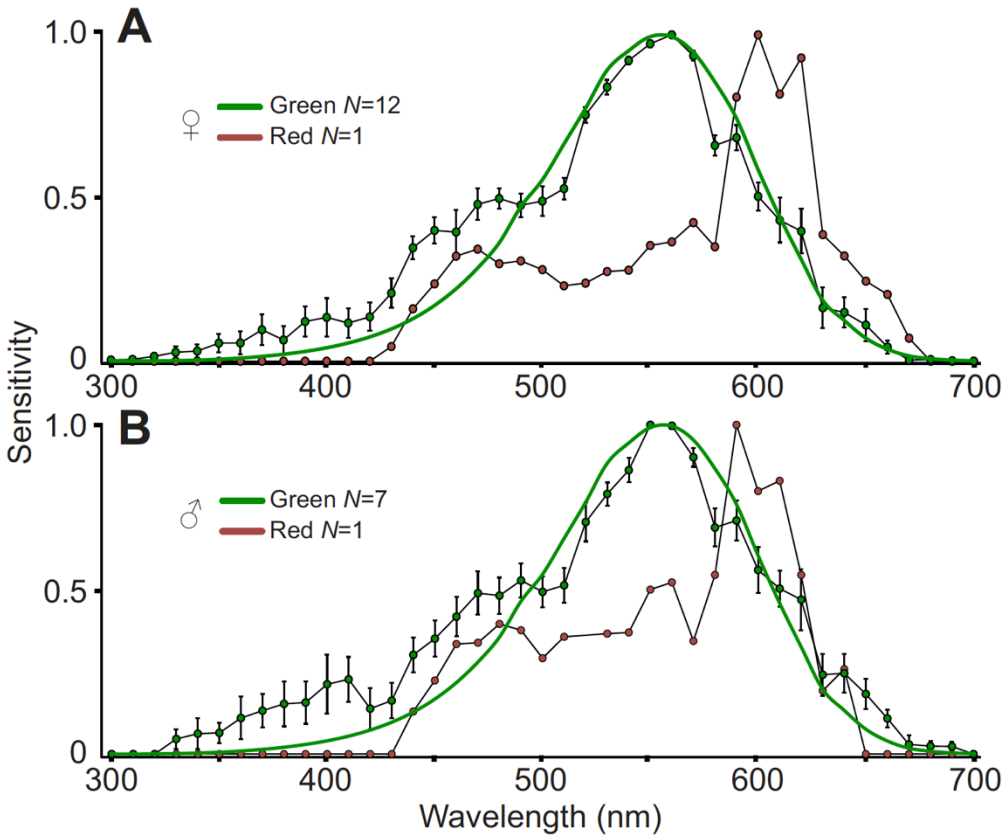

Figure 5. Long-wavelength (LW) photoreceptor cell spectral sensitivities in *H. erato*. Data are means±s.e.m. for (A) females and (B) males. Sensitivity was normalized to 1. Both sexes possess green- and red-sensitive spectral types of photoreceptor cell. Green-sensitive photoreceptor cells have λmax=555± 1.0 nm in females and λmax=556±2.2 nm in males. The red-sensitive photoreceptors have a depression in their sensitivity from 540 to 570 nm in both females and males, then show a narrow peak with λmax≈600 nm.

Discussion

Heliconius erato ommatidia resemble those of other insects, with the long visual fiber (LVF) receptors R1 and R2, containing SW opsins, while the short visual fibers R3-8, contain a single opsin, LWRh (Hadjieconomou, Timofeev, & Salecker, 2011; Wernet & Desplan, 2004; Wernet et al., 2015). *H. erato* compound eyes have at least five spectral types of photoreceptor and are sexually dimorphic, despite monomorphic wing patterns. We confirm the existence of R1 and R2 cells with sensitivity maxima (λ_{max}) ~355 nm, 390nm and 470 nm, based on UVRh1, UVRh2, and BRh expression, respectively, however

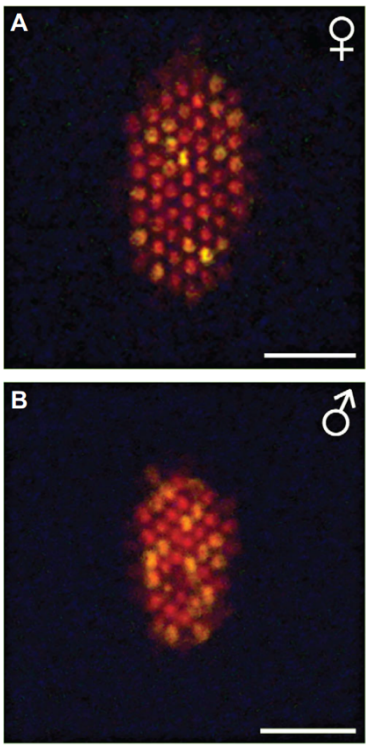

Figure 6. *Heliconius erato* eyeshine reflectance *in vivo.* (A) Female. (B) Male. Red and yellow ommatidia are inferred to be the result of heterogeneity of filtering pigments in the compound eye. Scale bars: 50 μm.

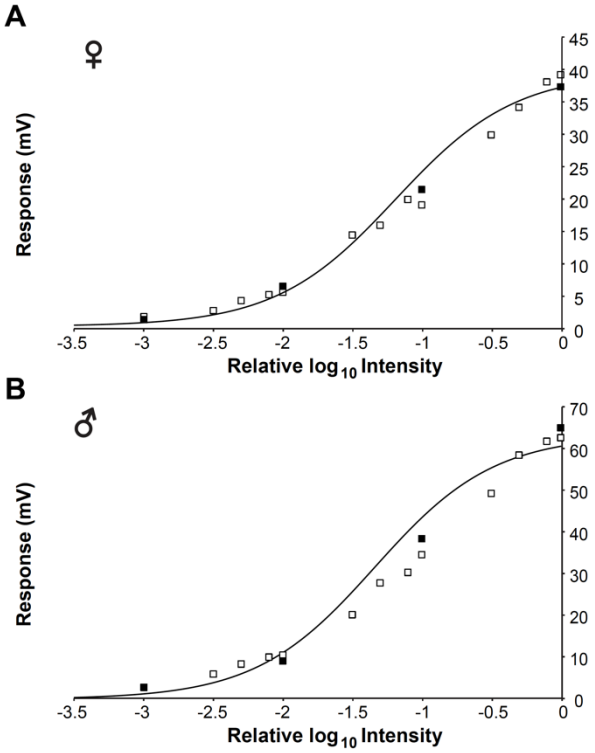

Fig. 7. Response log-intensity (Vlog-I) curves for two red-sensitive cells. The female (A) and male (B) red cells' responses are plotted before (white squares) and after (black squares) an experiment was performed, showing no significant change over time in either cell's response to varying intensities of white light. The Naka-Rushton model is fitted to the data for both cells (black line).

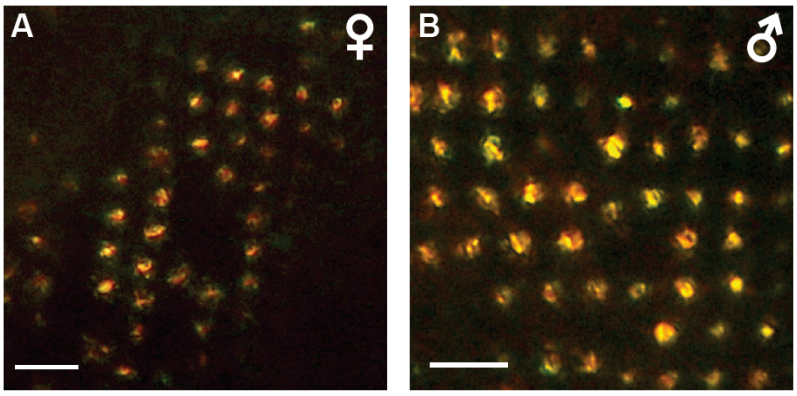

Fig. 8. Images of *H. erato* tapetal reflectance. from females (A) and males (B). Retinal tissue was lightly fixed in 4% paraformaldehyde. Tapeta were exposed by plucking away the photoreceptor cell layer, and epi-brightfield light was used to illuminate the exposed tapeta. Dark spots are due to incomplete removal of photoreceptor cell debris. Female and male tapeta were very uniform in reflectance compared to the red and yellow ommatidial eyeshine difference observed in Figure 6, suggesting the eyeshine differences are due to filtering pigment expression differences and not differences in tapetal reflectance.

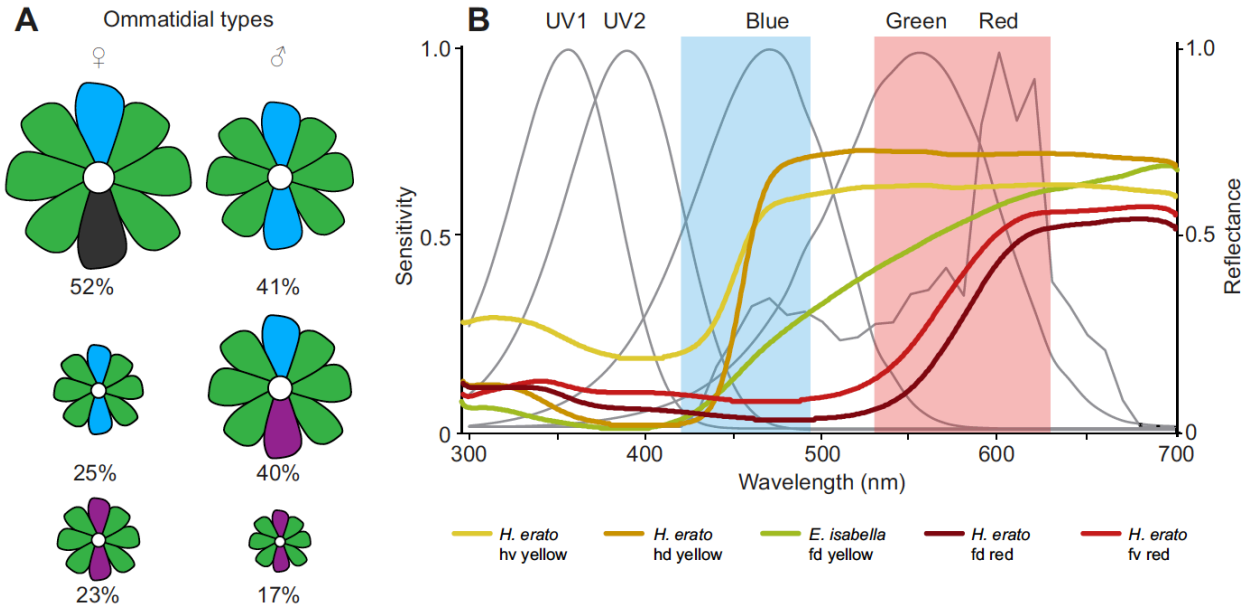

Fig. 9. Summary of *H. erato* retinal mosaic, photoreceptor physiology and wing reflectance spectra. (A) Ommatidial classes found in the sexually dimorphic eyes of H. erato. The size of the ommatidium is proportional to the average abundance of that class found in the eye of either females or males. Both differential regulation of opsin expression levels and the abundance of these ommatidial classes may be playing a role in color vision. (B) The five known spectral classes of photoreceptor in female *H. erato* overlayed with yellow and red wing reflectance spectra from *H. erato*, compared with the yellow wing reflectance spectrum of a *Heliconius* co-mimic, *Eueides isabella*. The blue shaded area indicates the overlap of the yellow reflectance spectra with the idealized sensitivity peak of the blue receptor, while the pink shaded area indicates the overlap of red wing reflectance spectra with the idealized sensitivities of the green and red receptors. Brightness differences between yellow wing colors may be detected by the *H. erato* blue receptor. Wing reflectance spectra data are from Briscoe et al. (2010) and Bybee et al. (2012). d, dorsal; v, ventral; f, forewing h, hindwing.

males lack UVRh1. Despite expression of only one long wavelength opsin, both sexes have green- ($_{max}$ ~555 nm) and red-sensitive photoreceptors (600 nm), with the longer wavelength peak attributable to the presence of lateral filtering.

UV photoreceptors and sexual dimorphism

Sexual size dimorphism is well documented in insect compound eyes (Lau, Ohba, Arikawa, & Meyer-Rochow, 2007; Victor Benno Meyer-Rochow & Lau, 2008; V. B. Meyer-Rochow & Reid, 1994), especially in Diptera, where males in several groups have larger eyes than females, probably due to the need for males to find females (Straw, Warrant, &

O'Carroll, 2006; C. Wehrhahn, 1979). In the butterfly *Bicyclus anynana*, the relative eye sizes of males and females are sexually dimorphic and differ according to the time of year together with opsin expression levels (Everett, Tong, Briscoe, & Monteiro, 2012; Macias-Munoz, Smith, Monteiro, & Briscoe, 2015). These differences can be interpreted as reflecting selection for optimal eye size, which is dependent on the behavioral requirements of the different sexes. In several dipteran species, males aerially chase and catch females for mating and the male-specific "love spot," is specifically adapted to this task (Land & Collett, 1974; Christian Wehrhahn, Poggio, & Bülthoff, 1982). In ommatidia found in the male love spot only, facet lenses are larger and an atypical R7 cell is present. Unlike other R7 cells in either sex, these love spot R7 cells resemble the outer R1-R6 cells; they express the same visual pigment and project their axons to the same region in the optic lobe as the R1-R6 cells (Franceschini, Hardie, Ribi, & Kirschfeld, 1981). Neuronal circuitry in the optic lobe is also sexually dimorphic, maximizing the male's spatial resolution and motion detection for tracking females while sacrificing color vision (Hornstein, O'Carroll, Anderson, & Laughlin, 2000). In honeybees (Hymenoptera), the male drone similarly has a dorsal acute zone with larger facet diameter and unique opsin expression for tracking females aerially, while the male ventral eye and the female worker bee eye are similar in opsin expression and morphology (Menzel, Wunderer, & Stavenga, 1991; Velarde, Sauer, Walden, Fahrbach, & Robertson, 2005). Most known examples of sex differences in opsin expression are from flies, bees, and butterflies (see below), where both sexes express the same opsins, and only the domain of expression (or filtering) changes.

There are few examples of sex differences in photoreceptor spectral sensitivities, and by implication color vision. Among vertebrates, in most New-World primate species, a

proportion of females can be trichromats, whereas all males are dichromats (Mollon, Bowmaker, & Jacobs, 1984). Males and females of the beetle *Rhagophthalmus ohbai* have different ERG response peaks, but opsin expression in the eyes is unknown (Lau et al., 2007). Several butterflies have sexually dimorphic spectral sensitivities due to lateral filtering pigments, which may be related to wing pattern dichromatism. For instance in the butterfly *Pieris rapae crucivora* (Pieridae), photoreceptors that express violet-absorbing visual pigments are tuned in males by filtering pigments to a narrow blue sensitivity to detect sexually dichroic wings displayed by females (Arikawa et al., 2005; Obara, 1970). In the European subspecies *P. r. rapae* wing colors are monomorphic (Obara & Majerus, 2000; Stavenga, Stowe, Siebke, Zeil, & Arikawa, 2004), and photoreceptor sensitivities lack this sex-specific filtering (D. Stavenga, unpublished observation); (Arikawa et al., 2005). Similarly, sexually dimorphic expression of filtering pigments in the clouded yellow butterfly, *Colias erate* (Pieridae), leads to differences in ommatidial classes (Ogawa et al., 2013). In the small copper butterfly, *Lycaena rubidus* (Lycaenidae), sexual dimorphism in the eye again coincides with wing dichromatism, and is based on differences in the spatial pattern of blue opsin expressing cells, as well as opsin co-expression in a subset of photoreceptors (Bernard & Remington, 1991; Sison-Mangus et al., 2006).

Thus despite the widespread occurrence of sexual dimorphism in insect compound eyes, *H. erato* is unusual among insects so far investigated in that the males lack protein expression of one of the visual opsins (UVRh1). Sexually dimorphic expression of opsin mRNA levels has been found in insects like the fig wasp, *Ceratosolen solmsi,* but protein spatial expression and spectral sensitivity data are missing (Wang et al., 2013). Furthermore, other known examples of sexually dimorphic eyes in butterflies are

accompanied by sexually dimorphic wings. *H. erato* wing patterns are sexually monomorphic. Other butterflies modify sex-specific color receptor differences with filtering pigments, however in *H. erato* filtering pigments do not contribute to sexual dimorphism. Lastly, we provide the first quantitative evidence in a butterfly that the relative abundance of shared photoreceptor and ommatidial classes are different between the sexes.

Given the new findings of this study, it is worthwhile to reconsider the hypothesis of Briscoe et al. (2010) who proposed that when the genus *Heliconius* arose, both sexes used both UV photoreceptors to facilitate detection of a UV-yellow wing signal that arose at the same time**.** However we find *H. erato* males lack one of the photoreceptors that should have given them an advantage in identifying conspecific females via UV color discrimination. This unexpected result raises the question of how selection may be acting on the visual systems of male and female *H. erato*. It may be less costly for males to mistake female co-mimics of another species because their investment in reproduction is small and they mate multiple times in their lifetime. Thus males may have lost the circuitry required for UV discrimination because it is metabolically costly and/or because of trade-offs with other uses of color vision. Females may benefit in discriminating the correct male colors, due to a much larger investment in egg production and the ability to mate with only a few males.

Sexual dimorphism exists in *H. erato* among blue photoreceptors as well, where males have 20% more BRh-expressing R1 and R2 photoreceptor cells compared to females (Figs. 3, 9A). This small but non-trivial sex difference might reflect differences in the costs and benefits for the chromatic and perhaps achromatic signals that can be derived from the different types of compound eye. The reflectance spectrum of the *H. erato* 3-OHK yellow

wing pigment has a step-like function peaking at about 470-480 nm, in the same range as the peak sensitivity of the blue photoreceptor (blue highlight, Figure 9B). Males and females might use the blue-sensitive cell to detect differences between *Heliconius* and non-*Heliconius* yellows (yellow vs. green spectra, Figure 9B) via either a chromatic or an achromatic channel. Males that lack UV discrimination could potentially benefit from more blue cells in the compound eyes than females.

Red receptors

Although the ancestral pterygote eye had only three opsin-based receptors: UV, B, and LW, red-sensitivity is widespread in insect compound eyes. Species in Odonata (Meinertzhagen, Menzel, & Kahle, 1983), Hymenoptera (Peitsch et al., 1992), and Lepidoptera have receptors with $\lambda_{max} > 570$ nm (Briscoe & Chittka, 2001). Earlier physiological studies (Bernhard, Boëthius, Gemne, & Struwe, 1970) and behavioural tests (Zaccardi et al., 2006a) have provided evidence for *Heliconius* red receptors, but to our knowledge these are the first intracellular recordings of red receptors in the retina of *H. erato*, and possibly any other nymphalid butterfly. Swihart (Swihart, 1972) predicted *H. erato* photoreceptors with peaks at 440 nm, 490 nm, and 600 nm based on single unit recordings from visual interneurons in the protocerebrum. Although the 440 nm estimate has not been replicated in subsequent experiments (Figs. 4,5, (Briscoe et al., 2010)), the 490 nm and 600 nm estimates match ours. Only one other nymphalid, *Polygonia c-album* ($\lambda_{max} = 580$ nm), has been found with a sensitivity $\lambda_{max} > 570$ nm, from electroretinograms (ERGs) (Eguchi, Watanabe, Hariyama, & Yamamoto, 1982).

For photoreceptors expressing non-A2 pigments including those found in insects, sensitivity maxima exceeding 580 nm are nearly always achieved by filters associated with an rhodopsin of λ_{max} <580 nm; the exception being the riodinid *Apodemia mormo,* which has a rhodopsin with λ_{max}=600 nm (Frentiu et al., 2007). Thus pierid and papilionid butterfly red receptors rely on photostable filters (Arikawa, Scholten, et al., 1999; Ogawa et al., 2013; Qiu & Arikawa, 2003). Consistent with this pattern our recordings of red receptors from a male and female *H. erato* indicate a peak sensitivity of 600 nm, which is significantly narrowed when compared to the predicted rhodopsin absorbance spectrum at a peak of 600 nm. *H. erato* ommatidia have red and yellow eyeshine, and it is theoretically possible that the red-shifted sensitivity is partly due to tuning of the tapetum, but tapetal reflectance is in fact uniform (Figure 8). Thus it is more likely that red eyeshine is due to the heterogeneous distribution of the red filter pigment between ommatidia. *H. erato* has a candidate photostable filter (possibly an ommine) that together with filtering by overlaying green cells, absorbs light at about 550 nm, near the peak sensitivity of the green cell (Langer & Struwe, 1972), which could explain the depression between 540 nm and 570 nm in the red cells' spectral sensitivities.

We did not label the red-sensitive cell, therefore we do not know which of the R3-9 cells correspond to the red-sensitive cells. However the rarity of our recordings (2 of 42) might not be reflective of a rarity of cells, as the abundance of dark red ommatidia in eyeshine reflectance suggests this cell type might be common (Figure 6). In plastic sections the red pigment was found adjacent to the rhabdom starting at approximately 320 μm below the cornea and extending to 480 μm (Zaccardi et al., 2006a). The location of the pigment suggests that if the *H. erato* retina is tiered or partially tiered, the red-sensitive

cells might be the more proximal R5-R9 cells. However in the absence of transmission electron microscopy data we cannot rule out the possibility that some R3/R4 cells might also be red-sensitive (Figure 1B). Heterogeneity of ommatidial classes as well as the location of the cell bodies in the proximal retina may make recording from these photoreceptors difficult. Although we did not examine R9 cells of *H. erato* specifically, previous *in situ* hybridization experiments of individual ommatidia in the compound eyes of *Papilio glaucus* (Briscoe, 2008) and *Vanessa cardui* (Briscoe et al., 2003), indicate butterfly R9 cells express *LWRh* mRNAs.

H. erato uses color vision to discriminate between wavelengths from 590-640 nm (Zaccardi et al. 2006b). We show here that the *H. erato* retina has two spectrally distinct LW receptors (Figure 5) forming the physiological basis of red-green color discrimination using only one LW opsin. Color vision has been demonstrated in *Papilio,* where tetrachromatic vision involves three typical insect receptors (UV, B, LW) plus an additional red receptor (Almut Kelber & Pfaff, 1999; Koshitaka, Kinoshita, Vorobyev, & Arikawa, 2008). Other studies further demonstrated that pierids and papilionids with red receptors use color discrimination to choose green leaves for oviposition (A. Kelber, 1999; Kolb & Scherer, 1982), as opposed to insects that lack a red receptor and use a monochromatic signal to choose yellow leaves for oviposition (Prokopy & Owens, 1983). Lythgoe proposed that using photoreceptors with λ_{max} above 580 nm would be suited to discriminating leaf colors, whose spectra tend to vary more in the red range from the reflectance maximum of chlorophyll (> 555 nm) (Lythgoe, 1979). Discriminating green leaves among many different plants would probably be difficult without chemosensory cues, but using the red receptor

for color discrimination may allow females to oviposit on leaves of an individual plant that are most suitable for offspring growth - typically younger leaves (A. Kelber, 1999).

As social and sexual signals, red wing colors of hetero- or conspecifics may be better discriminated by *Heliconius* using both green- and red-sensitive photoreceptors. Crane (Crane, 1955) showed behaviorally that the red colored band on the *H. erato* forewing is important for courtship and approach in both sexes. In *H. melpomene,* the gene responsible for the red color pattern is genetically linked to the preference for that same pattern (Merrill, Van Schooten, Scott, & Jiggins, 2011). It has been previously proposed that overlap in color receptor sensitivities should match steep slopes in the spectra of salient signals to better discriminate more color differences between similar signals (Chittka & Menzel, 1992). It is likely that *H. erato* are using the green and red receptors for color vision in the context of mate choice because the reflectance spectra of the red color patches on wings correspond to a region that quickly rises from low to very high in this range (~550-590) of the spectrum (Figure 9B) (Briscoe et al., 2010).

Here we show spectrally distinct UV photoreceptors due to a UV opsin duplication in the compound eye of *Heliconius erato.* We identify a new mechanism of sexual dimorphism among butterflies: namely, complete repression of expression of one UV opsin in males, together with a concomitant increase in the abundance of blue photoreceptors. Lastly, we physiologically characterize both green and red receptors that are likely to be responsible for color vision in the red range due to filtering of a LW rhodopsin. An open question remains as to how these sexual dimorphisms affect color and motion vision, and whether the 'unit of discrimination' is at the ommatidial level, the sum of all individual

photoreceptors found in the eye regardless of ommatidium structure, or some combination in between. The evolutionary and ecological consequences of this sexual dimorphism for *H. erato* behavior and life history have yet to be elucidated. We are only now able to frame these new questions in this long-studied system because of the novel work we present here.

References

Arikawa, K., Inokuma, K., & Eguchi, E. (1987). Pentachromatic visual system in a butterfly. *Naturwissenschaften, 74*(6), 297-298. doi:Doi 10.1007/Bf00366422

Arikawa, K., Mizuno, S., Kinoshita, M., & Stavenga, D. G. (2003). Coexpression of two visual pigments in a photoreceptor causes an abnormally broad spectral sensitivity in the eye of the butterfly *Papilio xuthus*. *J Neurosci, 23*(11), 4527-4532.

Arikawa, K., Mizuno, S., Scholten, D. G., Kinoshita, M., Seki, T., Kitamoto, J., & Stavenga, D. G. (1999). An ultraviolet absorbing pigment causes a narrow-band violet receptor and a single-peaked green receptor in the eye of the butterfly *Papilio*. *Vision Res, 39*(1), 1-8.

Arikawa, K., Scholten, D. G. W., Kinoshita, M., & Stavenga, D. G. (1999). Tuning of photoreceptor spectral sensitivities by red and yellow pigments in the butterfly *Papilio xuthus*. *Zoological Science, 16*(1), 17-24. doi:10.2108/zsj.16.17

Arikawa, K., Wakakuwa, M., Qiu, X., Kurasawa, M., & Stavenga, D. G. (2005). Sexual dimorphism of short-wavelength photoreceptors in the small white butterfly, *Pieris rapae crucivora*. *J Neurosci, 25*(25), 5935-5942. doi:10.1523/JNEUROSCI.1364-05.2005

Awata, H., Wakakuwa, M., & Arikawa, K. (2009). Evolution of color vision in pierid butterflies: blue opsin duplication, ommatidial heterogeneity and eye regionalization in *Colias erate*. *J Comp Physiol A, 195*(4), 401-408. doi:10.1007/s00359-009-0418-7

Aylward, G. W. (1989). A simple method of fitting the Naka-Rushton equation. *Clin. Vision Sci., 4*(3), 275-277.

Bates, H. W. (1862). Contributions to an insect fauna of the Amazon valley (Lepidoptera, Heliconidae). *Biological Journal of the Linnean Society, 16*(1), 41-54. doi:Doi 10.1111/J.1095-8312.1981.Tb01842.X

Bernard, G. D., & Remington, C. L. (1991). Color vision in *Lycaena* butterflies: spectral tuning of receptor arrays in relation to behavioral ecology. *Proceedings of the National Academy of Sciences, USA, 88*(7), 2783-2787.

Bernhard, C. G., Boëthius, J., Gemne, G., & Struwe, G. (1970). Eye ultrastructure, colour reception and behaviour. *Nature, 226*(5248), 865-866. doi:10.1038/226865a0

Bloch, N. I. (2015). Evolution of opsin expression in birds driven by sexual selection and habitat. *Proc R Soc Lond B Biol Sci, 282*(1798), 2014-2321. doi:10.1098/rspb.2014.2321

Bowmaker, J. K., & Hunt, D. M. (2006). Evolution of vertebrate visual pigments. *Current Biology, 16*(13), 484-489. doi:10.1016/j.cub.2006.06.016

Briscoe, A. D. (2000). Six opsins from the butterfly *Papilio glaucus*: molecular phylogenetic evidence for paralogous origins of red-sensitive visual pigments in insects. *J Mol Evol, 51*(2), 110-121.

Briscoe, A. D. (2008). Reconstructing the ancestral butterfly eye: focus on the opsins. *J Exp Biol, 211*(Pt 11), 1805-1813. doi:10.1242/jeb.013045

Briscoe, A. D., & Bernard, G. D. (2005). Eyeshine and spectral tuning of long wavelength-sensitive rhodopsins: no evidence for red-sensitive photoreceptors among five Nymphalini butterfly species. *J Exp Biol, 208*(Pt 4), 687-696. doi:10.1242/jeb.01453

Briscoe, A. D., Bernard, G. D., Szeto, A. S., Nagy, L. M., & White, R. H. (2003). Not all butterfly eyes are created equal: rhodopsin absorption spectra, molecular identification, and localization of ultraviolet-, blue-,

and green-sensitive rhodopsin-encoding mRNAs in the retina of *Vanessa cardui*. *J Comp Neurol, 458*(4), 334-349. doi:10.1002/cne.10582

Briscoe, A. D., Bybee, S. M., Bernard, G. D., Yuan, F., Sison-Mangus, M. P., Reed, R. D., . . . Chiao, C. C. (2010). Positive selection of a duplicated UV-sensitive visual pigment coincides with wing pigment evolution in *Heliconius* butterflies. *Proceedings of the National Academy of Sciences, USA, 107*(8), 3628-3633. doi:10.1073/pnas.0910085107

Briscoe, A. D., & Chittka, L. (2001). The evolution of color vision in insects. *Annu Rev Entomol, 46*, 471-510. doi:10.1146/annurev.ento.46.1.471

Brown, K. S. (1967). Chemotaxonomy and chemomimicry: the case of hydroxykynurenine. *Systematic Biology, 16*(3), 213-216.

Brown, K. S., Sheppard, P. M., & Turner, J. R. G. (1974). Quaternary refugia in tropical America: evidence from race formation in *Heliconius* butterflies. *Proc R Soc Lond B Biol Sci, 187*(1088), 369-378. doi:10.1098/rspb.1974.0082

Bybee, S. M., Yuan, F., Ramstetter, M. D., Llorente-Bousquets, J., Reed, R. D., Osorio, D., & Briscoe, A. D. (2012). UV photoreceptors and UV-yellow wing pigments in *Heliconius* butterflies allow a color signal to serve both mimicry and intraspecific communication. *Am Nat, 179*(1), 38-51. doi:10.1086/663192

Carleton, K. L., & Kocher, T. D. (2001). Cone opsin genes of african cichlid fishes: tuning spectral sensitivity by differential gene expression. *Molecular Biology and Evolution, 18*(8), 1540-1550.

Chen, P. J., Arikawa, K., & Yang, E. C. (2013). Diversity of the photoreceptors and spectral opponency in the compound eye of the Golden Birdwing, *Troides aeacus formosanus*. *PLoS One, 8*(4), e62240. doi:10.1371/journal.pone.0062240

Chittka, L., & Menzel, R. (1992). The evolutionary adaptation of flower colours and the insect pollinators' colour vision. *J Comp Physiol A, 171*(2), 171-181. doi:10.1007/bf00188925

Cong, Q., Borek, D., Otwinowski, Z., & Grishin, N. V. (2015). Tiger swallowtail genome reveals mechanisms for speciation and caterpillar chemical defense. *Cell Rep, 10*, 910-919. doi:10.1016/j.celrep.2015.01.026

Crane, J. (1955). Imaginal behavior of a Trinidad butterfly, *Heliconius erto hydara* Hewitson, with special reference to the social use of color. *Zoologica NY, 40*(16), 167-196.

Cronin, T. W., & Marshall, N. J. (1989). A retina with at least ten spectral types of photoreceptors in a mantis shrimp. *Nature, 339*(6220), 137-140. doi:10.1038/339137a0

Eguchi, E., Watanabe, K., Hariyama, T., & Yamamoto, K. (1982). A comparison of electrophysiologically determined spectral responses in 35 species of Lepidoptera. *Journal of Insect Physiology, 28*(8), 675-682. doi:10.1016/0022-1910(82)90145-7

Everett, A., Tong, X., Briscoe, A. D., & Monteiro, A. (2012). Phenotypic plasticity in opsin expression in a butterfly compound eye complements sex role reversal. *BMC Evolutionary Biology, 12*, 232. doi:10.1186/1471-2148-12-232

Franceschini, N., Hardie, R., Ribi, W., & Kirschfeld, K. (1981). Sexual dimorphism in a photoreceptor. *Nature, 291*(5812), 241-244. doi:10.1038/291241a0

Frentiu, F. D., Bernard, G. D., Sison-Mangus, M. P., Brower, A. V., & Briscoe, A. D. (2007). Gene duplication is an evolutionary mechanism for expanding spectral diversity in the long-wavelength photopigments of butterflies. *Mol Biol Evol, 24*(9), 2016-2028. doi:10.1093/molbev/msm132

Futahashi, R., Kawahara-Miki, R., Kinoshita, M., Yoshitake, K., Yajima, S., Arikawa, K., & Fukatsu, T. (2015). Extraordinary diversity of visual opsin genes in dragonflies. *Proceedings of the National Academy of Sciences, USA, 112*(11), 1247-1256. doi:10.1073/pnas.1424670112

Hadjieconomou, D., Timofeev, K., & Salecker, I. (2011). A step-by-step guide to visual circuit assembly in *Drosophila*. *Curr Opin Neurobiol, 21*(1), 76-84. doi:10.1016/j.conb.2010.07.012

Heliconius Genome Consortium, T. (2012). Butterfly genome reveals promiscuous exchange of mimicry adaptations among species. *Nature, 487*(7405), 94-98. doi:10.1038/nature11041

Henze, M. J., Dannenhauer, K., Kohler, M., Labhart, T., & Gesemann, M. (2012). Opsin evolution and expression in arthropod compound eyes and ocelli: insights from the cricket *Gryllus bimaculatus*. *BMC Evolutionary Biology, 12*, 163. doi:10.1186/1471-2148-12-163

Henze, M. J., & Oakley, T. H. (2015). The Dynamic Evolutionary History of Pancrustacean Eyes and Opsins. *Integr Comp Biol, 55*(5), 830-842. doi:10.1093/icb/icv100

Hines, H. M., Counterman, B. A., Papa, R., Albuquerque de Moura, P., Cardoso, M. Z., Linares, M., . . . McMillan, W. O. (2011). Wing patterning gene redefines the mimetic history of *Heliconius* butterflies. *Proceedings of the National Academy of Sciences, USA, 108*(49), 19666-19671.

doi:10.1073/pnas.1110096108
Hornstein, E. P., O'Carroll, D. C., Anderson, J. C., & Laughlin, S. B. (2000). Sexual dimorphism matches photoreceptor performance to behavioural requirements. *Proc R Soc Lond B Biol Sci, 267*(1457), 2111-2117. doi:10.1098/rspb.2000.1257
Hsu, R. (2001). Molecular evolution of a long wavelength-sensitive opsin in mimetic *Heliconius* butterflies (Lepidoptera: Nymphalidae). *Biological Journal of the Linnean Society, 72*(3), 435-449. doi:10.1006/bijl.2000.0511
Kelber, A. (1999). Ovipositing butterflies use a red receptor to see green. *Journal of Experimental Biology, 202*, 2619-2630.
Kelber, A., & Pfaff, M. (1999). True colour vision in the orchard butterfly, *Papilio aegeus*. *Naturwissenschaften, 86*(5), 221-224. doi:10.1007/s001140050601
Kitamoto, J., Ozaki, K., & Arikawa, K. (2000). Ultraviolet and violet receptors express identical mRNA encoding an ultraviolet-absorbing opsin: identification and histological localization of two mRNAs encoding short-wavelength-absorbing opsins in the retina of the butterfly *Papilio xuthus*. *J Exp Biol, 203*(Pt 19), 2887-2894.
Kitamoto, J., Sakamoto, K., Ozaki, K., Mishina, Y., & Arikawa, K. (1998). Two visual pigments in a single photoreceptor cell: identification and histological localization of three mRNAs encoding visual pigment opsins in the retina of the butterfly *Papilio xuthus*. *J Exp Biol, 201*(Pt 9), 1255-1261.
Kolb, G., & Scherer, C. (1982). Experiments on wavelength specific behavior of *Pieris brassicae* L. during drumming and egg-laying. *J Comp Physiol A, 149*(3), 325-332. doi:10.1007/bf00619148
Koshitaka, H., Kinoshita, M., Vorobyev, M., & Arikawa, K. (2008). Tetrachromacy in a butterfly that has eight varieties of spectral receptors. *Proc. Biol. Sci., 275*(1637), 947-954. doi:10.1098/rspb.2007.1614
Lampel, J., Briscoe, A. D., & Wasserthal, L. T. (2005). Expression of UV-, blue-, long-wavelength-sensitive opsins and melatonin in extraretinal photoreceptors of the optic lobes of hawk moths. *Cell Tissue Res, 321*(3), 443-458. doi:10.1007/s00441-004-1069-1
Land, M. F., & Collett, T. S. (1974). Chasing behaviour of houseflies (*Fannia canicularis*). *j comp physiol, 89*(4), 331-357. doi:10.1007/bf00695351
Langer, H., & Struwe, G. (1972). Spectral absorption by screening pigment granules in the compound eye of butterflies (*Heliconius*). *j comp physiol, 79*(2), 203-212. doi:10.1007/bf00697773
Lau, T. F. S., Ohba, N., Arikawa, K., & Meyer-Rochow, V. B. (2007). Sexual dimorphism in the compound eye of *Rhagophthalmus ohbai* (Coleoptera: Rhagophthalmidae): II. Physiology and function of the eye of the male. *Journal of Asia-Pacific Entomology, 10*(1), 27-31. doi:10.1016/s1226-8615(08)60327-1
Lythgoe, J. N. (1979). *Ecology of vision*: Clarendon Press; Oxford University Press.
Macias-Munoz, A., Smith, G., Monteiro, A., & Briscoe, A. D. (2015). Transcriptome-wide differential gene expression in *Bicyclus anynana* butterflies: female vision-related genes are more plastic. *Molecular Biology and Evolution*. doi:10.1093/molbev/msv197
Matsushita, A., Awata, H., Wakakuwa, M., Takemura, S. Y., & Arikawa, K. (2012). Rhabdom evolution in butterflies: insights from the uniquely tiered and heterogeneous ommatidia of the Glacial Apollo butterfly, *Parnassius glacialis*. *Proc R Soc Lond B Biol Sci, 279*(1742), 3482-3490. doi:10.1098/rspb.2012.0475
McCulloch, K. J., Osorio, D., & Briscoe, A. D. (2016). Determination of photoreceptor cell spectral sensitivity in an insect model from *in vivo* intracellular recordings. *JoVE, 108*(108), e53829. doi:10.3791/53829
Meinertzhagen, I. A., Menzel, R., & Kahle, G. (1983). The identification of spectral receptor types in the retina and lamina of the dragonfly *Sympetrum rubicundulum*. *J Comp Physiol A, 151*(3), 295-310. doi:10.1007/bf00623906
Menzel, J. G., Wunderer, H., & Stavenga, D. G. (1991). Functional morphology of the divided compound eye of the honeybee drone (*Apis mellifera*). *Tissue and Cell, 23*(4), 525-535. doi:10.1016/0040-8166(91)90010-q
Merrill, R. M., Dasmahapatra, K. K., Davey, J. W., Dell'Aglio, D. D., Hanly, J. J., Huber, B., . . . Yu, Q. (2015). The diversification of *Heliconius* butterflies: what have we learned in 150 years? *J Evol Biol, 28*(8), 1417-1438. doi:10.1111/jeb.12672
Merrill, R. M., Van Schooten, B., Scott, J. A., & Jiggins, C. D. (2011). Pervasive genetic associations between traits causing reproductive isolation in *Heliconius* butterflies. *Proc R Soc Lond B Biol Sci, 278*(1705), 511-518. doi:10.1098/rspb.2010.1493
Meyer-Rochow, V. B., & Lau, T. F. (2008). Sexual dimorphism in the compound eye of the moth *Operophtera*

brumata (Lepidoptera, Geometridae). *Invertebrate Biology, 127*(2), 201-216. doi:10.1111/j.1744-7410.2008.00131.x

Meyer-Rochow, V. B., & Reid, W. A. (1994). Male and female eyes of the Antarctic midge *Belgica antarctica* (Diptera, Chironomidae) - a scanning electron-microscope study. *Applied Entomology and Zoology, 29*(3), 439-442.

Mollon, J. D., Bowmaker, J. K., & Jacobs, G. H. (1984). Variations of colour vision in a New World primate can be explained by polymorphism of retinal photopigments. *Proc R Soc Lond B Biol Sci, 222*(1228), 373-399. doi:10.1098/rspb.1984.0071

Moran, D., Softley, R., & Warrant, E. J. (2015). The energetic cost of vision and the evolution of eyeless Mexican cavefish. *Science Advances, 1*(8), e1500363-e1500363. doi:10.1126/sciadv.1500363

Naka, K. I., & Rushton, W. A. (1966). S-potentials from luminosity units in the retina of fish (Cyprinidae). *J. Physiol., 185*(3), 587-599.

Niven, J. E., Anderson, J. C., & Laughlin, S. B. (2007). Fly photoreceptors demonstrate energy-information trade-offs in neural coding. *PLoS Biol, 5*(4), e116. doi:10.1371/journal.pbio.0050116

Niven, J. E., & Laughlin, S. B. (2008). Energy limitation as a selective pressure on the evolution of sensory systems. *J Exp Biol, 211*(Pt 11), 1792-1804. doi:10.1242/jeb.017574

Obara, Y. (1970). Studies on the mating behavior of the white cabbage butterfly, *Pieris rapae* crucivora Boisduval. *Z. Vergl. Physiologie, 69*(1), 99-116. doi:10.1007/bf00340912

Obara, Y., & Majerus, M. E. N. (2000). Initial mate recognition in the British cabbage butterfly, *Pieris rapae rapae*. *Zoological Science, 17*(6), 725-730. doi:10.2108/zsj.17.725

Ogawa, Y., Awata, H., Wakakuwa, M., Kinoshita, M., Stavenga, D. G., & Arikawa, K. (2012). Coexpression of three middle wavelength-absorbing visual pigments in sexually dimorphic photoreceptors of the butterfly *Colias erate*. *J Comp Physiol A Neuroethol Sens Neural Behav Physiol, 198*(12), 857-867. doi:10.1007/s00359-012-0756-8

Ogawa, Y., Kinoshita, M., Stavenga, D. G., & Arikawa, K. (2013). Sex-specific retinal pigmentation results in sexually dimorphic long-wavelength-sensitive photoreceptors in the eastern pale clouded yellow butterfly, *Colias erate*. *J Exp Biol, 216*(Pt 10), 1916-1923. doi:10.1242/jeb.083485

Osorio, D., & Vorobyev, M. (2005). Photoreceptor spectral sensitivities in terrestrial animals: adaptations for luminance and colour vision. *Proc Biol Sci, 272*(1574), 1745-1752. doi:10.1098/rspb.2005.3156

Osorio, D., & Vorobyev, M. (2008). A review of the evolution of animal colour vision and visual communication signals. *Vision Res, 48*(20), 2042-2051. doi:10.1016/j.visres.2008.06.018

Peitsch, D., Fietz, A., Hertel, H., de Souza, J., Ventura, D. F., & Menzel, R. (1992). The spectral input systems of hymenopteran insects and their receptor-based colour vision. *J Comp Physiol A, 170*(1), 23-40. doi:10.1007/bf00190398

Porter, M. L., Bok, M. J., Robinson, P. R., & Cronin, T. W. (2009). Molecular diversity of visual pigments in Stomatopoda (Crustacea). *Vis Neurosci, 26*(3), 255-265. doi:10.1017/S0952523809090129

Prokopy, R. J., & Owens, E. D. (1983). Visual detection of plants by herbivorous insects. *Annual Review of Entomology, 28*, 337-364. doi:DOI 10.1146/annurev.en.28.010183.002005

Qiu, X., & Arikawa, K. (2003). Polymorphism of red receptors: sensitivity spectra of proximal photoreceptors in the small white butterfly *Pieris rapae crucivora*. *Journal of Experimental Biology, 206*(Pt 16), 2787-2793. doi:10.1242/jeb.00493

Qiu, X., Vanhoutte, K. A., Stavenga, D. G., & Arikawa, K. (2002). Ommatidial heterogeneity in the compound eye of the male small white butterfly, *Pieris rapae crucivora*. *Cell Tissue Res, 307*(3), 371-379. doi:10.1007/s00441-002-0517-z

Sauman, I., Briscoe, A. D., Zhu, H., Shi, D., Froy, O., Stalleicken, J., . . . Reppert, S. M. (2005). Connecting the navigational clock to sun compass input in monarch butterfly brain. *Neuron, 46*(3), 457-467. doi:10.1016/j.neuron.2005.03.014

Schindelin, J., Arganda-Carreras, I., Frise, E., Kaynig, V., Longair, M., Pietzsch, T., . . . Cardona, A. (2012). Fiji: an open-source platform for biological-image analysis. *Nat Methods, 9*(7), 676-682. doi:10.1038/nmeth.2019

Sison-Mangus, M. P., Bernard, G. D., Lampel, J., & Briscoe, A. D. (2006). Beauty in the eye of the beholder: the two blue opsins of lycaenid butterflies and the opsin gene-driven evolution of sexually dimorphic eyes. *J Exp Biol, 209*(Pt 16), 3079-3090. doi:10.1242/jeb.02360

Sison-Mangus, M. P., Briscoe, A. D., Zaccardi, G., Knuttel, H., & Kelber, A. (2008). The lycaenid butterfly *Polyommatus icarus* uses a duplicated blue opsin to see green. *J Exp Biol, 211*(Pt 3), 361-369.

doi:10.1242/jeb.012617
Stalleicken, J., Labhart, T., & Mouritsen, H. (2006). Physiological characterization of the compound eye in monarch butterflies with focus on the dorsal rim area. *J Comp Physiol A, 192*(3), 321-331. doi:10.1007/s00359-005-0073-6
Stavenga, D. G. (2002a). Colour in the eyes of insects. *J Comp Physiol A, 188*(5), 337-348. doi:10.1007/s00359-002-0307-9
Stavenga, D. G. (2002b). Reflections on colourful ommatidia of butterfly eyes. *Journal of Experimental Biology, 205*(Pt 8), 1077-1085.
Stavenga, D. G. (2010). On visual pigment templates and the spectral shape of invertebrate rhodopsins and metarhodopsins. *J Comp Physiol A Neuroethol Sens Neural Behav Physiol, 196*(11), 869-878. doi:10.1007/s00359-010-0568-7
Stavenga, D. G., & Arikawa, K. (2006). Evolution of color and vision of butterflies. *Arthropod Struct Dev, 35*(4), 307-318. doi:10.1016/j.asd.2006.08.011
Stavenga, D. G., Stowe, S., Siebke, K., Zeil, J., & Arikawa, K. (2004). Butterfly wing colours: scale beads make white pierid wings brighter. *Proc R Soc Lond B Biol Sci, 271*(1548), 1577-1584. doi:10.1098/rspb.2004.2781
Straw, A. D., Warrant, E. J., & O'Carroll, D. C. (2006). A "bright zone" in male hoverfly (*Eristalis tenax*) eyes and associated faster motion detection and increased contrast sensitivity. *J Exp Biol, 209*(Pt 21), 4339-4354. doi:10.1242/jeb.02517
Swihart, S. L. (1972). The neural basis of colour vision in the butterfly, *Heliconius erato*. *Journal of Insect Physiology, 18*(5), 1015-1025. doi:10.1016/0022-1910(72)90038-8
Velarde, R. A., Sauer, C. D., Walden, K. K., Fahrbach, S. E., & Robertson, H. M. (2005). Pteropsin: a vertebrate-like non-visual opsin expressed in the honey bee brain. *Insect Biochem Mol Biol, 35*(12), 1367-1377. doi:10.1016/j.ibmb.2005.09.001
Wang, B., Xiao, J. H., Bian, S. N., Niu, L. M., Murphy, R. W., & Huang, D. W. (2013). Evolution and expression plasticity of opsin genes in a fig pollinator, *Ceratosolen solmsi*. *PLoS One, 8*(1), e53907. doi:10.1371/journal.pone.0053907
Wehrhahn, C. (1979). Sex-specific differences in the chasing behaviour of houseflies (*Musca*). *Biological Cybernetics, 32*(4), 239-241. doi:10.1007/bf00337647
Wehrhahn, C., Poggio, T., & Bülthoff, H. (1982). Tracking and chasing in houseflies (*Musca*). *Biological Cybernetics, 45*(2), 123-130. doi:10.1007/bf00335239
Wernet, M. F., & Desplan, C. (2004). Building a retinal mosaic: cell-fate decision in the fly eye. *Trends Cell Biol, 14*(10), 576-584. doi:10.1016/j.tcb.2004.09.007
Wernet, M. F., Perry, M. W., & Desplan, C. (2015). The evolutionary diversity of insect retinal mosaics: common design principles and emerging molecular logic. *Trends Genet, 31*(6), 316-328. doi:10.1016/j.tig.2015.04.006
Zaccardi, G., Kelber, A., Sison-Mangus, M. P., & Briscoe, A. D. (2006a). Color discrimination in the red range with only one long-wavelength sensitive opsin. *J Exp Biol, 209*(Pt 10), 1944-1955. doi:10.1242/jeb.02207
Zaccardi, G., Kelber, A., Sison-Mangus, M. P., & Briscoe, A. D. (2006b). Opsin expression in the eyes of *Heliconius erato*. *Perception, 35*(S), 142-143.

CHAPTER 3

Exceptional Retinal Mosaic Diversity and Evolution of a Violet Receptor in *Heliconius* Butterflies

Abstract

Numerous animal lineages for which color is ecologically important have independently expanded and diversified the opsin-based photoreceptors required for color vision(Arikawa, 2003; Cronin & Marshall, 1989; Futahashi et al., 2015; Hofmann & Carleton, 2009). Despite a high level of photoreceptor diversity observed in these lineages, the selective pressures giving rise to new photoreceptors and their spectral tuning remain mostly obscure (Bok, Porter, & Cronin, 2015; Carleton, Parry, Bowmaker, Hunt, & Seehausen, 2005; Chen, Awata, Matsushita, Yang, & Arikawa, 2016; Futahashi et al., 2015). In the butterfly *Heliconius erato*, both male and female eyes express a positively-selected violet receptor—which co-evolved with a specialized yellow pigment on their wings—while female eyes also express an ancestral UV receptor (McCulloch, Osorio, & Briscoe, 2016b). The UV receptor *UVRh1* and the violet receptor *UVRh2* are found in several *Heliconius* species, but whether sexually dimorphic opsin expression exists across the genus is unknown(Briscoe et al., 2010). We therefore compared UV opsin expression patterns in a phylogenetic context spanning both sexes in 23 species, using immunostaining and RNA-Seq. We identified five unique retinal mosaics and three distinct forms of sexual dimorphism based on ommatidial types. Further analysis revealed independent losses of opsin expression, pseudogenization events, and independent evolution of the same retinal mosaic. Opsin expression patterns are hyperdiverse within *Heliconius*. However, the retention of the positively-selected violet receptor across the

majority of species and sexes surveyed together with color space modeling of preferred yellow wing colors provides evidence that the violet receptor serves an adaptive role in *Heliconius* color vision in the context of conspecific recognition. Our observations give new insights into the selective pressures that underlie the spectral tuning of new visual photoreceptors.

Materials and Methods

Animals

We obtained pupae from The Butterfly Farm - Costa Rica Entomological Supply, or from Stratford Butterfly Farm, U.K. After eclosion, butterflies were kept alive for 2-3 days in a humidified chamber and fed a diluted honey solution daily before sacrificing. Other adult butterflies used for mRNA sequencing were collected in the field in Ecuador or México and preserved in RNALater (Life Technologies, Grand Island, NY). Only one color morph was used per species, except for *H. doris* where all three color morphs were sampled.

Cryosectioning

Butterfly heads were cut in two to separate the eyes. Both eyes were fixed in 4% paraformaldehyde (Electron Microscopy Sciences Cat. # 15710) in 0.1 M phosphate buffered saline (PBS) for 1 hour at room temperature. Eyes were then sucrose-protected in increasing concentrations of 10%, 20%, and 30% sucrose in PBS for either one hour at room temperature or overnight at 4°C. Excess cuticle was cut away around each eye before it was placed on a bed of Tissue Tek O.C.T. compound and frozen at -20°C. Frozen eyes

were sectioned at 14 μm thickness on an HM 500 OM microtome cryostat (Microm), and placed on slides to dry overnight at room temperature.

Immunohistochemistry

An antibody against the peptide DGLDSVDLAVIPEH in the N-terminal domain of the *Heliconius erato* UV1 opsin was generated in guinea pigs and immunoaffinity purified (Open Biosystems, Inc., Huntsville, Alabama). An anti-blue opsin antibody was generated in rats against the *H. erato* peptide RYRAELQKRLPWMGVREAD and also immunoaffinity purified (Thermo Fisher, MA, USA). The pan-UV antibody was described in Lampel *et al*. (Lampel, Briscoe, & Wasserthal, 2005). Dry slides were placed in 100% ice-cold acetone bath for 5 minutes, then washed 3 x 10 minutes in 0.1 M PBS. Slides were then placed in 0.5% sodium dodecyl sulfate in 0.1 M PBS for 5 minutes. Each slide was blocked for 30 minutes at room temperature using 8% (v/v) normal donkey serum and normal goat serum, and 0.3% Triton X-100 in 0.1 M PBS. Slides were incubated with 2:75 affinity-purified rabbit anti-pan-UV or rabbit anti-blue antibody and 1:15 affinity-purified guinea pig anti-UV1 antibody in blocking solution overnight at 4°C. Slides were washed 3 x 10 minutes in 0.1 M PBS and then incubated with 1:1000 goat anti-guinea pig Alexafluor 488 and 1:500 donkey anti-rabbit Cy3 or Alexafluor 555, in blocking solution for two hours at room temperature. Slides were washed once more 3 x 10 minutes in 0.1 M PBS. Slides were stored for imaging by coverslipping with Aqua Poly/Mount (Polysciences, Inc. Cat. # 18606). Slides were viewed with epifluorescence microscopy using a Zeiss Axioskop 2 under a 20x lens. Images were taken using a Zeiss Axiocam HRc and associated Axiovision

software. Contrast and brightness were adjusted for clarity using Adobe Photoshop CS4 and Fiji.

For each specimen we examined hundreds to thousands of fluorescently labeled ommatidia at multiple depths in the retina, and we noted different ommatidial types based on the combinations of UV-expressing R1 and R2 cells. For clarity, all images are presented as a small subset of the retina, where all possible ommatidial combinations can be seen in close proximity. We fluorescently labeled R1 and R2 cells expressing either BRh (blue) UVRh1 (green), or UVRh2 (magenta) (Fig. 1B-L, Fig. 2A-N). We did not distinguish which cell was R1 and which was R2. In double stains that did not label BRh expression, R1 and R2 cells that were not labeled were assumed to be blue opsin expressing cells, according to current and previous *in situ* hybridization and immunohistochemistry results (Fig. 1)(Zaccardi, Kelber, Sison-Mangus, & Briscoe, 2006). We then classified ommatidial types according to their combination of R1 and R2 cells, and identified retinal mosaics by the combinations of ommatidial types present in each (Fig. 1B).

RNA-Sequencing

Total RNAs were extracted from 64 individual adult butterfly heads using Trizol (Life Technologies, Grand Island, NY). A NucleoSpin RNA II kit (Macherey-Nagel, Bethlehem, PA) was used to purify 10 μg total RNA per sample. Purified total RNA was quantified using a Qubit 2.0 Fluorometer (Life Technologies, Grand Island, NY). The quality of the RNA samples was checked using an Agilent Bioanalyzer 2100 (Agilent Technologies, Santa Clara, CA). Four micrograms of purified total RNA were used to make cDNA libraries. A TruSeq RNA sample prep kit, set A (Illumina, San Diego, CA) was used to prepare individual cDNA

libraries. PCR-enriched individual cDNA libraries were quantified using the Qubit 2.0 Fluorometer and QC checked using the Agilent Bioanalyzer 2100. After being normalized according to their Qubit concentrations, the enriched individual libraries were pooled and then run on a 2% agarose gel. cDNA products ranging from 280 to 340 bp with an average of 310 bp were cut out and purified using a Geneclean III kit (MP Biomedicals, Solon, OH). After being re-purified using Agencourt AMPure XP magnetic beads (Beckman Coulter Genomics, Danvers, MA), the cDNA pool was quantified using the Qubit 2.0 Fluorometer, and QC checked using the Agilent Bioanalyzer 2100. The cDNA pool sample was then normalized to 10 nM and run on a HiSeq 2000 (Illumina, San Diego, CA) yielding ~200 million 100 bp paired-end reads per lane.

Cell Counting and Principal Component Analysis

Ommatidia were only counted if images captured more than 100 ommatidia, the tissue was not sheared or folded, and cell bodies were clearly labeled without a high level of background. Images were viewed at full resolution in Adobe Illustrator. The background autofluorescence found in all ommatidia was not removed, so as to see any ommatidia that might be unstained. Ommatidia were not counted if the staining was unclear or the sectioned tissue was of poor quality (e.g. folded). Total ommatidia were counted over as much area as possible for a single high quality section per individual and the percentages of each class of ommatidia were calculated. From these ommatidial classes we could count the total number of individual R1 and R2 photoreceptor subtypes found in each section. Principal components analysis was performed in R using the prcomp command. Ommatidial and cell count averages for each sex and species were used and log

transformed for the analysis. The results were plotted using the first two principal components as the x- and y-axes.

Ancestral state reconstruction and character mapping

Twenty-seven species of *Heliconius* and *E. isabella* were scored for the presence or absence of full-length *UVRh2* transcripts. All species expressed *UVRh1*. Fourteen species representing each of the major *Heliconius* lineages and the outgroup *Eueides isabella* that were examined using immunohistochemistry were additionally scored for the presence or absence of the following 5 traits: female UVRh2 PRC, male UVRh1 PRC and male UVRh2 PRC, female retinal mosaic I (3 ommatidia) and female retinal mosaic III (six ommatidia). Species from the *melpomene* and silvaniform clades which have a third female eye-type were excluded from ancestral state reconstructions of retinal mosaic I and retinal mosaic III. Each of these six characters were individually mapped onto the terminal nodes of the species tree from ref (Kozak et al., 2015a) in Mesquite (Maddison & Maddison, 2011) and ancestral states were then estimated using the maximum likelihood MK1 model with equal likelihood of gains and losses.

Opsin phylogenies

LWRh, BRh, UVRh1, and *UVRh2* opsin nucleotide sequences were gathered from GenBank or assembled from 64 newly-sequenced individual *Heliconius* and *Eueides* head transcriptomes (representing 21 species). Included in this data set are closely-related outgroups from three genera: *Eueides* (*E. isabella, E. procula, E. aliphera, E. lineata, E. vibilia), Dione* (*D. juno* and *D. moneta*) and *Agraulis vanillae*. mRNA-Seq data were *de novo*

assembled in CLC Genomics and opsin sequences were identified through local database BLAST searches, and then added to the MEGA alignments (Tamura et al., 2011). In cases where fragmented assemblies resulted from this procedure, full-length mRNAs from related individuals were used as a template against which reads from individual libraries were mapped. The read-mapping consensus sequence was then inspected by eye, exported and included in the nucleotide alignments. The number of nucleotide sites used to estimate each of the opsin phylogenies was as follows: *UVRh* (1137 bp), *BRh* (1143 bp) and *LWRh* (1143 bp). 298 newly sequenced mRNA sequences have been deposited in GenBank under accession numbers XXXXXXXX-XXXXXXXX, and may also be found in Appendix S1. Individual sequences were excluded from phylogenetic analysis if low expression levels resulted in large gaps. Opsin phylogenies were constructed in PhyML using the HKY85 substitution model and branch support was calculated with 1000 bootstrap replicates using aBayes (Anisimova, Gil, Dufayard, Dessimoz, & Gascuel, 2011; Guindon et al., 2010).

RELAX analysis

We used our *UVRh2* sequences to construct a gene tree using PhyML as described above. We defined all *melpomene/*silvaniform *UVRh2* branches as the test branches (T), and all other *UVRh2* and outgroup *UVRh* sequences as the reference branches (R), and ran the RELAX hypothesis test in HyPhy (Pond, Frost, & Muse, 2005) on the High Performance Computing cluster at UC Irvine. If relaxed selection is present, then the ω distribution in R should move closer to neutrality in T, that is, $\omega > 1$ in R should decrease toward 1 in T, while $\omega < 1$ in R should increase toward 1 in T (Fig. 5). RELAX sets the ω distribution of T equal to the ω distribution of R, raised to the power of k, or the relaxation parameter. In the

null model k = 1, so the ω distributions of T and R are equal. In the alternative model, k is allowed to vary, so that if k > 1 T is under stronger selection relative to R, and if k < 1, then T is under relaxed selection compared to R. The models are compared using a likelihood ratio test using a χ^2 distribution to test if the alternative model is a better fit.

Read-mapping of opsins

In order to validate the results of the immunohistochemistry and quantify the different levels of *UVRh1* and *UVRh2* transcript expression between major clades and sexes, we selected individual butterflies (males and females) for analysis. Our RNA-Seq reads were quality trimmed using the python script TQSfastq.py (http://genomics-pubs.princeton.edu/prv/resources/scripts/TQSfastq.py) with a quality threshold of 20 and a minimum read length of 30. Reads were paired using a second python script, paired_sequence_match.py (https://bitbucket.org/lance_parsons/paired_sequence_utils). We produced *de novo* assemblies of the transcriptome for each species using the programs Velvet (default settings and a kmer length of 31) (Zerbino & Birney, 2008) and Oases (Schulz, Zerbino, Vingron, & Birney, 2012). We then used BLAT (Kent, 2002) to locate the species-specific *UVRh1* and *UVRh2* opsin genes in our *de novo* transcriptomes utilizing the publically available *H. melpomene* sequences as references (NCBI Accession numbers: GU324678.1 (*UVRh1*) & GU324679.1 (*UVRh2*)). Next, we mapped the forward set of reads for each sample onto its species-specific *UVRh1* and *UVRh2* opsin sequences using the program Stampy (Lunter & Goodson, 2011). SAMtools was then used to sort the resulting mapped reads (Li et al., 2009), and htseq-count (http://www-huber.embl.de/users/anders/HTSeq/doc/overview.html) was employed to count the

number of unique reads that mapped to each opsin sequence. We calculated the reads per kilobase of transcript per million mapped (RPKM) for each gene in each sample. We also calculated the ratio of the average $\log_2$ *UVRh2* reads over the average $\log_2$ *UVRh1* reads. Lastly, for any species and sex combination in which we had two or more samples, we determined whether there was a significant difference in the expression of *UVRh1* and *UVRh2* using a two-sample t-test with equal variances.

Species phylogeny

Five representative species of the major *Heliconius* clades were included in this analysis; *H. melpomene*, *H. erato*, *H. doris*, *H. sara* and *H. charithonia*. A *de novo* assembly of RNA-Seq data was performed and transcriptomic data from each of the five species was mapped back to the assembly using Velvet (Zerbino & Birney, 2008) and Oases (Schulz et al., 2012). Contigs were filtered for the presence of sequence data in each of the five species, for contig lengths of >200 bp and for BLAST matches with >90% sequence identity and >100 bp long. In total, 634 loci were obtained and alignments for each locus were produced using Clustal W (Larkin et al., 2007) and variable positions flanking indels were masked by Ns to reduce misalignment error in the data set. The 634 loci from the five representative species were concatenated and a partition annotation file denoting the coordinates of each locus was generated. This partitioned data was run in RAxML (Stamatakis, 2006) with rapid bootstrapping (1000 bootstraps) and a maximum likelihood search under the General Time Reversible (GTR) substitution model, with a gamma distribution. The alignment file for the 634 loci was deposited in Dryad under data identifier: doi:XX.XXX/dryad.XXXX.

Color space modeling

Models of color vision take into account how receptor signals contribute to chromatic (e.g., color opponent) mechanisms (Kelber, Vorobyev, & Osorio, 2003). For *H. erato* males, whose yellow color preferences have been tested experimentally (Finkbeiner, Briscoe, & Reed, 2014; Finkbeiner, Fishman, Osorio, & Briscoe, In Review) and shown to prefer 3-OHK yellow models, we calculated chromaticity loci for the actual *H. erato* male trichromatic system consisting of UV2, blue and green receptors and a hypothetical male trichromatic system in which UV2 is replaced by UV1. Equations of Kelber et al. (2003; their eqq. [A1]–[A5], [A8]–[A12]) were used to model the trichromatic color spaces. This model incorporates a von Kries's transformation, that is, normalization by the illumination spectrum, which models the way in which low-level mechanisms such as photoreceptor adaptation give color constancy (Kelber et al., 2003). The sunny open habitat illumination spectrum of Briscoe et al. (2010) was used in the model because it was taken in a locality in Oaxaca, MX where *Heliconius* fly. For *H. erato* photoreceptor absorbance spectra were based on λmax value estimates (*H. erato*: 355 (UV1), 398 (UV2), 470 (B), and 555 (G) nm; (Briscoe et al., 2010; Frentiu, Bernard, Sison-Mangus, Brower, & Briscoe, 2007; McCulloch et al., 2016b; Struwe, 1972a, 1972b) and a visual pigment template (Palacios et al. 1996). The rhodopsin templates do not incorporate effects of intraocular filtering but for our purposes are reasonable estimates of the spectral sensitivity curves.

Results and Discussion

Opsin Protein and mRNA Expression in *Heliconius*

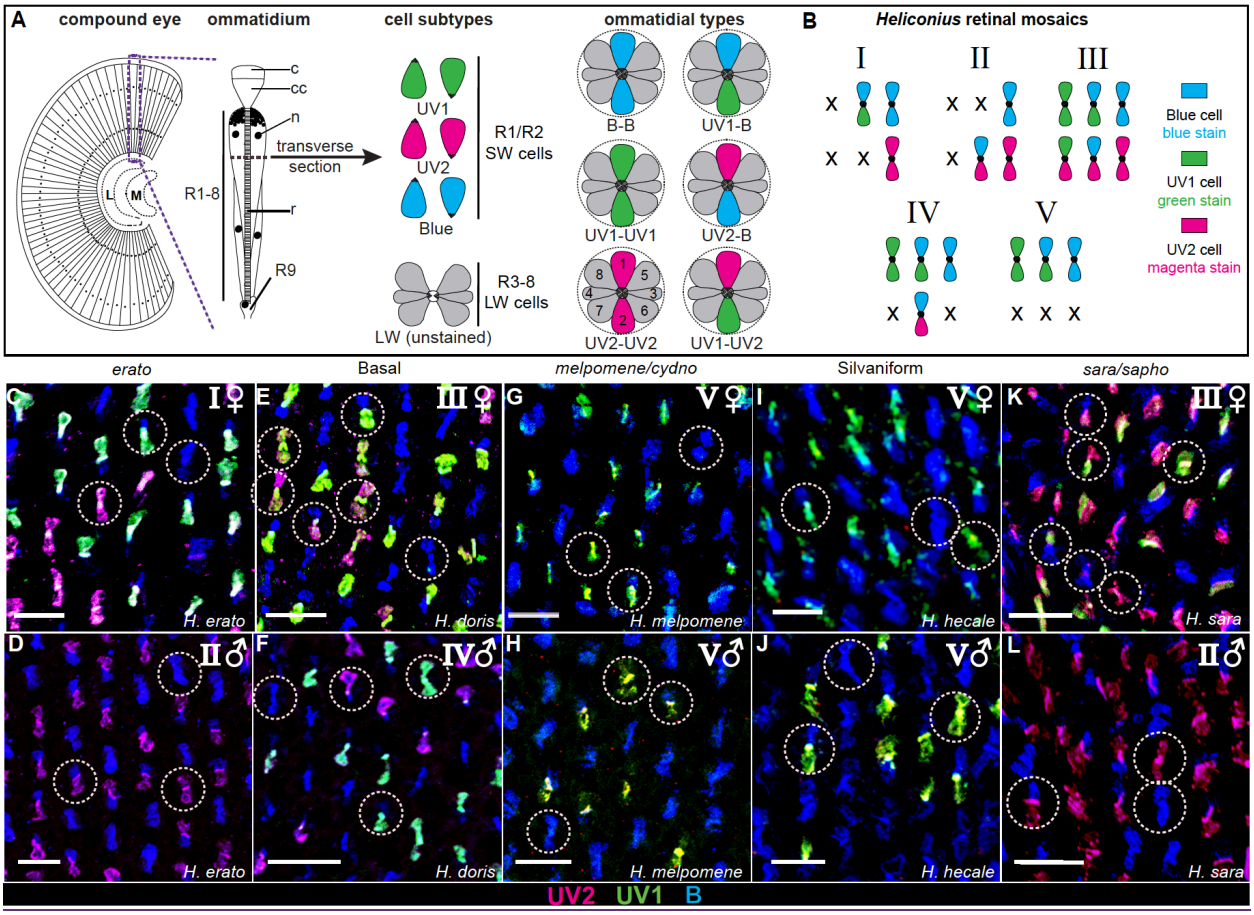

Figure 1. **At least five retinal mosaics are found in *Heliconius*.** (A) From left to right: schematic of the compound eye, longitudinal section of a single ommatidium, individual photoreceptor cell subtypes, and total number of ommatidial types showing variable opsin expression in the main retina across surveyed *Heliconius* species. Short wavelength (SW) R1/R2 cells express blue (blue), UV1 (green), or UV2 (magenta) opsins. Cells R3-9 are long wavelength (LW) opsin-expressing cells. L, lamina; M, medulla c, cornea; cc, crystalline cone; n, nucleus; r, rhabdom. (B) Retinal mosaics are identified based on patterns of SW opsin expression and numbered I - V. (C-L) Female and male transverse sections of *Heliconius* compound eyes, representing each major clade in the genus. Roman numerals in each panel indicate the retinal mosaic for each species and sex. (C and D) *H. erato.* (E and F) *H. doris*. (G and H) *H. melpomene*. (I and J) *H. hecale*. (K and L) *H. sara*. Circles highlight ommatidial types. Scale bars, 25 μm.

A key question in visual ecology is concerned with how animal eyes have evolved to handle the variety of colorful stimuli they encounter in their world. What costs or benefits might there be to evolving a new receptor and a specialized visual system? Famous for their spectacular wing evolution and mimicry, *Heliconius* butterflies are also interesting for

their eyes. *Heliconius* have an ultraviolet (UV) opsin duplication, identified in all species so far investigated, together with a 3-hydroxykynurenine yellow pigment on their wings; both traits are synapomories of the genus. Positive selection of *UVRh2* suggests a new adaptive function for the UV2 opsin in *Heliconius* (Briscoe et al., 2010). Recently we determined photoreceptor sensitivity and opsin expression in the eye of *H. erato* (McCulloch, Osorio, & Briscoe, 2016a). We found that females have UV1, UV2, blue (B) and long wavelength (L) opsin-expressing cells with peak sensitivities at 355, 390, 470, and 555 nm respectively, while males have the same opsins and sensitivities except they lack UV1 (McCulloch et al., 2016b). Each sex possesses a distinct set of three ommatidial types, exhibiting a sexually dimorphic retinal mosaic (Fig 1A-D). To better understand the origins of the positively-selected violet receptor (UV2) and how it came to replace the ancestral UV1 receptor in the male eye, we asked whether the observed sexual dimorphism is found throughout the genus.

We therefore immunostained transverse sections of ommatidia in the compound eyes of males and females of 14 species in five major clades within *Heliconius* using anti-opsin antibodies. R1 and R2 photoreceptor cells are defined by the short-wavelength (SW) opsin they express (blue, UV1, or UV2) (Fig. 1A). R1 and R2 cell subtypes express SW opsins in different combinations resulting in up to six possible ommatidial types (Fig. 1A). We discovered at least five distinct retinal mosaics in *Heliconius* based on the different ommatidial types present in the eye, all but one incorporating the positively-selected violet receptor UV2 (Fig 1B-L). Across the genus, all species within a clade (except *H. charithonia,* see below) share the same retinal mosaic (Figs. 1, 2).

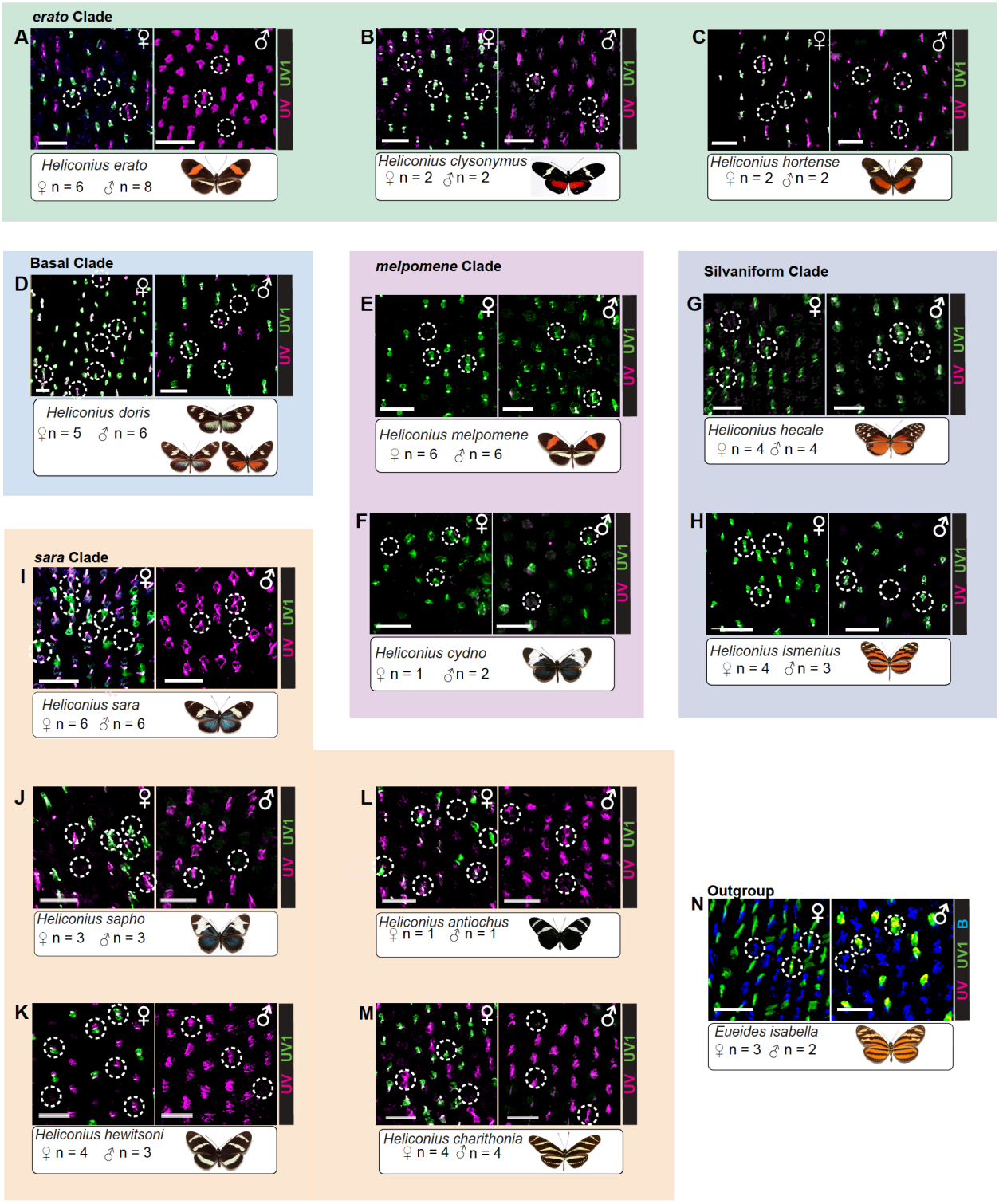

Figure 2. Eye sections of *Heliconius* and outgroup species immunostained for UV1 (green), UV2 (magenta) and blue (blue) opsins. (A-N) Images of each sex for all species immunostained in this study. The orientation of ommatidia in all images matches that of the R1 and R2 PRCs in Fig. 1A. Sample size refers to number of individuals with ommatidia counted in each species and sex. Dashed circles identify the different types of ommatidia in each species and sex. Scale bars, 25 μm.

Despite similarities among species within each clade, retinal mosaics differ considerably between clades and sexes. Other *erato* clade members (2 species) have the same expression pattern as *H. erato*, where UV1 opsin expression is absent in the male eye and UV2 is present in both sexes (females, mosaic I; males, mosaic II, Figs. 1C,D, 2A-C) (McCulloch et al., 2016b). Unlike *H. erato,* both *H. doris* sexes make use of UV1 and UV2, in six ommatidial types in females (mosaic III, Fig. 1E) and four ommatidial types in males (mosaic IV, Fig. 1F). The *melpomene* (2 species) and silvaniform (2 species) sister clades have yet another retinal mosaic. Both sexes have lost the UV2 cell, resulting in mosaic V (Fig. 1G-J, 2E-H). *Eueides isabella,* a sister taxon to *Heliconius,* is also similar to *melpomene* and silvaniform clades with respect to ancestral UV1 staining, but does not have the UV2 duplication (Fig. 2N). A third form of sexual dimorphism is found in the *sara* clade (5 species). Females in this clade are similar to *H. doris* females (mosaic III), while males are similar to *H. erato* males (mosaic II, Fig. 1K,L).

To complement our protein data, we sequenced and quantified levels of opsin mRNA expression in 19 species (n=64 butterflies) (Appendix 2, Table 1). In the *erato* (4 species) and *sara* (5 species) clades, *UVRh1* expression is nearly absent in males and *UVRh2* expression is high, while females highly express both *UVRh1* and *UVRh2* (Table 1). Both sexes in the basal clade (3 species) express both *UVRh1* and *UVRh2,* consistent with the *H. doris* opsin staining pattern (Table 1). Consistent with our protein expression data, all *melpomene* and silvaniform species (5 species) have very low expression of *UVRh2* in both sexes, while *UVRh1* remains highly expressed (Table 1). RNA-Sequencing also revealed that *UVRh2* is pseudogenized in several silvaniform species (see below), but not in *H. melpomene*.

Table 1. Sex-specific differential *UVRh* expression in *Heliconius.*

		Males					Females				
Clade	**Species**	**N**	**Average RPKM UV1**	**Average RPKM UV2**	**log2(ÛV2)/ log2(ÛV1)**	**p-value**	**N**	**Average RPKM UV1**	**Average RPKM UV2**	**log2(ÛV2) /log2(ÛV1)**	**p-value**
basal	*H. doris*	3	385.67	718	1.076	0.006	3	693.62	651.7	0.993	0.837
	H. hecuba	1	1760.67	1014.5	0.942	ND	1	3214.53	290.35	0.775	ND
	H. wallacei	1	979.51	921.8	0.993	ND	0	ND	ND	ND	ND
melpomene	*H. melpomene*	2	684.98	181.3	0.808	0.274	2	554.12	66.35	0.74	0.017
silvaniform	*H. atthis*	1	2114.9	11.9	0.463	ND	1	4075.18	0.61	0.2	ND
	H. hecale	2	334.59	4.5	0.435	0.023	2	1184.19	6.07	0.404	0.04
	H. ismenius	2	807.98	3.1	0.365	0.003	2	971.14	1.65	0.306	0.006
	H. numata	2	637.35	8.5	0.49	0.013	2	757.06	6.29	0.416	0.026
sara	*H. charithonia*	2	0.77	2359.3	5.535	0.011	3	748.48	1210.36	1.05	0.564
	H. eleuchia	1	0.17	4631.06	10.291	ND	1	423.12	5515.05	1.312	ND
	H. hewitsoni	2	0.68	1105.2	7.845	0.021	2	373.13	1327.59	1.158	0.003
	H. sapho	1	0.11	1387	ND	ND	1	277.85	1039.18	1.172	ND
	H. sara	3	0.36	1349.6	11.074	<0.001	4	284.58	1152.47	1.164	0.01
erato	*H. clysonimus*	2	0.93	3879.8	7.518	0.028	2	1043.01	1033.01	0.998	0.98
	H. erato	2	0.35	1886.1	12.251	0.008	2	519.83	867.88	1.058	0.502
	H. hortense	1	0.13	2664.2	ND	ND	1	1491.18	1507.52	1.001	ND
	H. telesiphe	1	0.52	1515.1	6.749	ND	1	847.3	1037	1.022	ND

Uniquely-mapped reads to each *UVRh* opsin mRNA were quantified by calculating reads per kilobase of transcript per million mapped (RPKM). For $\log_2$ ratios with N > 1, a t-test was performed to test for significant differences between *UVRh1* and *UVRh2* expression. Significant ($p < 0.05$) p-values are in bold. Green indicates expression of *UVRh1* > *UVRh2*, orange is *UVRh2* > *UVRh1*, and purple indicates no significant difference between *UVRh1* and *UVRh2*. ND: p-value not determined.

Evidence for sexually dimorphic patterns of opsin expression as seen in *erato* and *sara* clades is limited in other insects. Sexual dimorphism in other investigated butterflies is accomplished via sex differences in eye filter pigment distributions that cause shifts in photoreceptor sensitivity, or via sex-specific co-expression of opsins in a subset of photoreceptor cells (Arikawa, Wakakuwa, Qiu, Kurasawa, & Stavenga, 2005; Ogawa et al., 2012; Ogawa, Kinoshita, Stavenga, & Arikawa, 2013; Sison-Mangus, Bernard, Lampel, & Briscoe, 2006). In addition to butterflies, known examples of sexual dimorphism in the compound eyes of honeybees and houseflies involve differences in the domain of opsin expression rather than loss of opsin expression in one sex (Franceschini, Hardie, Ribi, & Kirschfeld, 1981; Menzel, Wunderer, & Stavenga, 1991). Some evidence for sex differences in *LWRh* opsin expression has been observed in the fig wasp *Ceratosolen solmsi* (Wang et al., 2013), but mRNA expression alone does not reveal opsin spatial expression, or whether

differences in spectral sensitivity exist. Male-specific loss of the UV1 cell represents a novel form of sexual dimorphism in insects.

Photoreceptor Cell and Ommatidial Counts

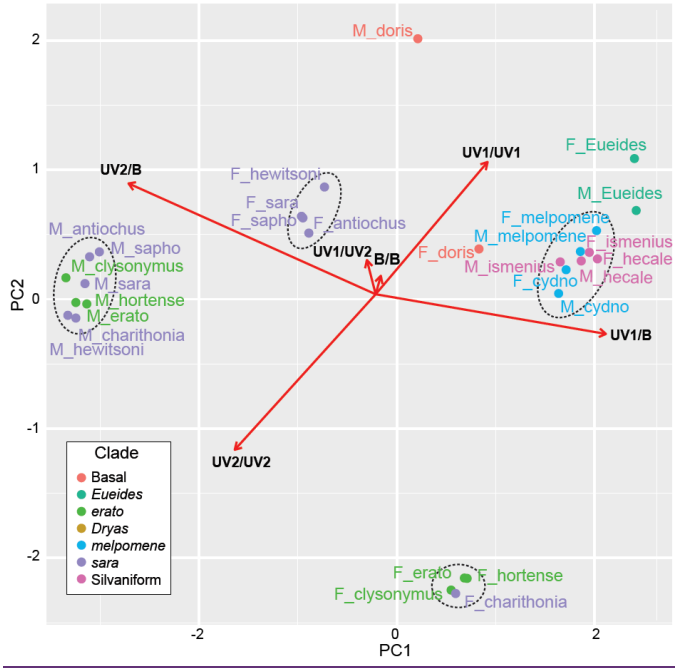

Figure 3. Principal component analysis of ommatidial type abundances in each species and sex. Data is plotted in two dimensions using the first two principal components, totaling 73% of the variance in the analysis. Eigenvectors are shown for this analysis with each vector representing an ommatidial type (red arrows). Averages of ommatidial percentages were used for analysis. Labels list the sex and species for each point, colors correspond to the clade in which the species belongs. Dotted circles indicate clustering of *sara/erato* clade males (left), *sara* clade females (center), *melpomene*/silvaniform clades both sexes (right), and *erato* clade/*H. charithonia* females (bottom). *Eueides isabella* is plotted here as its UV cells were labeled with the UV1 antibody, but this species does not have a *UVRh* gene duplication so formal comparison with *Heliconius* UV1 cannot be made.

If opsin regulatory mechanisms are conserved in *Heliconius*, then we would expect fixed proportions of stochastically distributed ommatidial types (Wernet, Perry, & Desplan, 2015). Similar proportions of ommatidial types in related species might provide evidence of a single evolutionary origin of changes to retinal mosaic developmental pathways. We therefore calculated average percentages of ommatidial types in multiple individuals for each species and sex. Within each clade, the abundance of each ommatidial type is similar

Table 2. Percentages of ommatidial types in *Heliconius*.

Clade	Sex	Species	Om. Counted	UV2/UV2	UV2/B	B/B	UV1/UV1	UV1/UV2	UV1/B
erato	Female	*H. clysonymus*	155	28.4	0	25.8	0	0	45.8
erato	Female	*H. erato*	2428	23.5 ± 1.1	0	24.6 ± 1.0	0	0	52 ± 1.2
erato	Female	*H. hortense*	181	23.2	0	22.7	0	0	54.1
sara	Female	*H. charithonia*	2051	28.3 ± 0.93	0	22.6 ± 0.67	0	0	49.1 ± 0.44
sara	Female	*H. antiochus*	270	8.1	24.8	33.7	3.3	8.5	21.5
sara	Female	*H. hewitsoni*	1153	7.7 ± 1.5	28.9 ± 0.57	25.3 ± 1.8	7.7 ± 0.83	6.7 ± 1.7	23.7 ± 1.5
sara	Female	*H. sapho*	742	6.1	27.9	37.7	2.7	6.5	19.1
sara	Female	*H. sara*	1063	8.8 ± 1.1	29.9 ± 0.72	28.1 ± 4.4	4.5 ± 0.38	7.0 ± 1.5	21.7 ± 1.6
basal	Female	*H. doris*	2445	4.1 ± 1.6	4.8 ± 0.57	30.1 ± 1.4	8.6 ± 0.70	4.3 ± 0.91	48.1 ± 1.2
melp	Female	*H. cydno*	940	0	0	62.2	4.6	0	33.2
melp	Female	*H. melpomene*	1812	0	0	48.5 ± 1.9	10.5 ± 1.1	0	41.0 ± 2.2
Silvan	Female	*H. hecale*	198	0	0	43.4	7.1	0	49.5
Silvan	Female	*H. ismenius*	1194	0	0	49.3 ± 4.6	7.2 ±2.3	0	43.6 ± 2.6
Eueides	Female	*E. isabella*	303	0	0	15.2	39.9	0	44.9
erato	Male	*H. clysonymus*	219	15.5	59.8	24.7	0	0	0
erato	Male	*H. erato*	2356	17.7 ± 1.5	40.6 ± 1.7	41.6 ± 2.0	0	0	0
erato	Male	*H. hortense*	113	18.6	46.9	34.5	0	0	0
sara	Male	*H. charithonia*	2719	21.7 ± 1.9	43.2 ± 4.1	35.1 ± 5.5	0	0	0
sara	Male	*H. antiochus*	273	10.6	50.5	38.8	0	0	0
sara	Male	*H. hewitsoni*	255	22.4	48.6	29	0	0	0
sara	Male	*H. sapho*	309	9.4	46	44.7	0	0	0
sara	Male	*H. sara*	1106	14.6 ± 1.7	45.8 ± 0.71	39.6 ± 1.3	0	0	0
basal	Male	*H. doris*	1758	0	25 ± 1.4	31.3 ± 3.6	18.5 ± 2.1	0	25.1 ± 0.39
melp	Male	*H. cydno*	213	0	0	62.8	2.6	0	34.5
melp	Male	*H. melpomene*	1594	0	0	56.3 ± 4.4	6.8 ± 0.94	0	36.9 ± 3.6
Silvan	Male	*H. hecale*	171	0	0	53.8	5.8	0	40.4
Silvan	Male	*H. ismenius*	1232	0	0	65.8 ± 1.7	4.9 ± 0.70	0	29.3 ± 2.3
Eueides	Male	*E. isabella*	232	0	0	15.9	19.8	0	64.2

Species are organized by clade and sex. Averages ± S.E. Colors correspond to percentages, in increments of 10 percentage points: 0%, dark blue; >0%, blue; >10%, light blue; >20%, turquoise; >30% green; >40%, green-yellow, >50%, yellow; >60%, yellow-orange. Bolded borders highlight groups of retinal mosaics with similar ommatidial percentages.

among both individuals and species; between clades there are notable differences (Table 3). To visualize these differences, we plotted the results of a principal component analysis (PCA) using the percentages of ommatidial types from each of 14 species and sex (Fig. 3). Four clusters are evident (Fig. 3).

Two cases where proportions of ommatidial types are similar in sister clades - one in *sara* and *erato* males, and another in the *melpomene* and silvaniform clades - suggest a common origin of retinal mosaics II and V before the extant clades diverged (Table 3). *H. doris* are distinct within the genus in that neither sex obviously clusters with other clades in the PCA plot. *H. doris* males are the only males that express both UV1 and UV2 (Fig. 1F). *H. doris* females, despite sharing retinal mosaic III with *sara* females, differ in ommatidial

type abundances (Table 3). *H. doris* females are also the only individuals where our staining sometimes indicated possible coexpression of UV1 and UV2 in the same photoreceptor cell. This could be an artifact of our staining procedure, or, more likely, *H. doris* females may represent yet another retinal mosaic in *Heliconius*, due to coexpression of UV1 and UV2.

Stochastic spatial expression yet fixed proportions of ommatidial subtypes are found in numerous insects (Arikawa, 2003; Wernet et al., 2015). In the *D. melanogaster* retina, expression of *spalt, prospero, senseless, spineless, warts,* and *melted* leads to stereotypical ratios of two ommatidial types defined by stochastic expression of opsins (Cook, Pichaud, Sonneville, Papatsenko, & Desplan, 2003; Domingos et al., 2004; Mikeladze-Dvali et al., 2005; Wernet et al., 2006). Recently two butterfly species were shown to have two cells homologous to the single *D. melanogaster* R7 subtype (Perry et al., 2016). The resulting butterfly R1 and R2 color-sensing cells depend on *spineless* expression for either a UV or blue cell fate, thus producing the three ancestral types of ommatidia seen throughout Lepidoptera (UV/UV, UV/B, or B/B) (Perry et al., 2016). *Heliconius* species may have added an extra step in this pathway, where lack of *spineless* expression indicates a UV cell, and then another transcription factor determines whether this cell is a UV1 or UV2 cell, allowing for up to six ommatidial types. Other mechanisms are probably responsible for the restriction to three ommatidial types in *erato* clade females—despite expression of UV1, UV2, and blue cell subtypes—as well as the suppression of the UV1 cell subtype in *erato* and *sara* clade males in favor of UV2, which further work should address.

Other intriguing questions raised by *Heliconius* diversity of opsin expression are related to the neural processing of color. Although *H. erato* females do not have an ommatidial type that contains a UV1 and UV2 cell within it, it is clear that *H. erato* females

are able to discriminate within UV wavelengths, suggesting downstream neural processing that compares information from distinct ommatidia in the eye. If *H. erato* is able to distinguish within UV wavelengths with just three ommatidial types, what might be the adaptive function, if any, of the *H. sara* and *H. doris* females' six ommatidial types? Having six ommatidial types (*sara, H. doris* females) may allow for finer color discrimination with more types of spectral comparisons within single ommatidial cartridges. Restricting the types of ommatidia in the eye (*erato* females, *H. doris* males) may represent an alternative strategy that reduces the complexity of the downstream neural circuitry, allowing a more energetically and computationally efficient signaling pathway while maintaining UV discrimination.

Additionally, in comparison to *Heliconius* that have two UV cells, those with only a single type of UV cell (*melpomene,* silvaniforms, both sexes; *erato, sara* males) have a consistently higher ratio of blue cells to UV cells. One explanation could be that in the absence of UV discrimination, blue cells become important for detecting brightness rather than color of *Heliconius* UV-yellow wing signals, where a steep increase in reflectance coincides with the blue cell's peak sensitivity in *H. erato.* This is in contrast to a non-*Heliconius* yellow wing pigment, where the reflectance increases more gradually, and a single cell would be all that is needed to detect differences in brightness between these two reflectances (Chapter 2, Figure 8) (McCulloch et al., 2016b). Further electrophysiological and behavioral work is needed to address the importance of the ratios of specific cell and ommatidial subtypes to color vision.

Loss of UV2 in *melpomene* and Silvaniform Clades

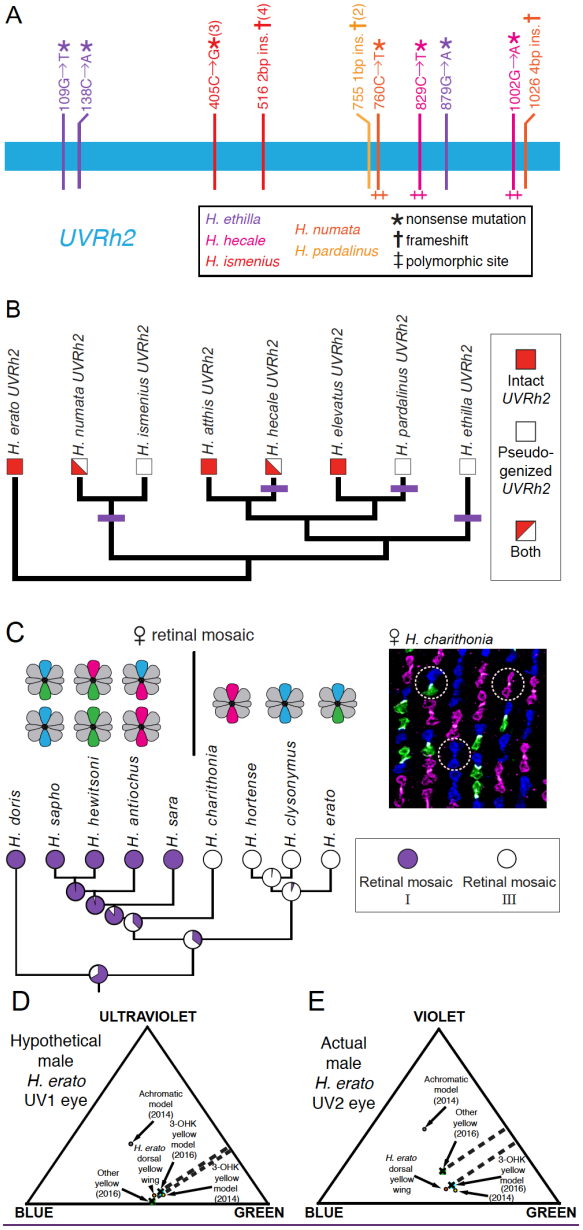

Fig. 4. Parallel loss of *UVRh2* mRNAs, reversible eye evolution in *Heliconius* and color space modeling. (A) Schematic of identified silvaniform loss-of-function mutations in *UVRh2.* Color of the mutation corresponds to the species in which it was identified. Symbols indicate the type of mutation. Numbers in parentheses indicate the number of individuals identified with the same mutation. No number indicates only one individual identified with the mutation. (B) Silvaniform species phylogeny with outgroup *H. erato*. Expressed transcripts were either intact (red boxes) or pseudogenized (white boxes). Some individuals were heterozygous (half red, half white). Purple bars indicate loss-of-function events. Phylogeny from Ref. (Kozak et al., 2015b). (C) *sara* and *erato* clade retinal mosaics mapped on to the species phylogeny with outgroup *H. doris*. *sara* clade females have retinal mosaic type III (purple circles) with six ommatidial types except for *H. charithonia*, with retinal mosaic I (white circles) and three ommatidial types. Inset shows immunostain of female *H. charithonia* with UV1 (green), UV2 (magenta) and blue opsins (blue). Maximum likelihood ancestral state reconstruction indicates loss of retinal mosaic III at the base of the *erato* and *sara* clades and re-gain of retinal mosaic III within the *sara* clade after divergence of *H. charithonia*. (D) Locations of natural and model yellow wing colors used in mate choice tests of Finkbeiner et al. (2014) and (2016) (Finkbeiner et al., 2014;

Finkbeiner et al., In Review) in chromaticity diagrams based on receptor signals for *H. erato*. Trichromatic plots for the three receptors in a hypothetical *H. erato* eye consisting of UV1 (ultraviolet), B (blue) and LW (green) receptors and (E) and for the actual male *H. erato* eye consisting of UV2 (violet), B and LW receptors. Dotted lines indicate the contribution of a UV-G (panel D) or V-G (panel E) chromatic mechanism to the detection of model colors used in behavioral tests. 3-OHK yellows are preferred by male *H. erato* over other yellow or grey (achromatic) colors in mate-choice tests.

Table 3. Mutations found in the *UVRh2* mRNAs of silvaniform clade species.

Species	Specimen ID	Sex	Full length *UVRh2?*	Nucleotide position	Type of mutation
H. atthis	AB304	M	yes		
	AB371	F	yes		
H. elevatus	GenBank accession: GU324676.1	?	yes		
H. ethilla	ENA accession: ERS235669	M	no	109	G-->T resulting in STOP
				138	C-->A resulting in STOP
				879	G-->A resulting in STOP
H. hecale	HHE26	F	yes/no	829	polymorphic stie, C-->T results in STOP
	HHE221	M	yes		
	HHE234	F	yes		
	HHE235	M	yes/no	1002	polymorphic site, T-->A results in STOP
H. ismenius	AB123	M	no	405	C-->G resulting in STOP
				516	2 bp insertion (GA) resulting in frameshift
	HIS13	F	no	405	C-->G resulting in STOP
				516	2 bp insertion (GA) resulting in frameshift
	HIS439	F	no	516	2 bp insertion (GA) resulting in frameshift
	HIS441	M	no	405	C-->G resulting in STOP
				516	2 bp insertion (GA) resulting in frameshift
H. numata	HNU473	F	yes/no	760	polymorphic site, C-->T results in STOP
				1026	4 bp insertion (ACAG)
	HNU475	M	yes		
	HNU501	M	yes		
	HNU503	F	?		missing full sequence due to low read count
H. pardalinus	ENA accession: ERS235667	M	no	755	1 bp insertion (A) resulting in frameshift
	ENA accession: ERS235668	M	no	755	1 bp insertion (A) resulting in frameshift

Despite evolving a new violet receptor at the base of the genus *Heliconius,* it appears that UV2 is being lost in some *melpomene* and silvaniform species and that these species have reverted to an ancestral UV1-expressing retina. In previous work we identified full-length *UVRh2* mRNA in *melpomene*-clade species (Briscoe et al., 2010), however *H. melpomene* and *H. cydno* lack a UV2-expressing photoreceptor cell in the compound eye (Figs. 1*G,H,* S1E,F). In *H. melpomene* whole heads (n = 4), full-length *UVRh2* mRNA is present in low levels, but otherwise encodes a full-length protein (Table 1). This suggests that *UVRh2* may be degraded before translation or lowly expressed in the brain in an extra-retinal receptor (Lampel et al., 2005).

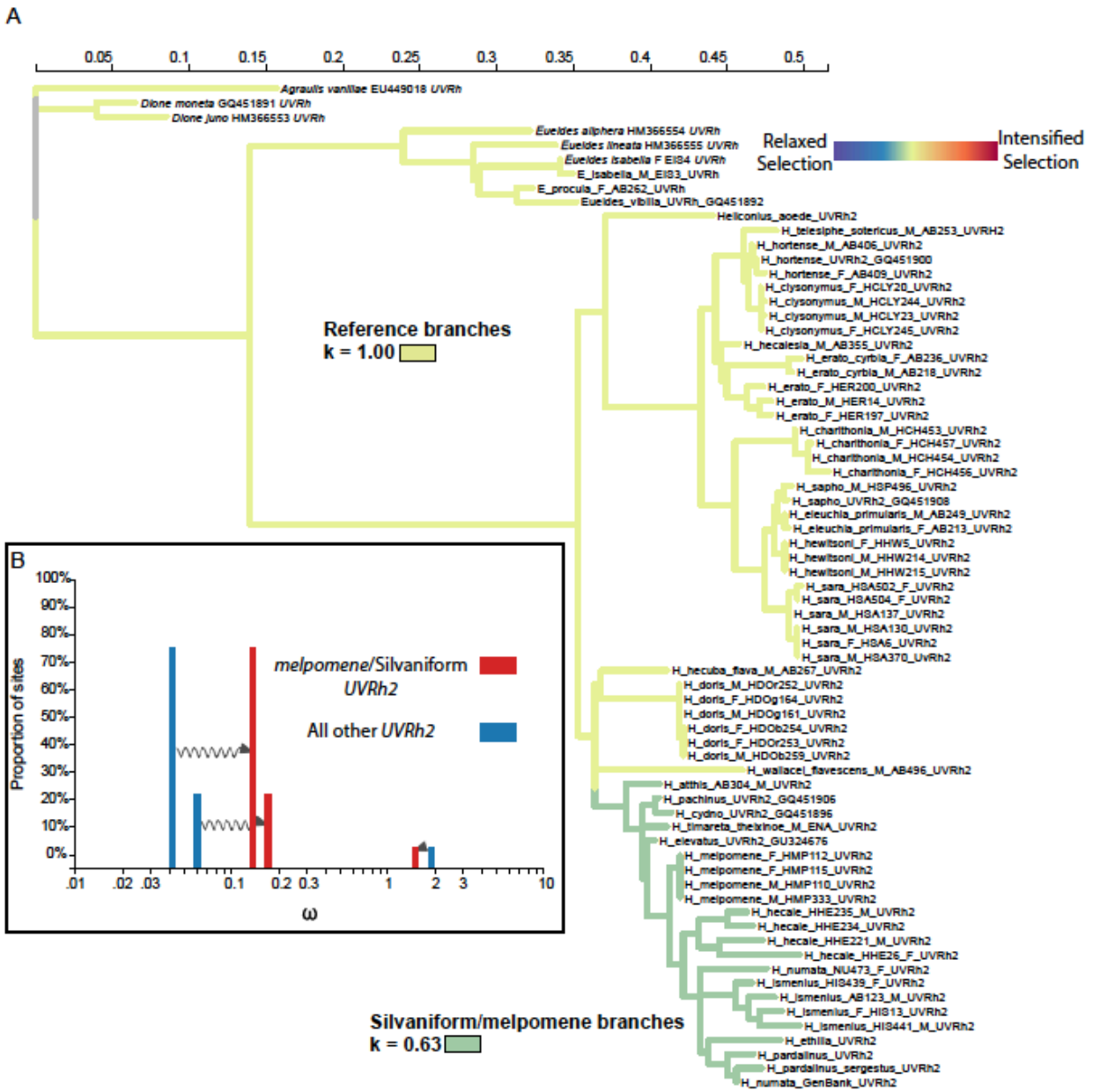

Figure 5. Selection is relaxed on *UVRh2* in *melpomene*/Silvaniform clades. (A) Gene tree showing test branches of silvaniform/*melpomene UVRh2* (light green) associated with a relaxation parameter, k < 1, relative to reference UVRh branches (yellow) set at k = 1, signifying relaxed selection in the test branches. The legend represents the relative value of the selection parameter, k, where cooler colors show relaxed selection and warmer colors show intensified selection. (B) Comparison of ω distributions from *melpomene*/silvaniform *UVRh2* branches (red) and all other *UVRh* branches (blue) under the alternative model of relaxed selection. Sites under positive ($\omega > 1$) or purifying ($\omega < 1$) selection in other *UVRh* branches move toward neutrality in the *melpomene*/silvaniform *UVRh2* branches ($\omega = 1$). In the BS-REL model, ω values for each site are binned into three ω distributions corresponding to sites under strong purifying, weakly purifying/nearly neutral, and positive selection, totaling 100% of all sites. Arrows indicate that when comparing sites in the reference branches to the corresponding sites in the test branches, all three ω distributions move toward neutrality in the test branches.

Unlike *H. melpomene*, several silvaniform species have pseudogenized *UVRh2* (Fig 4A,B, Table 3). Specifically, *H. atthis* and *H. elevatus* have full-length *UVRh2* mRNAs, whereas *H. pardalinus* and *H. ethilla* do not. RNA-Seq shows that *H. numata* and *H. hecale* are polymorphic for full-length and truncated *UVRh2* mRNAs (Fig. 4B, Table 3). Character mapping of *UVRh2* pseudogenes on a species phylogeny reveals at least four independent loss-of-function events in silvaniform *UVRh2* evolutionary history (Fig. 4).

Since *UVRh2* has lost its role in vision in the *melpomene*/silvaniform clades, we expect relaxed selection on *UVRh2* in these clades. We formally tested this hypothesis using RELAX in HYPHY (See Supplemental Experimental Procedures) (Wertheim, Murrell, Smith, Kosakovsky Pond, & Scheffler, 2015). We found a significant difference favoring a model where *melpomene*/silvaniform *UVRh2* genes are evolving under relaxed selection compared to the null model where *melpomene*/silvaniform branches have the same selection pressures as all other *UVRh2* branches (relaxation parameter, k = 0.6292; k = 1 means our test branch is evolving under either purifying or positive selection at the same rate as the reference branches at each site) (chi-squared test, p = 0.0005367, Fig. 5).

H. charithonia and the Independent Evolution of a Similar Retinal Mosaic in Two Clades

While some *Heliconius* lineages have lost UV2, it appears that the female-specific retinal mosaic expressing both UV opsins in six ommatidial types has evolved twice. Male *H. charithonia* are like other *sara* clade males (mosaic II, Figs. 1D,L, 4C). However females have three ommatidial types, similar to *erato*-clade females (mosaic I), rather than having the six ommatidial types (mosaic III) found in other *sara* clade females (Fig. 4C). In opsin

gene phylogenies (298 sequences total), *H. charithonia UVRh1, UVRh2, BRh,* and *LWRh* opsins each fall within a monophyletic clade together with other *sara* clade opsins (Fig. 6A-C). A species phylogeny using 634 orthologous genes from whole transcriptomes of five species, also gives strong support for *H. charithonia'*s inclusion within the *sara* clade (Fig. 6D). Maximum likelihood reconstruction of ancestral states suggests that female-specific *erato* mosaic I arose in the common ancestor to the *erato* and *sara* clades from mosaic III. After *H. charithonia* diverged, retinal mosaic III arose a second time in *sara*-clade females (Fig. 4C). The presence of retinal mosaic III in the distant basal and *sara* clade females implies an instance of reversion to a previously lost ancestral state.

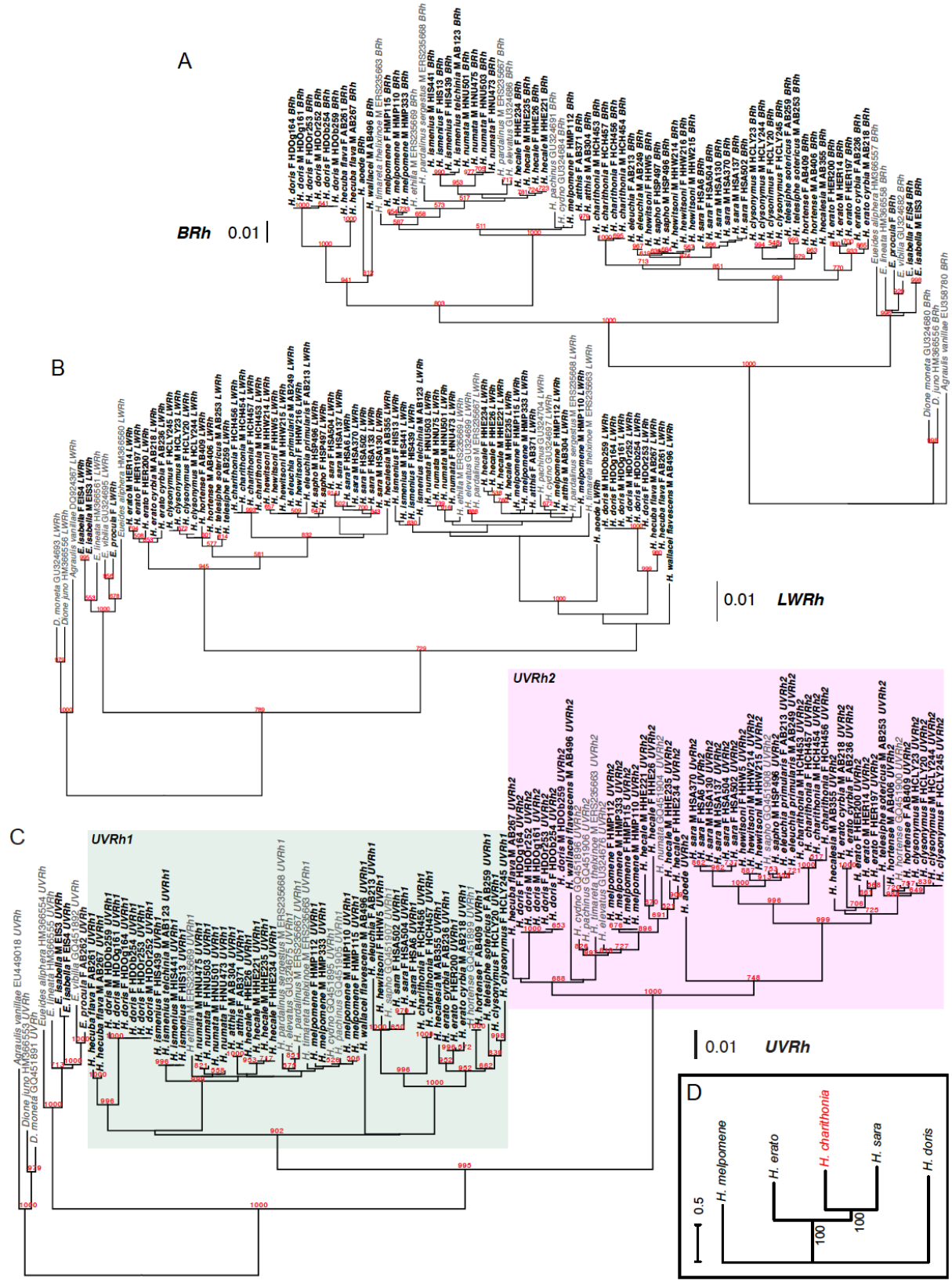

Figure 6. Phylogenies of opsin coding sequences and species phylogeny with *H. charithonia*. Opsin phylogenies were constructed using PhyML, using all available full-length mRNA sequences for the *BRh* (A),

LWRh (B)*, UVRh1,* and *UVRh2* (C) opsins found in *Heliconius* and outgroups. Bold indicates new sequences from RNA-seq data. Bootstrap values are out of 1000 and are shown only at branch support values greater than 500. Scale bar indicates branch length. (D) Maximum likelihood species phylogeny. 634 orthologous genes were concatenated and aligned to produce the species tree, giving strong support for *H. charithonia* as part of the *sara/sapho* clade.

Evolutionary History of the UV2 Receptor in the Genus *Heliconius*

To trace the evolution of the UV2 receptor and the specialized UV2-dominated eye of *erato* and *sara*-clade males, we reconstructed ancestral states for several traits (Fig. 7A-H). Maximum likelihood models indicate that both sexes probably had UV1 and UV2 cell subtypes in the common ancestor of *Heliconius* (Fig. 7A-D). Downregulation of *UVRh1* in males appears to have evolved once in the ancestor to the *erato* and *sara* clade (Fig. 7C). In the *sara*/*erato* clade ancestor, female eyes were restricted to three ommatidial types (mosaic I). After the divergence of *H. charithonia* from the rest of the *sara* clade, *sara* lineage female eyes evolved six ommatidial types (mosaic III) (Fig. 7G,H). As the *melpomene*/silvaniform lineage split from the rest of the genus, both sexes lost the UV2 cell subtype (Fig. 7B,D), giving rise to retinal mosaic V. Relaxed selection of *UVRh2* resulted in multiple parallel pseudogenizations following the loss of the UV2 cell as the silvaniforms diverged from the *melpomene* clade (Figs. 2E-H, 4A,B, 7F).

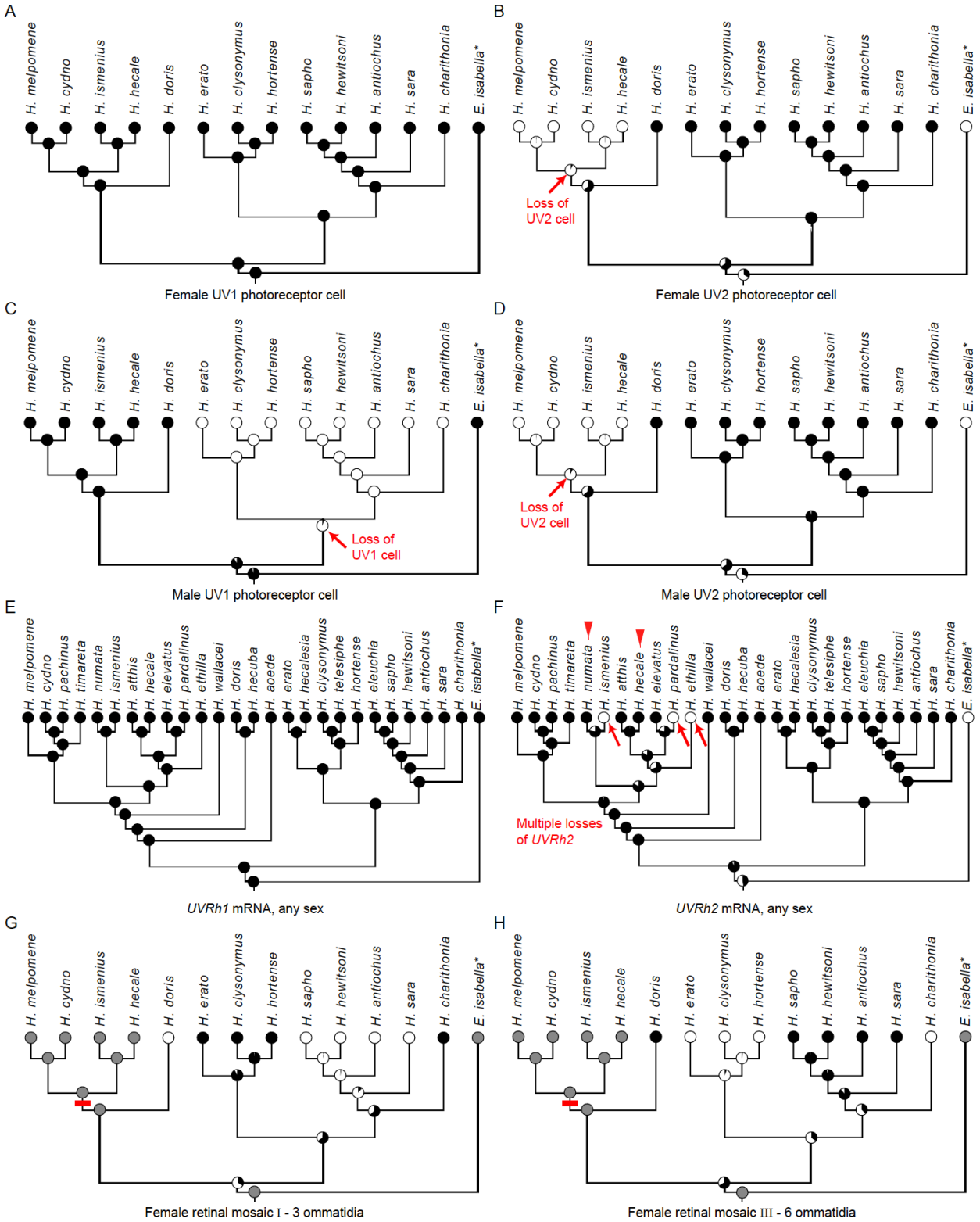

Figure 7. Maximum likelihood ancestral state reconstructions for traits associated with *UVRh1* and *UVRh2* opsin expression. (*A-H*) Reconstructions were implemented in Mesquite using species for which either mRNA or protein expression data were available. Black circles indicate presence of trait; white circles indicate absence. Gray circles indicate species that were not used in Maximum Likelihood (ML) estimates. Pie charts at ancestral nodes signify ML ratios indicating whether the trait was present or absent at that node. (*A*)

All females have a UV1-expressing PRC. (*B*) Arrow indicates node where the UV2 PRC was inferred to be absent in the female ancestor of the *melpomene* and silvaniform clades. (*C*) Arrow indicates node where the UV1 PRC was lost in the male ancestor of the *sara* and *erato* clades. (*D*) Arrow indicates node where the UV2 PRC was lost in the male ancestor of the *melpomene* and silvaniform clades. (*E*) All members of *Heliconius* express *UVRh1* mRNA in at least one sex. (*F*) *UVRh2* is expressed in at least one sex for most species, except for three silvaniforms indicated by red arrows. Arrowheads indicate species that express both functional and non-functional *UVRh2*. These species were coded as having the trait present. (*G, H*) The female ancestor at the base of the genus *Heliconius* most likely expressed eye-type I, with six ommatidia. At the base of the *sara* and *erato* clades, eye-type I switched to eye-type V, with three ommatidia in females. After *H. charithonia* diverged from the other species in the *sara* group, eye-type V switched back to eye-type I where females again expressed 6 ommatidia. Red bar indicates secondary loss of UV2 PRC in the *melpomene* and silvaniform groups, and so they were excluded from the maximum likelihood analysis. Asterisk, *E. isabella* lacks two UV opsins but is coded as UV1 present, due to conserved UV1 antibody staining, though is excluded from analysis in *G* and *H* due to lack of both opsins.

Modeling of 3-OHK Yellow Coloration and the Benefit of the Violet Receptor

The newly-evolved violet receptor (UV2) appears in the majority of *Heliconius* lineages in both sexes (n=12 species, Table 1), despite being lost in the *melpomene* and silvaniform lineages (n=5 species, Table 1, Fig. 8). What might be the benefit of evolving a new violet receptor and a visual system making use of this receptor? While the UV2 receptor appears in retinal mosaics with three, four and even six kinds of ommatidia within *Heliconius,* functionally the biggest impact on color vision is expected to be due to its spectral tuning. Previously we used modelling to show that a color vision system similar to the female *H. erato* eye consisting of UV, V, B and L receptors would outperform both avian and butterfly visual systems lacking the duplicated UVs in classifying *Heliconius* 3-hydroxykynurenine (3-OHK) yellow from other yellow coloration (Bybee et al., 2012). These results suggested that the co-evolution of the duplicated UVs together with 3-OHK coloration was beneficial for conspecific communication in the context of mimicry. Why then would male *H. erato* only express V, B and L photoreceptors?

To understand the potential benefit of the specialized male eye, we performed mate choice experiments with achromatic and chromatic stimuli resembling *Heliconius* 3-OHK

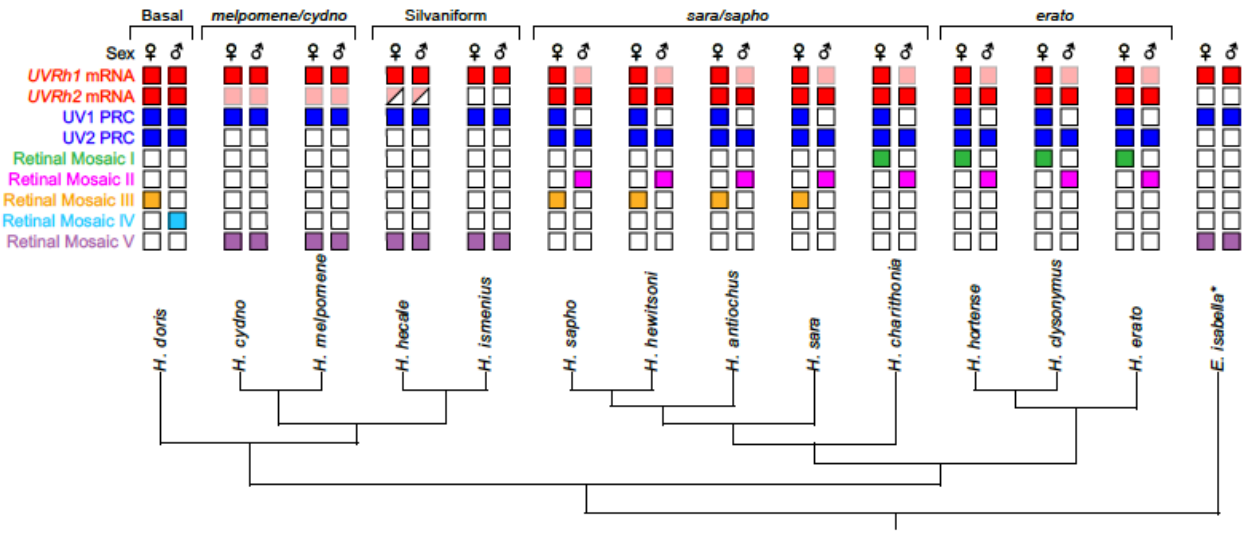

Figure 8. Summary of UV opsin character states on the *Heliconius* phylogeny. Each trait was scored for presence (filled box) or absence (open box) based on immunohistochemistry of adult eyes and mRNA-Seq of adult heads. Some species are polymorphic for the trait (half-filled boxes). For all species, traits are listed for both sexes. *UVRh1* and *UVRh2* mRNAs (red) signify full-length transcripts for UV1 and UV2 opsins respectively. Lighter-shaded (pink) boxes indicate low-level mRNA expression. mRNA expression data only for six other species are given in Table 1. Photoreceptor cell subtypes found in either males or females are indicated according to UV1 or UV2 opsin expression (dark blue). Retinal mosaic types I-V (green, magenta, orange, light blue and purple), characterized by the type of ommatidia expressed in each species and sex, are also mapped on the species phylogeny of Kozak et al. (Kozak et al., 2015b).

yellow and other yellows (Finkbeiner et al., 2014; Finkbeiner et al., In Review) and mapped these loci in the trichromatic color space of male *H. erato* with V, B and L receptors. Here we compare the distances between these loci against the loci distances in the color space of a hypothetical *H. erato* eye with UV, B and L receptors. Evidence suggests that a V-L chromatic mechanism provides superior separation of the *Heliconius* yellow preferred by *H. erato* males from the non-preferred other yellow, compared to a hypothetical UV-L mechanism (Fig 4D,E, dotted lines). Therefore, the use of a distinctive yellow wing pigment for signaling in *Heliconius* helps explain the origins of the specialized male *H. erato* eye, in which a V receptor replaced an ancestral UV receptor.

The loss of UV2 in some *Heliconius* lineages, nonetheless, suggests costs associated with evolving a new color receptor. Both UV2 cell loss and *UVRh2* pseudogenization in the *melpomene*/silvaniform clades represent recent and ongoing processes. If

*melpomene/*silvaniform species retain a UV1 receptor with similar sensitivity as *H. erato* UV1, these species may be less able to discern variation in yellow wing coloration than species in the *erato/sara/doris* clades. Interestingly, rampant hybridization exists between species in the *melpomene* and silvaniform clades. We propose that loss of UV2 in these clades many have contributed to increased hybridization via reduced ability to recognize conspecifics (Consortium, 2012; Estrada & Jiggins, 2008). The multiple instances of pseudogenizing mutations in *UVRh2* suggests that other kinds of cues such as olfaction, may play an increasingly critical role in mate recognition and foraging in species that have lost the duplicate UV opsin.

In summary, we have identified an unprecedented diversity of opsin expression patterns and retinal mosaics among closely related species. Changes in opsin expression have resulted in multiple forms of sexual dimorphism, multiple parallel losses of UV cells and the *UVRh2* gene, and repeated independent evolution of retinal mosaics (Fig. 8). Nonetheless a majority of males and females retain the newly-evolved UV2 opsin, which facilitates discrimination of 3-OHK yellow from other yellow coloration in behavioral tests. Our findings substantiate and elaborate our understanding of the origins and spectral tuning of a new opsin-based violet receptor and its relationship to yellow signaling in *Heliconius*.

References

Anisimova, M., Gil, M., Dufayard, J. F., Dessimoz, C., & Gascuel, O. (2011). Survey of branch support methods demonstrates accuracy, power, and robustness of fast likelihood-based approximation schemes. *Syst Biol, 60*(5), 685-699. doi:10.1093/sysbio/syr041

Arikawa, K. (2003). Spectral organization of the eye of a butterfly, *Papilio*. *J Comp Physiol A Neuroethol Sens Neural Behav Physiol, 189*(11), 791-800. doi:10.1007/s00359-003-0454-7

Arikawa, K., Wakakuwa, M., Qiu, X., Kurasawa, M., & Stavenga, D. G. (2005). Sexual dimorphism of short-wavelength photoreceptors in the small white butterfly, *Pieris rapae crucivora*. *J Neurosci, 25*(25),

5935-5942. doi:10.1523/JNEUROSCI.1364-05.2005
Bok, M. J., Porter, M. L., & Cronin, T. W. (2015). Ultraviolet filters in stomatopod crustaceans: diversity, ecology and evolution. *J Exp Biol, 218*(Pt 13), 2055-2066. doi:10.1242/jeb.122036
Briscoe, A. D., Bybee, S. M., Bernard, G. D., Yuan, F., Sison-Mangus, M. P., Reed, R. D., . . . Chiao, C. C. (2010). Positive selection of a duplicated UV-sensitive visual pigment coincides with wing pigment evolution in *Heliconius* butterflies. *Proc Natl Acad Sci U S A, 107*(8), 3628-3633. doi:10.1073/pnas.0910085107
Bybee, S. M., Yuan, F., Ramstetter, M. D., Llorente-Bousquets, J., Reed, R. D., Osorio, D., & Briscoe, A. D. (2012). UV photoreceptors and UV-yellow wing pigments in *Heliconius* butterflies allow a color signal to serve both mimicry and intraspecific communication. *Am Nat, 179*(1), 38-51. doi:10.1086/663192
Carleton, K. L., Parry, J. W., Bowmaker, J. K., Hunt, D. M., & Seehausen, O. (2005). Colour vision and speciation in Lake Victoria cichlids of the genus *Pundamilia*. *Mol Ecol, 14*(14), 4341-4353. doi:10.1111/j.1365-294X.2005.02735.x
Chen, P.-J., Awata, H., Matsushita, A., Yang, E.-C., & Arikawa, K. (2016). Extreme spectral richness in the eye of the common bluebottle butterfly, *Graphium sarpedon*. *Frontiers in Ecology and Evolution, 4*. doi:10.3389/fevo.2016.00018
Consortium, H. G. (2012). Butterfly genome reveals promiscuous exchange of mimicry adaptations among species. *Nature, 487*(7405), 94-98. doi:10.1038/nature11041
Cook, T., Pichaud, F., Sonneville, R., Papatsenko, D., & Desplan, C. (2003). Distinction between color photoreceptor cell fates Is controlled by Prospero in *Drosophila*. *Developmental Cell, 4*(6), 853-864. doi:10.1016/s1534-5807(03)00156-4
Cronin, T. W., & Marshall, N. J. (1989). A retina with at least ten spectral types of photoreceptors in a mantis shrimp. *Nature, 339*(6220), 137-140. doi:10.1038/339137a0
Domingos, P. M., Brown, S., Barrio, R., Ratnakumar, K., Frankfort, B. J., Mardon, G., . . . Mollereau, B. (2004). Regulation of R7 and R8 differentiation by the *spalt* genes. *Dev Biol, 273*(1), 121-133. doi:10.1016/j.ydbio.2004.05.026
Estrada, C., & Jiggins, C. D. (2008). Interspecific sexual attraction because of convergence in warning colouration: is there a conflict between natural and sexual selection in mimetic species? *J Evol Biol, 21*(3), 749-760. doi:10.1111/j.1420-9101.2008.01517.x
Finkbeiner, S. D., Briscoe, A. D., & Reed, R. D. (2014). Warning signals are seductive: relative contributions of color and pattern to predator avoidance and mate attraction in *Heliconius* butterflies. *Evolution, 68*(12), 3410-3420. doi:10.1111/evo.12524
Finkbeiner, S. D., Fishman, D. A., Osorio, D., & Briscoe, A. D. (In Review). How butterflies use special pigments to signal during cloudy weather. *Proceedings of the Royal Society B: Biological Sciences*.
Franceschini, N., Hardie, R., Ribi, W., & Kirschfeld, K. (1981). Sexual dimorphism in a photoreceptor. *Nature, 291*(5812), 241-244. doi:10.1038/291241a0
Frentiu, F. D., Bernard, G. D., Sison-Mangus, M. P., Brower, A. V., & Briscoe, A. D. (2007). Gene duplication is an evolutionary mechanism for expanding spectral diversity in the long-wavelength photopigments of butterflies. *Mol Biol Evol, 24*(9), 2016-2028. doi:10.1093/molbev/msm132
Futahashi, R., Kawahara-Miki, R., Kinoshita, M., Yoshitake, K., Yajima, S., Arikawa, K., & Fukatsu, T. (2015). Extraordinary diversity of visual opsin genes in dragonflies. *Proc Natl Acad Sci U S A, 112*(11), E1247-1256. doi:10.1073/pnas.1424670112
Guindon, S., Dufayard, J. F., Lefort, V., Anisimova, M., Hordijk, W., & Gascuel, O. (2010). New algorithms and methods to estimate maximum-likelihood phylogenies: assessing the performance of PhyML 3.0. *Systematic Biology, 59*(3), 307-321. doi:10.1093/sysbio/syq010
Hofmann, C. M., & Carleton, K. L. (2009). Gene duplication and differential gene expression play an important role in the diversification of visual pigments in fish. *Integr Comp Biol, 49*(6), 630-643. doi:10.1093/icb/icp079
Kelber, A., Vorobyev, M., & Osorio, D. (2003). Animal colour vision – behavioural tests and physiological concepts. *Biological Reviews of the Cambridge Philosophical Society, 78*(1), 81-118. doi:10.1017/s1464793102005985
Kent, W. J. (2002). BLAT--the BLAST-like alignment tool. *Genome Research, 12*, 656-664. doi:10.1101/gr.229202
Kozak, K. M., Wahlberg, N., Neild, A., Dasmahapatra, K. K., Mallet, J., & Jiggins, C. D. (2015a). Multilocus Species Trees Show the Recent Adaptive Radiation of the Mimetic Heliconius Butterflies. *Systematic Biology*. doi:10.1093/sysbio/syv007

Kozak, K. M., Wahlberg, N., Neild, A. F., Dasmahapatra, K. K., Mallet, J., & Jiggins, C. D. (2015b). Multilocus species trees show the recent adaptive radiation of the mimetic heliconius butterflies. *Syst Biol, 64*(3), 505-524. doi:10.1093/sysbio/syv007

Lampel, J., Briscoe, A. D., & Wasserthal, L. T. (2005). Expression of UV-, blue-, long-wavelength-sensitive opsins and melatonin in extraretinal photoreceptors of the optic lobes of hawk moths. *Cell Tissue Res, 321*(3), 443-458. doi:10.1007/s00441-004-1069-1

Larkin, M. A., Blackshields, G., Brown, N. P., Chenna, R., McGettigan, P. A., McWilliam, H., . . . Higgins, D. G. (2007). Clustal W and Clustal X version 2.0. *Bioinformatics, 23*(21), 2947-2948. doi:10.1093/bioinformatics/btm404

Li, H., Handsaker, B., Wysoker, A., Fennell, T., Ruan, J., Homer, N., . . . Genome Project Data Processing, S. (2009). The Sequence Alignment/Map format and SAMtools. *Bioinformatics, 25*(16), 2078-2079. doi:10.1093/bioinformatics/btp352

Lunter, G., & Goodson, M. (2011). Stampy: a statistical algorithm for sensitive and fast mapping of Illumina sequence reads. *Genome Res, 21*(6), 936-939. doi:10.1101/gr.111120.110

Maddison, W. P., & Maddison, D. R. (2011). Mesquite: A modular system for evolutionary analysis (Version 2.75). Retrieved from http://mesquiteproject.org/

McCulloch, K. J., Osorio, D., & Briscoe, A. D. (2016a). Determination of photoreceptor cell spectral sensitivity in an insect model from *in vivo* intracellular recordings. *J Vis Exp*(108). doi:10.3791/53829

McCulloch, K. J., Osorio, D., & Briscoe, A. D. (2016b). Sexual dimorphism in the compound eye of *Heliconius erato*: a nymphalid butterfly with at least five spectral classes of photoreceptor. *J Exp Biol*. doi:10.1242/jeb.136523

Menzel, J. G., Wunderer, H., & Stavenga, D. G. (1991). Functional morphology of the divided compound eye of the honeybee drone (*Apis mellifera*). *Tissue Cell, 23*(4), 525-535.

Mikeladze-Dvali, T., Wernet, M. F., Pistillo, D., Mazzoni, E. O., Teleman, A. A., Chen, Y. W., . . . Desplan, C. (2005). The growth regulators *warts/lats* and *melted* interact in a bistable loop to specify opposite fates in *Drosophila* R8 photoreceptors. *Cell, 122*(5), 775-787. doi:10.1016/j.cell.2005.07.026

Ogawa, Y., Awata, H., Wakakuwa, M., Kinoshita, M., Stavenga, D. G., & Arikawa, K. (2012). Coexpression of three middle wavelength-absorbing visual pigments in sexually dimorphic photoreceptors of the butterfly *Colias erate*. *J Comp Physiol A Neuroethol Sens Neural Behav Physiol, 198*(12), 857-867. doi:10.1007/s00359-012-0756-8

Ogawa, Y., Kinoshita, M., Stavenga, D. G., & Arikawa, K. (2013). Sex-specific retinal pigmentation results in sexually dimorphic long-wavelength-sensitive photoreceptors in the eastern pale clouded yellow butterfly, *Colias erate*. *J Exp Biol, 216*(Pt 10), 1916-1923. doi:10.1242/jeb.083485

Perry, M., Kinoshita, M., Saldi, G., Huo, L., Arikawa, K., & Desplan, C. (2016). Molecular logic behind the three-way stochastic choices that expand butterfly colour vision. *Nature*. doi:10.1038/nature18616

Pond, S. L., Frost, S. D., & Muse, S. V. (2005). HyPhy: hypothesis testing using phylogenies. *Bioinformatics, 21*(5), 676-679. doi:10.1093/bioinformatics/bti079

Schulz, M. H., Zerbino, D. R., Vingron, M., & Birney, E. (2012). Oases: robust *de novo* RNA-seq assembly across the dynamic range of expression levels. *Bioinformatics, 28*(8), 1086-1092. doi:10.1093/bioinformatics/bts094

Sison-Mangus, M. P., Bernard, G. D., Lampel, J., & Briscoe, A. D. (2006). Beauty in the eye of the beholder: the two blue opsins of lycaenid butterflies and the opsin gene-driven evolution of sexually dimorphic eyes. *J Exp Biol, 209*(Pt 16), 3079-3090. doi:10.1242/jeb.02360

Stamatakis, A. (2006). RAxML-VI-HPC: maximum likelihood-based phylogenetic analyses with thousands of taxa and mixed models. *Bioinformatics, 22*(21), 2688-2690. doi:10.1093/bioinformatics/btl446

Struwe, G. (1972a). Spectral sensitivity of single photoreceptors in the compound eye of a tropical butterfly (*Heliconius numata*). *Journal of Comparative Physiology, 79*(2), 197-201. doi:10.1007/bf00697772

Struwe, G. (1972b). Spectral sensitivity of the compound eye in butterflies (*Heliconius*). *Journal of Comparative Physiology, 79*(2), 191-196. doi:10.1007/bf00697771

Tamura, K., Peterson, D., Peterson, N., Stecher, G., Nei, M., & Kumar, S. (2011). MEGA5: molecular evolutionary genetics analysis using maximum likelihood, evolutionary distance, and maximum parsimony methods. *Mol Biol Evol, 28*(10), 2731-2739. doi:10.1093/molbev/msr121

Wang, B., Xiao, J. H., Bian, S. N., Niu, L. M., Murphy, R. W., & Huang, D. W. (2013). Evolution and expression plasticity of opsin genes in a fig pollinator, *Ceratosolen solmsi*. *PLoS One, 8*(1), e53907. doi:10.1371/journal.pone.0053907

Wernet, M. F., Mazzoni, E. O., Celik, A., Duncan, D. M., Duncan, I., & Desplan, C. (2006). Stochastic *spineless* expression creates the retinal mosaic for colour vision. *Nature, 440*(7081), 174-180. doi:10.1038/nature04615

Wernet, M. F., Perry, M. W., & Desplan, C. (2015). The evolutionary diversity of insect retinal mosaics: common design principles and emerging molecular logic. *Trends Genet, 31*(6), 316-328. doi:10.1016/j.tig.2015.04.006

Wertheim, J. O., Murrell, B., Smith, M. D., Kosakovsky Pond, S. L., & Scheffler, K. (2015). RELAX: detecting relaxed selection in a phylogenetic framework. *Mol Biol Evol, 32*(3), 820-832. doi:10.1093/molbev/msu400

Zaccardi, G., Kelber, A., Sison-Mangus, M. P., & Briscoe, A. D. (2006). Color discrimination in the red range with only one long-wavelength sensitive opsin. *J Exp Biol, 209*(Pt 10), 1944-1955. doi:10.1242/jeb.02207

Zerbino, D. R., & Birney, E. (2008). Velvet: algorithms for de novo short read assembly using de Bruijn graphs. *Genome Res, 18*(5), 821-829. doi:10.1101/gr.074492.107

SUMMARY AND CONCLUSIONS

Heliconius butterflies have highly diverse retinal mosaics that are both clade- and sex-specific across the genus. From work presented here and previous behavioral work in the lab, it is likely that these differences in retinal mosaics correspond to an equally diverse set of visual systems among these closely-related butterflies. As part of this work, I have attempted to develop a well-established but difficult to reproduce technique, and make it more accessible to other visual and sensory ecologists and biologists. I used this technique along with opsin protein staining to characterize the phenotypic effects of a gene duplication in *Heliconius erato*. *H. erato*, males and females have photoreceptors with max sensitivity in the UV (UV2 cell, 390 nm) blue (470 nm) green (555 nm) and red (590 nm). I unexpectedly discovered that males lack UV1 opsin, and that only females have a UV cell with max sensitivity at 355 nm. I next expanded my investigation to include 23 different species, measuring opsin protein and mRNA expression, and found that the UV opsin gene duplication had led to extensive variation in the retinal mosaics of *Heliconius* species. *Heliconius* clade- and sex-specific opsin expression patterns have led to at least five distinct retinal mosaics within the genus. Multiple independent losses of expression in one or both sexes are also common and clade-specific. Reconstructing the evolutionary history of vision-related phenotypes associated with opsin expression, I found that *Heliconius* have independently evolved the same retinal mosaic in at least two clades.

Through a combination of sensory physiology, protein spatial expression, and gene expression studies we were able to characterize different aspects of the specific patterns of diversity within the genus, which any of these techniques alone would miss. This highlights

the advantage of using a multifaceted approach to gain a better understanding of both genetic and phenotypic evolutionary changes, rather than relying on sequencing and prediction of protein function by itself. Although *Heliconius* has been a major model system for the evolution of wing patterns, reproductive isolation, and speciation, until now little was known about the visual system in the genus. Characterization of the effects of the UV opsin gene duplication presented in this dissertation has shown that these butterflies have much more complex eyes than previously thought and this work will give new insight into how mate choice and visual behavior affect *Heliconius* evolution. Many questions related to the evolution of visual systems in *Heliconius* remain to be solved, which will open many new directions for research in this well-studied system. Current work in the lab is investigating tuning of spectral sensitivities and visual behavior in the UV range in several other *Heliconius* species. Further work should determine the selection pressures that have caused differences in *Heliconius* retinal mosaics, as well as the evolutionary developmental mechanisms of opsin expression and retinal mosaic diversity.

In this work, I have identified that the UV opsin gene duplication has resulted in neofunctionalization, and this has altered the course of *Heliconius* visual trait evolution during speciation generating a high level of diversity among *Heliconius* retinal mosaics. In my investigation of the *H. erato* eye, I identified a novel form of sexual dimorphism in any insect eye so far investigated, via the loss of UVRh1, which is also found in other *erato* and *sara* clade males. *Heliconius* diversity in retinal mosaics is unprecedented in other taxa well known for diversity in color receptors. By comparatively investigating *Heliconius* expression patterns, I have captured a unique snapshot of the initial steps of divergent

evolution of color receptors following gene duplication; a process which through time, has resulted in the grand diversity of visual systems across all animals.

APPENDIX A

Materials for Setup of an Electrophysiology Rig

Name of Material/ Equipment	Company	Catalog Number	Comments/Description
Butterfly pupae			Several local species available, need USDA permits for shipping. Carolina Bio Supply has several insect species that may be ordered within the U.S. without the need for additional permits
Large plastic cylinder			Any chamber that remains humidified will work
Insect pins, size 2	BioQuip	1208B2	
100% Desert Mesquite Honey	Trader Joe's		Any honey or sucrose solution will work
Xenon Arc Lamp	Oriel Instruments	66003	Oriel is now a part of Newport Corporation
Universal Power Supply	Oriel Instruments	68805	Oriel is now a part of Newport Corporation
Optical Track	Oriel Instruments	11190	Oriel is now a part of Newport Corporation
Rail Carrier, Large (2x)	Oriel Instruments	11641	Oriel is now a part of Newport Corporation
Rail Carrier, Small (4x)	Oriel Instruments	11647	Oriel is now a part of Newport Corporation
Thread Adaptor, 8-32 Male to 1/4-20 Male, pack of 10	Newport Corporation	TA-8Q20-10	
Optical Mounting Post, 1.0 in., 0.5 in. Dia. Stainless, 8-32 & 1/4-20 (5x)	Newport Corporation	SP-1	
No Slip Optical Post Holder, 2 in., 0.5 in. Diameter Posts, 1/4-20 (5x)	Newport Corporation	VPH-2	
Fixed lens mount, 50.8 mm	Newport Corporation	LH-2	
Fixed lens mount, 25.4 mm	Newport Corporation	LH-1	
Condenser lens assembly	Newport Corporation	60006	
Convex silica lens, 50.8 mm	Newport Corporation	SPX055	
Six Position Filter Wheel, x2	Newport Corporation	FW1X6	
Filter Wheel Mount Hub	Newport Corporation	FWM	
Concave silica lens, 25.4 mm	Newport Corporation	SPC034	
Collimator holder	Newport Corporation	77612	
Collimating beam probe	Newport Corporation	77644	
Ferrule Converter, SMA Termination to 11 mm Standard Ferrule	Newport Corporation	77670	This adapter allows the fiber optic to fit into the collimator holder
600 µm diameter UV-vis fiber obtic cable	Oriel Instruments	78367	Oriel is now a part of Newport Corporation
Shutter with drive unit	Uniblitz	100-2B	
UV Fused Silica Metallic ND Filter, 0.1 OD	Newport	FRQ-ND01	
UV Fused Silica Metallic ND Filter, 0.3 OD	Newport	FRQ-ND03	
UV Fused Silica Metallic ND Filter, 0.5 OD	Newport	FRQ-ND05	
UV Fused Silica Metallic ND Filter, 1.0 OD	Newport	FRQ-ND10	
UV Fused Silica Metallic ND Filter, 2.0 OD	Newport	FRQ-ND30	
UV Fused Silica Metallic ND Filter, 3.0 OD	Newport	FRQ-ND50	
LS-1-Cal lamp	Ocean Optics	LS-1-Cal	
Spectrometer	Ocean Optics	USB-2000	
SpectraSuite Software	Ocean Optics		
Interference bandpass filter, 300 nm	Edmund Optics	67749	
Interference bandpass filter, 310 nm	Edmund Optics	67752	
Interference bandpass filter, 320 nm	Edmund Optics	67754	
Interference bandpass filter,	Edmund Optics	67756	

330 nm		
Interference bandpass filter, 340 nm	Edmund Optics	65614
Interference bandpass filter, 350 nm	Edmund Optics	67757
Interference bandpass filter, 360 nm	Edmund Optics	67760
Interference bandpass filter, 370 nm	Edmund Optics	67761
Interference bandpass filter, 380 nm	Edmund Optics	67762
Interference bandpass filter, 390 nm	Edmund Optics	67763
Interference bandpass filter, 400 nm	Edmund Optics	65732
Interference bandpass filter, 410 nm	Edmund Optics	65619
Interference bandpass filter, 420 nm	Edmund Optics	65621
Interference bandpass filter, 430 nm	Edmund Optics	65622
Interference bandpass filter, 440 nm	Edmund Optics	67764
Interference bandpass filter, 450 nm	Edmund Optics	65625
Interference bandpass filter, 460 nm	Edmund Optics	67765
Interference bandpass filter, 470 nm	Edmund Optics	65629
Interference bandpass filter, 480 nm	Edmund Optics	65630
Interference bandpass filter, 492 nm	Edmund Optics	65633
Interference bandpass filter, 500 nm	Edmund Optics	65634
Interference bandpass filter, 510 nm	Edmund Optics	65637
Interference bandpass filter, 520 nm	Edmund Optics	65639
Interference bandpass filter, 532 nm	Edmund Optics	65640
Interference bandpass filter, 540 nm	Edmund Optics	65642
Interference bandpass filter, 550 nm	Edmund Optics	65644
Interference bandpass filter, 560 nm	Edmund Optics	67766
Interference bandpass filter, 570 nm	Edmund Optics	67767
Interference bandpass filter, 580 nm	Edmund Optics	65646
Interference bandpass filter, 589 nm	Edmund Optics	65647
Interference bandpass filter, 600 nm	Edmund Optics	65648
Interference bandpass filter, 610 nm	Edmund Optics	65649
Interference bandpass filter, 620 nm	Edmund Optics	65650
Interference bandpass filter, 632 nm	Edmund Optics	65651
Interference bandpass filter, 640 nm	Edmund Optics	65653
Interference bandpass filter, 650 nm	Edmund Optics	65655
Interference bandpass filter, 660 nm	Edmund Optics	67769
Interference bandpass filter, 671 nm	Edmund Optics	65657
Interference bandpass filter,	Edmund Optics	67770

680 nm			
Interference bandpass filter, 690 nm	Edmund Optics	65659	
Interference bandpass filter, 700 nm	Edmund Optics	67771	
Faraday cage			Any metal structure will work that can be grounded and that fits the experimental setup.
Stereomicroscope, 6x, 12x, 25x, 50x magnification	Wild Heerbrugg	Wild M5	Any Stereomicroscope will do
Microscope stand with swinging arm and heavy base	McBain Instruments		Any heavy base with arm will do
Cardan arm			Custom built, See Figure 4
Fiber-lite high intensity illuminator	Dolan-Jenner	MI-150	For lighting specimen
Fiber-lite goose-neck light guide	Dolan-Jenner	EEG 2823	Any goose-neck light guide will do
Marble table			
Raised wooden table			Hole should be cut through this table so that the sandbox can rest on the marble table underneath
Wooden box filled with sand			custom built, any box with sand
Manipulator	Carl Zeiss - Jena		
Electrode holder			
Specimen stage			
Alligator clip wires for grounding			
Insulated copper wire			
Silver wire, 0.125 mm diameter	World Precision Instruments	AGW0510	
BNC cables			
Preamplifier with headstage	Dagan Corporation	IX2-700	
Humbug Noise reducer	Quest Scientific	Humbug	
Oscilloscope, 30MHz, 2CH, Dual Trace, Alt-triggering, without probe	EZ Digital	os-5030	
BNC T-adapter			
Powerlab hardware 2/20	ADI instruments	ML820	
Labchart software	ADI instruments	Chart 5	
10 MHz Pulse Generator	BK Precision	4030	
Glass pipette puller	Sutter Instruments	P-87	
Borosillicate glass capillaries with filament	World Precision Instruments	1B120F-4	
Potassium chloride, 3 M			
Slotted plastic tube			
Low melting temperature wax			
Soldering Iron	Weller		
Platform with ball-and-socket magnetic base	Hama photo and video		
Double edge carbon steel, breakable razor blade	Electron Microscopy Sciences	72004	
Vaseline			
Microsoft Excel	Microsoft		

APPENDIX B

All Specimens, Locations, and Opsins Sequenced

Tissue type, sequencing type, gene name, accession number are listed when possible. Newly sequenced individuals are in bold.

Species	Locality	Specimen ID	Sex	Tissue type	Library type	Illumina Sequencing	Gene Name	ENA Run Accession Number	Comments
Agraulis vanillae	Huntington Beach, CA						*LWRh*	DQ924367	Frentiu et al. 2007
							BRh	EU358780	Pohl et al. 2009
							UVRh	EU449018	Pohl et al. 2009
Dione juno	Oaxaca, México						*LWRh*	HM366559	This Study
							BRh	HM366556	This Study
							UVRh	HM366553	Bybee et al. 2012
D. moneta	El Guajolote, Loxicha, Oaxaca, Mexico	AB55					*LWRh*	GU324693	Yuan et al. 2010
							BRh	GU324680	Yuan et al. 2010
							UVRh	GQ451891	Yuan et al. 2010
Eueides aliphera	Oaxaca, México						*LWRh*	HM366560	This Study
							BRh	HM366557	This Study
							UVRh	HM366554	Bybee et al. 2012
E. isabella	The Butterfly Farm - Costa Rica Entomological Supply	**EIS3**	♂	Head	RNA-seq	100 bp PE	***LWRh***		
							BRh		
							UVRh		
	The Butterfly Farm - Costa Rica Entomological Supply	**EIS4**	♀	Head	RNA-seq	100 bp PE	***LWRh***		
							BRh		
							UVRh		
E. lineata	Oaxaca, México						*LWRh*	HM366561	This Study
							BRh	HM366558	This Study
							UVRh	HM366555	Bybee et al. 2012
E. procula	The Butterfly Farm - Costa Rica Entomological Supply	**AB262**					***LWRh***		
							BRh		
							UVRh		
E. vibilia	Yurimaguas, Peru	R83					*LWRh*	GU324695	Yuan et al. 2010
							BRh	GU324682	Yuan et al. 2010
							UVRh	GQ451892	Yuan et al. 2010
Heliconius	The Butterfly	**Neruda**	?	Head	RNA-	100 bp PE	***LWRh***		

aoede	Farm - Costa Rica Entomological Supply				seq		
H. atthis	Pichincha, Ecuador	**AB304**	♂	Head	RNA-seq	100 bp PE	***BRh UVRh2 LWRh***
	Santo Domingo, Ecuador	**AB371**	♀	Head	RNA-seq	100 bp PE	***BRh UVRh1 UVRh2 LWRh***
H. charithonia	England Stratford Butterfly Farm - Costa Rica	**HCH453**	♂	Head	RNA-seq	100 bp PE	***BRh UVRh1 UVRh2 LWRh***
	England Stratford Butterfly Farm - Costa Rica	**HCH454**	♂	Head	RNA-seq	100 bp PE	***BRh UVRh1 UVRh2 LWRh***
	England Stratford Butterfly Farm - Costa Rica	**HCH456**	♀	Head	RNA-seq	100 bp PE	***BRh UVRh1 UVRh2 LWRh***
	England Stratford Butterfly Farm - Costa Rica	**HCH457**	♀	Head	RNA-seq	100 bp PE	***BRh UVRh1 UVRh2 LWRh***
H. clysonymus	The Butterfly Farm - Costa Rica Entomological Supply	**HCLY20**	♀	Head	RNA-seq	100 bp PE	***BRh UVRh1 UVRh2 LWRh***
	The Butterfly Farm - Costa Rica Entomological Supply	**HCLY23**	♂	Head	RNA-seq	100 bp PE	***BRh UVRh1 UVRh2 LWRh***
	The Butterfly Farm - Costa Rica Entomological Supply	**HCLY244**	♂	Head	RNA-seq	100 bp PE	***BRh UVRh1 UVRh2 LWRh***
	The Butterfly	**HCLY245**	♀	Head	RNA-	100 bp PE	***BRh UVRh1 UVRh2 LWRh***

	Farm - Costa Rica Entomological Supply				seq				
							BRh UVRh1 UVRh2		
H. cydno	Atlantic slope, Costa Rica						*LWRh*	GU324697	Yuan et al. 2010
							BRh	GU324684	Yuan et al. 2010
							UVRh1	GQ451895	Briscoe et al. 2010
							UVRh2	GQ451896	Briscoe et al. 2010
H. doris	The Butterfly Farm - Costa Rica Entomological Supply	**HDOb254**	♀	Head	RNA-seq	100 bp PE	***LWRh***		
							BRh UVRh1 UVRh2		
	The Butterfly Farm - Costa Rica Entomological Supply	**HDOb259**	♂	Head	RNA-seq	100 bp PE	***LWRh***		
							BRh UVRh1 UVRh2		
	The Butterfly Farm - Costa Rica Entomological Supply	**HDOg161**	♂	Head	RNA-seq	100 bp PE	***LWRh***		
							BRh UVRh1 UVRh2		
	The Butterfly Farm - Costa Rica Entomological Supply	**HDOg164**	♀	Head	RNA-seq	100 bp PE	***LWRh***		
							BRh UVRh1 UVRh2		
	The Butterfly Farm - Costa Rica Entomological Supply	**HDOr252**	♂	Head	RNA-seq	100 bp PE	***LWRh***		
							BRh UVRh1 UVRh2		
	The Butterfly Farm - Costa Rica Entomological Supply	**HDOr253**	♀	Head	RNA-seq	100 bp PE	***LWRh***		
							BRh UVRh1 UVRh2		
H. eleuchia primularis	Santo Domingo, Ecuador	**AB213**	♀	Head	RNA-seq	100 bp PE	***LWRh***		
							BRh UVRh1 UVRh2		
	Pichincha,	**AB249**	♂	Head	RNA-	100 bp PE	***LWRh***		

	Ecuador				seq				
							BRh		
							UVRh1		
							UVRh2		
H. elevatus	Micaela Bastida Rd, Peru						*LWRh*	GU324699	Yuan et al. 2010
							BRh	GU324686	Yuan et al. 2010
							UVRh1	GU324675	Yuan et al. 2010
							UVRh2	GU324676	Yuan et al. 2010
H. erato	The Butterfly Farm - Costa Rica Entomological Supply	**HER14**	♂	Head	RNA-seq	100 bp PE	***LWRh***		
							BRh		
							UVRh1		
							UVRh2		
	The Butterfly Farm - Costa Rica Entomological Supply	**HER197**	♀	Head	RNA-seq	100 bp PE	***LWRh***		
							BRh		
							UVRh1		
							UVRh2		
	The Butterfly Farm - Costa Rica Entomological Supply	**HER200**	♀	Head	RNA-seq	100 bp PE	***LWRh***		
							BRh		
							UVRh1		
							UVRh2		
H. erato cyrbia	Santo Domingo, Ecuador	**AB218**	♂	Head	RNA-seq	100 bp PE	***LWRh***		
							BRh		
							UVRh1		
							UVRh2		
	Pichincha, Ecuador	**AB236**	♀	Head	RNA-seq	100 bp PE	***LWRh***		
							BRh		
							UVRh1		
							UVRh2		
H. ethilla	6.4667 S, 76.3347 W, Peru	09-67	♂	Whole body	DNA-seq	100 bp PE	*LWRh*	ERS235669	Martin et al. 2013
							BRh		
							UVRh1		
							UVRh2		
H. hecale	The Butterfly Farm - Costa Rica Entomological Supply	**HHE221**	♂	Head	RNA-seq	100 bp PE	***LWRh***		
							BRh		
							UVRh1		
							UVRh2		
	The Butterfly Farm - Costa Rica Entomological Supply	**HHE234**	♀	Head	RNA-seq	100 bp PE	***LWRh***		
							BRh		
							UVRh1		
							UVRh2		

	The Butterfly Farm - Costa Rica Entomological Supply	**HHE235**	♂	Head	RNA-seq	100 bp PE	***LWRh***
	The Butterfly Farm - Costa Rica Entomological Supply	**HHE26**	♀	Head	RNA-seq	100 bp PE	***BRh*** ***UVRh1*** ***UVRh2*** ***LWRh***
H. hecalesia	Pichincha, Ecuador	**AB355**	♂	Head	RNA-seq	100 bp PE	***BRh*** ***UVRh1*** ***UVRh2*** ***LWRh***
H. hecuba flava	Napo, Ecuador	**AB261**	♀	Head	RNA-seq	100 bp PE	***BRh*** ***UVRh1*** ***UVRh2*** ***LWRh***
	Napo, Ecuador	**AB267**	♂	Head	RNA-seq	100 bp PE	***BRh*** ***UVRh1*** ***UVRh2*** ***LWRh***
H. hewitsoni	The Butterfly Farm - Costa Rica Entomological Supply	**HHW214**	♂	Head	RNA-seq	100 bp PE	***BRh*** ***UVRh1*** ***UVRh2*** ***LWRh***
	The Butterfly Farm - Costa Rica Entomological Supply	**HHW215**	♂	Head	RNA-seq	100 bp PE	***BRh*** ***UVRh1*** ***UVRh2*** ***LWRh***
	The Butterfly Farm - Costa Rica Entomological Supply	**HHW216**	♀	Head	RNA-seq	100 bp PE	***BRh*** ***UVRh1*** ***UVRh2*** ***LWRh***
	The Butterfly Farm - Costa Rica Entomological Supply	**HHW5**	♀	Head	RNA-seq	100 bp PE	***BRh*** ***UVRh1*** ***UVRh2*** ***LWRh***
H. hortense	Oaxaca, Mexico	**AB406**	♂	Head	RNA-seq	100 bp PE	***BRh*** ***UVRh1*** ***UVRh2*** ***LWRh***
	Oaxaca, Mexico	**AB409**	♀	Head	RNA-seq	100 bp PE	***BRh*** ***UVRh1*** ***UVRh2*** ***LWRh***

H. ismenius	The Butterfly Farm - Costa Rica Entomological Supply	**HIS13**	♀	Head	RNA-seq	100 bp PE	***BRh UVRh1 UVRh2 LWRh***
	The Butterfly Farm - Costa Rica Entomological Supply	**HIS439**	♀	Head	RNA-seq	100 bp PE	***BRh UVRh1 UVRh2 LWRh***
	The Butterfly Farm - Costa Rica Entomological Supply	**HIS441**	♂	Head	RNA-seq	100 bp PE	***BRh UVRh1 UVRh2 LWRh***
	Oaxaca, Mexico	**AB123**	♂	Head	RNA-seq	100 bp PE	***BRh UVRh1 UVRh2 LWRh***
H. melpomene	The Butterfly Farm - Costa Rica Entomological Supply	**HMP110**	♂	Head	RNA-seq	100 bp PE	***BRh UVRh1 UVRh2 LWRh***
	The Butterfly Farm - Costa Rica Entomological Supply	**HMP112**	♀	Head	RNA-seq	100 bp PE	***BRh UVRh1 UVRh2 LWRh***
	The Butterfly Farm - Costa Rica Entomological Supply	**HMP115**	♀	Head	RNA-seq	100 bp PE	***BRh UVRh1 UVRh2 LWRh***
	The Butterfly Farm - Costa Rica Entomological Supply	**HMP333**	♂	Head	RNA-seq	100 bp PE	***BRh UVRh1 UVRh2 LWRh***
H. numata	England Stratford Butterfly Farm - Ecuador	**HNU473**	♀	Head	RNA-seq	100 bp PE	***BRh UVRh1 UVRh2 LWRh***
							BRh UVRh1

	England Stratford Butterfly Farm - Ecuador	**HNU475**	♂	Head	RNA-seq	100 bp PE	***UVRh2 LWRh***		
	England Stratford Butterfly Farm - Ecuador	**HNU501**	♂	Head	RNA-seq	100 bp PE	***BRh UVRh1 UVRh2 LWRh***		
	England Stratford Butterfly Farm - Ecuador	**HNU503**	♀	Head	RNA-seq	100 bp PE	***BRh UVRh1 UVRh2 LWRh***		
H. pachinus	Sirena, Costa Rica						***BRh UVRh1 UVRh2*** *LWRh*	GU324704	Yuan et al. 2010
							BRh	GU324691	Yuan et al. 2010
							UVRh1	GQ451905	Briscoe et al. 2010
							UVRh2	GQ451906	Briscoe et al. 2010
H. pardalinus	8.3425 S, 74.5922 W Peru	09-371	♂	Whole body	DNA-seq		*BRh UVRh1 UVRh2 LWRh*	ERS235667	Martin et al. 2013
H. pardalinus sergestus	6.4778 S, 76.3517 W Peru	09-202	♂	Whole body	DNA-seq		*BRh UVRh1 UVRh2 LWRh*	ERS235668	Martin et al. 2013
H. sapho	England Stratford Butterfly Farm - Costa Rica	**HSP496**	♂	Head	RNA-seq	100 bp PE	***BRh UVRh1 UVRh2 LWRh***		
	England Stratford Butterfly Farm - Costa Rica	**HSP497**	♀	Head	RNA-seq	100 bp PE	***BRh UVRh1 UVRh2 LWRh***		
H. sara	The Butterfly Farm - Costa Rica Entomological Supply	**HSA130**	♂	Head	RNA-seq	100 bp PE	***BRh UVRh1 UVRh2 LWRh***		
	The Butterfly Farm - Costa Rica Entomological Supply	**HSA133**	♀	Head	RNA-seq	100 bp PE	***BRh***		

	The Butterfly Farm - Costa Rica Entomological Supply	**HSA137**	♂	Head	RNA-seq	100 bp PE	***UVRh1 UVRh2 LWRh***		
	The Butterfly Farm - Costa Rica Entomological Supply	**HSA370**	♂	Head	RNA-seq	100 bp PE	***BRh UVRh1 UVRh2 LWRh***		
	The Butterfly Farm - Costa Rica Entomological Supply	**HSA502**	♀	Head	RNA-seq	100 bp PE	***BRh UVRh1 UVRh2 LWRh***		
	The Butterfly Farm - Costa Rica Entomological Supply	**HSA504**	♀	Head	RNA-seq	100 bp PE	***BRh UVRh1 UVRh2 LWRh***		
	The Butterfly Farm - Costa Rica Entomological Supply	**HSA6**	♀	Head	RNA-seq	100 bp PE	***BRh UVRh1 UVRh2 LWRh***		
H. telesiphe sotericus	Napo, Ecuador	**AB253**	♂	Head	RNA-seq	100 bp PE	***BRh UVRh1 UVRh2 LWRh***		
	Napo, Ecuador	**AB259**	♀	Head	RNA-seq	100 bp PE	***BRh UVRh1 UVRh2 LWRh***		
H. timareta thelxinoe	6.4550 S, 76.2983 W, Peru	09-57	♂	Whole body	DNA-seq		*LWRh*	ERS235663	Martin et al. 2013
H. wallacei flavescens	Sucumbios, Ecuador	**AB496**	♂	Head	RNA-seq	100 bp PE	*BRh UVRh1 UVRh2* ***LWRh***		
							BRh UVRh1 UVRh2		